

METAL-POOR STARS AND THE CHEMICAL ENRICHMENT OF THE UNIVERSE

ANNA FREBEL

Harvard-Smithsonian Center for Astrophysics, 60 Garden St., Cambridge, MA 02138, USA; email: afrebel@cfa.harvard.edu

JOHN E. NORRIS

Research School of Astronomy & Astrophysics, The Australian National University,
Mount Stromlo Observatory, Cotter Road, Weston, ACT 2611, Australia; email: jen@mso.anu.edu.au
To appear in Vol. 5 of “Planets, Stars and Stellar Systems”, by Springer, in 2012

ABSTRACT

Metal-poor stars hold the key to our understanding of the origin of the elements and the chemical evolution of the Universe. This chapter describes the process of discovery of these rare stars, the manner in which their surface abundances (produced in supernovae and other evolved stars) are determined from the analysis of their spectra, and the interpretation of their abundance patterns to elucidate questions of origin and evolution.

More generally, studies of these stars contribute to other fundamental areas that include nuclear astrophysics, conditions at the earliest times, the nature of the first stars, and the formation and evolution of galaxies – including our own Milky Way. This is illustrated with results from studies of lithium formed during the Big Bang; of stars dated to within ~ 1 Gyr of that event; of the most metal-poor stars, with abundance signatures very different from all other stars; and of the build-up of the elements over the first several Gyr. The combination of abundance and kinematic signatures constrains how the Milky Way formed, while recent discoveries of extremely metal-poor stars in the Milky Way’s dwarf galaxy satellites constrain the hierarchical build-up of its stellar halo from small dark-matter dominated systems.

Two areas needing priority consideration are discussed. The first is improvement of abundance analysis techniques. While one-dimensional, Local Thermodynamic Equilibrium (1D/LTE) model atmospheres provide a mature and precise formalism, proponents of more physically realistic 3D/non-LTE techniques argue that 1D/LTE results are not accurate, with systematic errors often of order ~ 0.5 dex or even more in some cases. Self-consistent 3D/non-LTE analysis as a standard tool is essential for meaningful comparison between the abundances of metal-poor stars and models of chemical enrichment.

The second need is for larger samples of metal-poor stars, in particular those with $[\text{Fe}/\text{H}] < -4$ and those at large distances (20 – 50 kpc), including the Galaxy’s ultra-faint dwarf satellites. With future astronomical surveys and facilities these endeavors will become possible. This will provide new insights into small-scale details of nucleosynthesis as well as large-scale issues such as galactic formation.

Subject headings: Galaxy: formation – Galaxy: halo – stars: abundances – early Universe – nuclear reactions, nucleosynthesis, abundances

1. INTRODUCTION

A few minutes after the beginning of the Universe, the only chemical elements that existed were hydrogen (~ 0.75 by mass fraction), helium (~ 0.25), and a minuscule amount of lithium ($\sim 2 \times 10^{-9}$). Today, some 13.7 Gyr later, the mass fraction of the elements Li – U in the Milky Way galaxy stands at ~ 0.02 , essentially all of it created by stellar nucleosynthesis. Metal-poor stars provide the foundation for our understanding of the intricate details of the manner in which this enrichment occurred.

The astronomer Carl Sagan summarized cosmic chemical evolution in just one sentence, “We are made from star stuff”. Studying stars that are extremely under-abundant in their heavy elements (collectively referred to as “metals”) takes us right to the heart of this statement. These objects allow us to study the origin of the elements that were subsequently recycled in stellar generations over billions of years until ending up in the human

body.

The rationale for analyzing metal-poor stars is that they are long-lived, low-mass objects, the majority of which are main-sequence and giant stars that have preserved in their atmospheres the chemical signatures of the gas from which they formed. Given that the overall Universe was largely devoid of metals at the earliest times, it is generally assumed (and borne out by analysis) that low metallicity indicates old age. For these objects to be still observable, their masses are of order $0.6 - 0.8 M_{\odot}$. By measuring their surface composition today, one can “look back” in time and learn about the nature of the early Universe. Another vital assumption is that the stellar surface composition has not been significantly altered by any internal “mixing” processes or by external influences such as accretion of interstellar material that would change the original surface abundance.

Analysis of old, metal-poor stars to study the early Universe is often referred to as “stellar archaeology” and “near-field cosmology”. This fossil record of local Galac-

tic metal-poor stars provides unique insight into the enrichment of the Universe, complementing direct studies of high-redshift galaxies.

1.1. *The Role of Metal-Poor Stars*

The abundances of the elements in stars more metal-poor than the Sun have the potential to inform our understanding of conditions from the beginning of time – the Big Bang – through the formation of the first stars and galaxies, and up to the relatively recent time when the Sun formed. An incomplete list of the rationale for studying metal-poor stars includes the following.

- The most metal-poor stars ($[\text{Fe}/\text{H}] \lesssim -4.0$), with primitive abundances of the heavy elements (atomic number $Z > 3$), are most likely the oldest stars so far observed.
- The lithium abundances of extremely metal-poor near main-sequence-turnoff stars have the potential to directly constrain conditions of the Big Bang.
- The most metal-poor objects were formed at epochs corresponding to redshifts $z > 6$, and probe conditions when the first heavy element producing objects formed. The study of objects with $[\text{Fe}/\text{H}] < -3.5$ permits insight into conditions at the earliest times that is not readily afforded by the study of objects at high redshift.
- They constrain our understanding of the nature of the first stars, the initial mass function, the explosion of super- and hyper-novae, and the manner in which their ejecta were incorporated into subsequent early generations of stars.
- Comparison of detailed observed abundance patterns with the results of stellar evolution calculations and models of galactic chemical enrichment strongly constrains the physics of the formation and evolution of stars and their host galaxies.
- In some stars with $[\text{Fe}/\text{H}] \sim -3.0$, the overabundances of the heavy-neutron-capture elements are so large that measurement of Th and U is possible and leads to independent estimates of their ages and hence of the Galaxy.
- Stars with $[\text{Fe}/\text{H}] \lesssim -0.5$ inform our understanding of the evolution of the Milky Way system. Relationships between abundance, kinematic, and age distributions – the defining characteristics of stellar populations – permit choices between the various paradigms of how the system formed and has evolved.

1.2. *Background Matters*

1.2.1. *Essential Reading*

The study of metal-poor stars for insight into the chemical evolution of the Universe has resulted in a rich literature, embracing diverse areas. The reader will find the following topics and reviews of considerable interest.

For the context of the early chemical enrichment of the Universe, and how one might use metal-poor stars to explore back in time to the Big Bang see Bromm & Larson

(2004), Frebel (2010), and Pagel (1997). To understand how one determines the chemical abundances of stars, the important abundance patterns, and how reliable the results are, refer to Wheeler et al. (1989), Sneden et al. (2008), and Asplund (2005). Other relevant questions and reviews include the following. How does one discover metal-poor stars: Beers & Christlieb (2005). What is the role of abundance in the stellar population paradigm: Sandage (1986), Gilmore et al. (1989), and Freeman & Bland-Hawthorn (2002). How do the abundances constrain galactic chemical enrichment: McWilliam (1997). What progress has been made in understanding the supernovae and hypernovae that produce the chemical elements: Timmes et al. (1995), Arnett (1996), and Kobayashi et al. (2006), and references therein. These reviews are of course not one-dimensional, and in many cases they describe matters in several of the topics highlighted above. They will repay close reading by the interested student.

1.2.2. *Abundance Definitions*

Most basically, $\epsilon(\text{A})$, the abundance of element A is presented logarithmically, relative to that of hydrogen (H), in terms of N_{A} and N_{H} , the numbers of atoms of A and H.

$$\log_{10} \epsilon(\text{A}) = \log_{10}(N_{\text{A}}/N_{\text{H}}) + 12$$

(For lithium, the abundance is mostly expressed as $\text{A}(\text{Li}) = \log \epsilon(\text{Li})$; and for hydrogen, by definition, $\log_{10} \epsilon(\text{H}) = 12$.) For stellar abundances in the literature, results are generally presented relative to their values in the Sun, using the so-called “bracket notation”,

$$\begin{aligned} [\text{A}/\text{H}] &= \log_{10}(N_{\text{A}}/N_{\text{H}})_{\star} - \log_{10}(N_{\text{A}}/N_{\text{H}})_{\odot} \\ &= \log_{10} \epsilon(\text{A})_{\star} - \log_{10} \epsilon(\text{A})_{\odot}, \end{aligned}$$

and for two elements A and B, one then has

$$[\text{A}/\text{B}] = \log_{10}(N_{\text{A}}/N_{\text{B}})_{\star} - \log_{10}(N_{\text{A}}/N_{\text{B}})_{\odot}$$

In the case of the Fe metallicity, $[\text{Fe}/\text{H}] = \log_{10}(N_{\text{Fe}}/N_{\text{H}})_{\star} - \log_{10}(N_{\text{Fe}}/N_{\text{H}})_{\odot}$. For example, $[\text{Fe}/\text{H}] = -4.0$ corresponds to an iron abundance 1/10000 that of the Sun.

For completeness, it should be noted that with the bracket notation one needs to know the abundance not only of the star being analyzed, but also of the Sun, the chemical composition of which has recently been revised substantially for some elements (Asplund et al. 2009).

1.2.3. *Nomenclature*

Baade (1944), in his seminal paper on the subject, defined two groups of stars, Type I and Type II, which today are referred to as Population I and Population II. The first referred to young stars, including open clusters, which reside in the disk of the Galaxy, while the second includes its globular clusters, and essentially all of its known metal-poor stars. In what follows, Population II will be referred to as the “halo”, which defines the spatial distribution of the population. It has been speculated that a so-called Population III exists, which

TABLE 1
METAL-POOR STAR RELATED DEFINITIONS

Description	Definition	Abbreviation ^a
Population III stars	postulated first stars, formed from zero-metallicity gas	Pop III
Population II stars	old (halo) stars formed from low-metallicity gas	Pop II
Population I stars	young (disk) metal-rich stars	Pop I
Solar	$[\text{Fe}/\text{H}] = 0.0$	
Metal-poor	$[\text{Fe}/\text{H}] < -1.0$	MP
Very metal-poor	$[\text{Fe}/\text{H}] < -2.0$	VMP
Extremely metal-poor	$[\text{Fe}/\text{H}] < -3.0$	EMP
Ultra metal-poor	$[\text{Fe}/\text{H}] < -4.0$	UMP
Hyper metal-poor	$[\text{Fe}/\text{H}] < -5.0$	HMP
Carbon-rich stars	$[\text{C}/\text{Fe}] > +0.7$ for $\log(L/L_{\odot}) \leq 2.3$ $[\text{C}/\text{Fe}] \geq (+3.0 - \log(L/L_{\odot}))$ for $\log(L/L_{\odot}) > 2.3$	CEMP
n-capture-rich stars	$0.3 \leq [\text{Eu}/\text{Fe}] \leq +1.0$ and $[\text{Ba}/\text{Eu}] < 0$	CEMP
n-capture-rich stars	$[\text{Eu}/\text{Fe}] > +1.0$ and $[\text{Ba}/\text{Eu}] < 0$	r-I
n-capture-rich stars	$[\text{Ba}/\text{Fe}] > +1.0$ and $[\text{Ba}/\text{Eu}] > +0.5$	r-II
n-capture-rich stars	$0.0 < [\text{Ba}/\text{Eu}] < +0.5$	s
n-capture-normal stars	$[\text{Ba}/\text{Fe}] < 0$	r/s no

NOTE. — Carbon-rich stars appear with r- and s-process enhancements also. The CEMP definitions are from Aoki et al. (2007) and differ somewhat from Beers & Christlieb (2005).

^a Commonly used in the literature.

comprises the elusive first stars. With the advent of detailed cosmological simulations of primordial star formation, the term “Population III” is now widely used only for stars that first formed from zero-metallicity gas that consisted only of hydrogen, helium and traces of lithium. The most metal-poor stars currently known are thus extreme members of Population II.

Following Beers & Christlieb (2005) (with some modifications and additions) the nomenclature listed in Table 1 will be adopted for different types of metal-poor stars in terms of population, metallicity and chemical signatures. As can be seen, the main metallicity indicator is the iron abundance, $[\text{Fe}/\text{H}]$. Iron has the advantage that among the elements it has the richest absorption line spectrum in the optical region, facilitating determination of Fe abundance independent of the wavelength range covered by the spectrum. With few exceptions, $[\text{Fe}/\text{H}]$ traces the overall metallicity of the stars fairly well.

1.3. Plan of Attack

For convenience, and the purposes of this chapter, the term “metal-poor” will be taken to mean stars in the Milky Way system having $[\text{Fe}/\text{H}] < -1.0$. This embraces all of the “metal-poor” categories of Beers & Christlieb (2005) shown here in Table 1. It will confine our attention principally to field stars and globular clusters of the Galactic halo and the Galaxy’s dwarf galaxy satellites. Further, if one accepts the Galactic age-metallicity relationship presented, for example, by Freeman & Bland-Hawthorn (2002), this restricts discussion to star formation and associated chemical enrichment that occurred during the first ~ 4 Gyr following the Big Bang. Our abundance restriction also includes part of the so-called “metal-weak thick disk (MWTD)” (see Chiba & Beers 2000) and the Galactic bulge, neither of which will be discussed here. Currently, no major works have been carried out that attempt to elucidate differ-

ences between halo and MWTD abundance patterns. The bulge, on the other hand, is believed to be the site of some of the very first star formation, the result of which is seen today admixed with overwhelming later generations at the Galaxy’s center, precluding insight into its metal-poor population. This is work for the future.

In Section 2, the search for metal-poor stars will be briefly outlined, and what has been discovered so far. Section 3 is concerned with the manner in which chemical abundances are determined (and their reliability). An overview of metallicity distribution functions (MDF) of globular clusters, field stars, and satellite dwarf galaxies is also given. A major focus of this chapter is an introduction to the interpretation of the relative abundances, $[\text{X}/\text{Fe}]$, and the corresponding chemical patterns observed in metal-poor stars. Against this background, in Section 4, the body of metal-poor stellar abundances is presented, and the general abundance trends are discussed in light of expectations set by models of stellar evolution and galactic chemical evolution (GCE). In Section 5, age determination in a small class of extremely metal-poor stars which have huge r-process element enhancement is described. In Section 6, the implications of deduced abundances for the cosmogony of the early Universe and the Milky Way system are considered. Finally, in Section 7, the possibilities and challenges of the future are outlined.

2. DISCOVERY – THE SEARCH FOR NEEDLES IN THE HAYSTACK

2.1. Historical Perspective

Chemical abundance (along with spatial distribution, kinematics, and age) is one of the basic parameters that define stellar populations (see e.g., Sandage 1986). In the middle of the twentieth century, however, as noted by Sandage, “There had grown up a general opinion, shared by nearly all spectroscopists, that there was a single universal curve of all the elements, and that the Sun and all

the stars shared ... precisely ... this property of identical ratios of any element A to hydrogen”. Subtle spectroscopic differences that had been documented at that time were thought to result from differences in physical conditions in the atmospheres of stars rather than in chemical composition. Chamberlain & Aller (1951) profoundly changed this concept with their chemical abundance analysis of the “A-type subdwarfs” HD 19445 and HD 140243, for which they reported $[\text{Fe}/\text{H}]$ ($[\text{Ca}/\text{H}]$) = -0.8 (-1.4) and -1.0 (-1.6), respectively. Their work clearly established the existence of stars with elemental abundances (relative to that of hydrogen) lower than in the Sun, and that these lower abundances played a critical role in determining the strength of their spectral features. (It should be noted in passing that these early values are believed to have been overestimates, with the currently accepted values for Fe being $[\text{Fe}/\text{H}] \sim -2.0$ and -2.5 , respectively. See Sandage (1986, Footnote 2) for an interesting sociological comment on the differences between the earlier and current values.) Soon after that work, Burbidge et al. (1957) reviewed the case for the nucleosynthesis of almost all of the chemical elements within stars. In the decades that followed, exhaustive searches for, and analysis of “metal-poor” stars – as illustrated in Figure 1 – have led to the discovery of stars with lower and lower values of $[\text{Fe}/\text{H}]$ until, at time of writing, two objects with $[\text{Fe}/\text{H}] \sim -5.5$ are known.

Two major developments, relevant to the present discussion, occurred in parallel with the early chemical abundance analyses of stars. The first was the wide acceptance of the “Big Bang” paradigm as the most likely description of the Universe. The second was the demonstration by Wagoner et al. (1967), for example, that at the era of decoupling of radiation and matter, some minutes after the singularity, no elements beyond lithium had been produced (if isotropy and homogeneity were assumed).

One might then enquire how best observationally to examine the manner in which the chemical enrichment of the Universe proceeded. A first approach would be to investigate objects at high redshift, such as galaxies and the Lyman- α clouds seen in the spectra of quasars. Songaila (2001) and Ryan-Weber et al. (2009) report that for redshifts $z = 5.0$ and 6.0 , measures of Si IV and C IV (Songaila) and C IV (Ryan-Weber et al.) observed column densities imply intergalactic metallicity $Z_{\text{IGM}} \gtrsim 3.5 \times 10^{-4} Z_{\odot}$ and $(9 \pm 5) \times 10^{-5} Z_{\odot}$, respectively. Assuming solar abundance ratios, these intergalactic values correspond to $[\text{Fe}/\text{H}] \gtrsim -3.4$ and -4.0 . It is also important to note in this context the recent analyses of very metal-poor Damped Lyman- α systems (see Cooke et al. 2011) that are currently observed out to redshifts $z \sim 2 - 3$, and which report abundances of ~ 6 elements, down to $[\text{Fe}/\text{H}] \sim -3.0$. Far-field cosmological measurements thus currently reach to abundance limits 30 times larger than those observed in the most metal-poor stars in the Milky Way. Further, while to date only C and Si are observed at high redshift ($z \gtrsim 5$), some 8 – 9 elements are measurable in Galactic stars observed to have $[\text{Fe}/\text{H}] = -5.5$ (Christlieb et al. 2002; Frebel et al. 2005). That is to say, it seems reasonable to suggest that the most metal-poor stars have the potential to serve as the best cosmological probes of chemical enrichment at the earliest times.

2.2. Search Techniques

Metal-poor field stars are rare. To begin with, the proportion of stars in the solar neighborhood that belong to the halo population is only $\sim 10^{-3}$ (see e.g., Bahcall & Soneira 1980). Further, as a rule of thumb, the simple chemical enrichment model of the halo of Hartwick (1976; see Section 3.2.1 below) suggests that the number of stars should decrease by a factor of ten for each factor of ten decrease in abundance. For example, the number of stars with $[\text{Fe}/\text{H}] < -3.5$ should be smaller by a factor 100 than the number with $[\text{Fe}/\text{H}] < -1.5$. (For observational support for this suggestion, down to $[\text{Fe}/\text{H}] \sim -4.0$, below which it breaks down, see Norris (1999)). Roughly speaking, given that the stellar halo MDF peaks at $[\text{Fe}/\text{H}] = -1.5$, in the solar neighborhood one might expect to find ~ 1 in 200,000 stars with $[\text{Fe}/\text{H}] < -3.5$.

One thus needs to filter out disk stars if one wishes to find metal-poor stars. While important bright extremely metal-poor stars have been discovered somewhat serendipitously (e.g., the red giant CD-38° 245 with $[\text{Fe}/\text{H}] = -4.0$ and $V = 12.8$; Bessell & Norris 1984), for stars brighter than $B \sim 16$ this has to date been systematically achieved in one of two ways. The first uses the fact that the halo does not share the rotation of the Galactic disk, and a large fraction of its members have relatively high proper motions. The first star with $[\text{Fe}/\text{H}] < -3.0$ (G64-12; Carney & Peterson 1981) was discovered in this way. The major surveys to date that utilized this technique are those of Ryan & Norris (1991a) and Carney et al. (1996), whose samples each comprise a few hundred halo main-sequence dwarfs with $[\text{Fe}/\text{H}] < -1.0$, and who together report ~ 10 stars having $[\text{Fe}/\text{H}] < -3.0$.

The second method has been more prolific and utilizes objective-prism spectroscopy with Schmidt telescopes, which permit one to simultaneously obtain low-resolution spectra (resolving power $R (= \lambda/\Delta\lambda) \sim 400$) of many stars over several square degrees. Examination of the strength of the Ca II K line at 3933.6 \AA with respect to that of nearby hydrogen lines or an estimate of the color of the star permits one to obtain a first estimate of whether the star is metal-weak or not. Candidate metal-poor stars are then observed at intermediate resolution ($R \sim 2000$) to obtain a measurement of the metal abundance of the star. The techniques are described in detail by Beers & Christlieb (2005), who also document important surveys that have obtained first abundance estimates for some tens of thousands of stars brighter than $B \sim 16.5$ with $[\text{Fe}/\text{H}] < -1.0$.

The most important Schmidt surveys to date have been the HK survey (Beers et al. 1992) and the Hamburg/ESO Survey (HES) (Christlieb et al. 2008). In order to give the reader an appreciation of the scope and many steps involved in the process, here is a brief description of the HES. According to N. Christlieb, the HES consists of some 12 million stars in the magnitude range $10 < B < 18$. In an effective survey area of some 6700 square degrees, $\sim 21,000$ candidate metal-poor stars were selected, for which, at the time of writing, follow-up spectroscopy has been obtained of ~ 5200 . Preliminary metal-poor candidates were selected in several steps to arrive at candidate lists for which medium-resolution spectroscopy was sought. Due to limitations of telescope

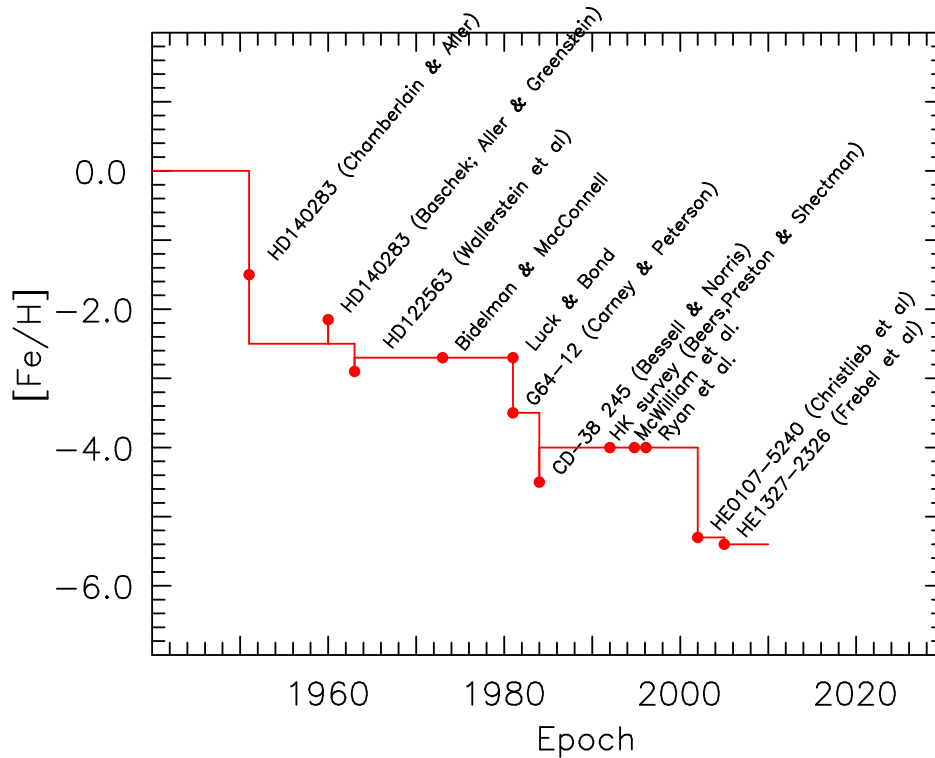


FIG. 1.— $[\text{Fe}/\text{H}]$ for the most metal-poor star then known as a function of epoch. The symbols denote the abundance determined by the authors, while the horizontal lines refer, approximately, to currently accepted values. (The abundances are based on one-dimensional, Local Thermodynamic Equilibrium model atmosphere analysis. See Section 3.1.)

time and target faintness, it was common that not all stars could be observed. In the magnitude range $13.0 \lesssim B \lesssim 17.5$ there were ~ 3700 red giants of which about 1700 were observed at medium-resolution (Schörck et al. 2009), together with ~ 3400 near-main-sequence-turnoff stars, of which ~ 700 have follow-up spectroscopy (Li et al. 2010). There is also a bright sample of ~ 1800 stars having $B < 14.5$, for all of which medium resolution spectra were obtained by Frebel et al. (2006). From these samples, the most metal-poor candidates were selected for high-resolution observation. Various considerations determined whether a star was ultimately observed. These include telescope time allocations, observability and weather conditions during observing time, target brightness, reliability of the medium-resolution result, science questions to be addressed, and of course the preliminary metallicity of the star. Given these limitations, fainter stars remain unobserved on the target lists due to time constraints.

To this point the discussion has been confined to surveys that have concentrated on discovering candidate metal-poor stars with $B \lesssim 17.5$, with follow-up medium-resolution spectroscopy complete in most cases to only somewhat brighter limits. Surveys that reach to considerably fainter limits are the Sloan Digital Sky Survey (SDSS) and the subsequent SEGUE-I and II surveys (see <http://www.sdss.org>), which have obtained spectra with resolving power $R \sim 2000$, and are also proving to be a prolific source of metal-poor stars. In a sample of some 400,000 stars, SDSS/SEGUE has discovered 26,000 stars with spectra having $S/N > 10$, and $[\text{Fe}/\text{H}] < -2.0$ (based on these intermediate-resolution spectra), while some 400

have $[\text{Fe}/\text{H}] < -3.0$.

The search for metal-poor stars remains a very active field, with several exciting projects coming to completion, currently in progress, and planned. This matter will be further discussed in Section 7.

2.3. High-Resolution, High S/N Follow-Up Spectroscopy

The final observational step in the discovery process is spectroscopy of the most significant objects (e.g., most metal-poor, or most chemically peculiar) at very high resolving power ($R \sim 10^4 - 10^5$) and $S/N \gtrsim 100$, in order to reveal the fine detail required for the determination of parameters such as accurate chemical abundances, isotope ratios, and in some cases stellar ages. This is best achieved with 6 – 10 m telescope/échelle spectrograph combinations – currently HET/HRS, Keck/HIRES, Magellan/MIKE, Subaru/HDS, and VLT/UVES.

In order to give the reader a feeling for both the role of increased resolution and the manner in which decreasing metallicity affects the observed flux, Figure 2 shows the increase in spectroscopic detail between intermediate ($R \sim 1600$) and high ($R \sim 40000$) resolving power for four metal-poor red giants of similar effective temperature (T_{eff}) and surface gravity ($\log g$) as metal abundance decreases from $[\text{Fe}/\text{H}] = -0.9$ to -5.4 (for HE 0107-5240, the most metal-poor giant currently known).

2.4. Census of the Most Metal-Poor Stars

This section presents a census of stars having $[\text{Fe}/\text{H}] < -3.0$ and for which detailed high-resolution, high S/N , published abundance analyses are available. The data

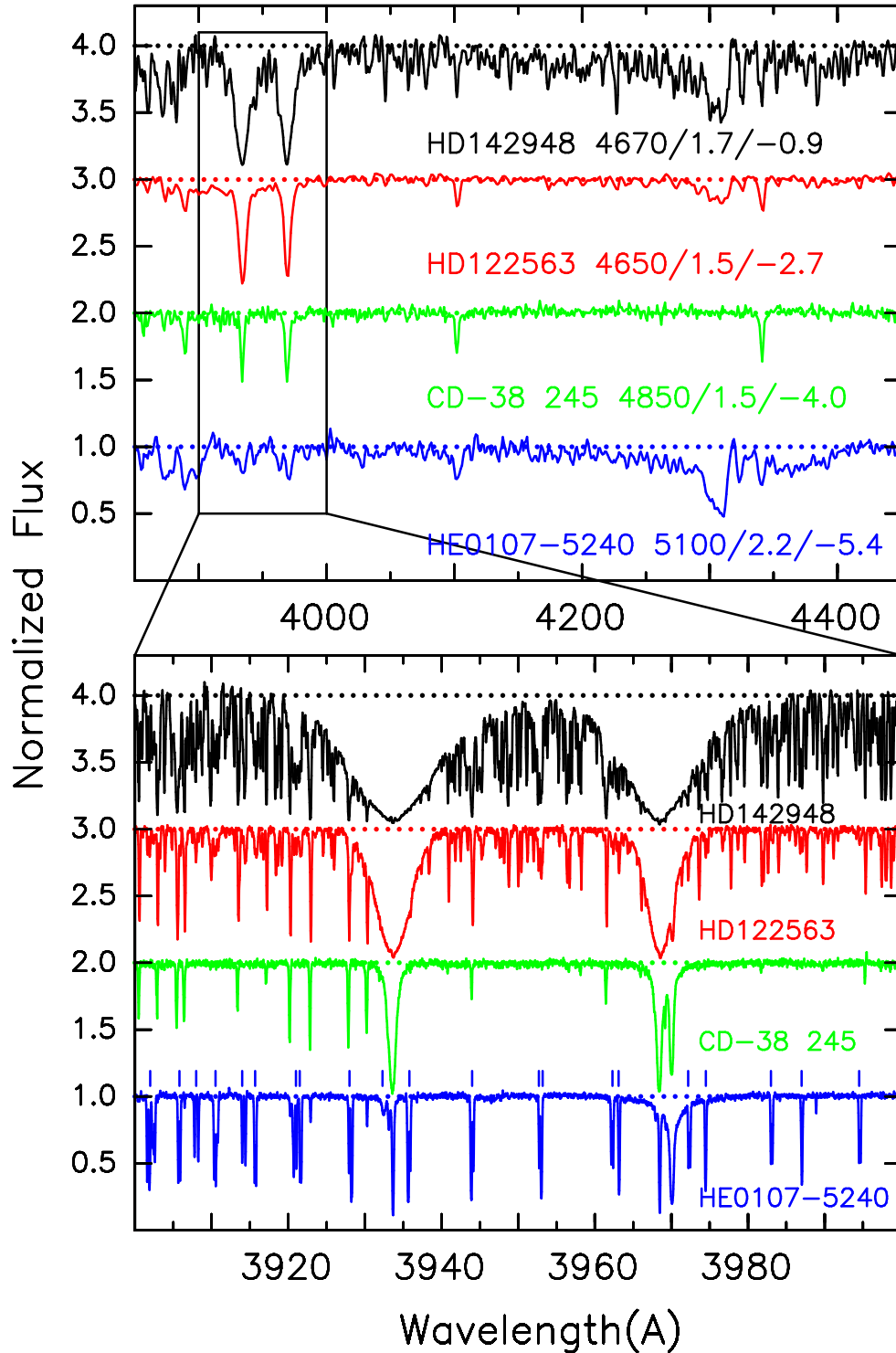


FIG. 2.— (Upper panel) Spectra at intermediate resolution ($R \sim 1600$) of metal-poor red giants over the range $-5.4 < [\text{Fe}/\text{H}] < -0.9$. Note the strong decrease in the strengths of the Ca II H & K lines at 3933.6 and 3968.4 Å. The numbers in the panel represent $T_{\text{eff}}/\log g/[\text{Fe}/\text{H}]$. (Lower panel) Spectra of the same stars at $R \sim 40000$ on the range $3900 - 4000$ Å. (Note that while the Ca II H & K lines are very weak in the most metal-poor giant, HE 0107-5240, many more lines have appeared. These are features of CH (the positions of which are indicated immediately above the spectrum) resulting from an extremely large overabundance of carbon relative to iron in this object.

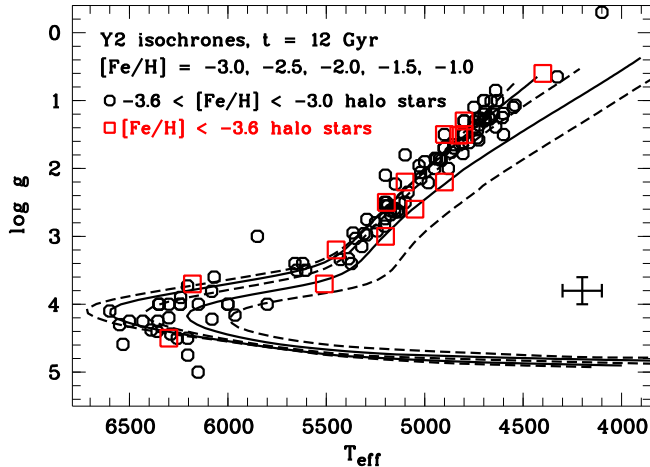


FIG. 3.— Hertzsprung-Russell diagram of the ~ 130 known metal-poor stars with $[\text{Fe}/\text{H}] < -3.0$ studied at high-resolution (from the compilation of Frebel 2010). 14 stars with $[\text{Fe}/\text{H}] < -3.6$ are marked with open squares. Typical error bars are indicated at bottom right. Several 12 Gyr isochrone tracks (from <http://www.astro.yale.edu/demarque/yyiso.html>) for different metallicities are overplotted for illustration. As can be seen, the main-sequence turnoff shifts significantly to hotter temperatures at $[\text{Fe}/\text{H}] < -2.0$, whereas the giant branch is less affected.

set comprises some 130 objects, and may be found in the compilation of Frebel (2010). Figure 3 shows the distribution of the stellar parameters effective temperature, T_{eff} , and surface gravity, $\log g$, of these objects, in comparison with several 12 Gyr isochrones of different metallicities, $[\text{Fe}/\text{H}]$, in the Hertzsprung-Russell diagram. The vast majority of the stars are luminous red giants ($4000 \text{ K} < T_{\text{eff}} < 5500 \text{ K}$, $0.0 < \log g < 3.5$), but about 25 main-sequence stars near the turnoff ($5800 \text{ K} < T_{\text{eff}} < 6600 \text{ K}$, $3.5 < \log g < 4.5$) are also known. A similar ratio is maintained for metallicities below $[\text{Fe}/\text{H}] = -3.6$. (The atmospheric parameters T_{eff} , $\log g$, and $[\text{Fe}/\text{H}]$ are the essential stellar parameters that determine the structure of a star’s outer layers and the details of its emergent flux, as will be discussed in Section 3.1.)

Figure 4 presents the histogram of $[\text{Fe}/\text{H}]$ for the same group of objects. Two things are worth noting from this diagram. First, the number of stars decreases precipitously as one moves towards lowest abundance, and second, the proportion of carbon-rich objects increases dramatically. The implications of this remarkable behavior are discussed further in Section 6.1. More generally, roughly 10% of the objects in this sample (often those with enhanced carbon) reveal a chemical nature that is different from that of “normal” halo stars. These objects are of particular interest as they can be used to address a variety of astrophysically important questions. Arguably, the most interesting stars in the sample are those with metallicities $[\text{Fe}/\text{H}] \lesssim -3.5$. It is probably reasonable to say that all stars known to have $[\text{Fe}/\text{H}] \lesssim -3.5$ from medium-resolution spectroscopy and $B < 16.5$ are included in this diagram, given their potential for insight into the early Universe.

There are eight stars known to have $[\text{Fe}/\text{H}] \sim -4.0$ or less. One of them is CD-38° 245 (Bessell & Norris 1984;

Norris et al. 2001), the first star with $[\text{Fe}/\text{H}] \sim -4.0$. It was discovered some 30 years ago, and was a long-standing record holder for the most iron-poor object in the Milky Way. It has been observed and analyzed many times by most research groups working in the field. Only four stars in this very small sample have $[\text{Fe}/\text{H}] < -4.3$, with two having $[\text{Fe}/\text{H}] < -5.0$. In 2001, the first star with $[\text{Fe}/\text{H}] < -5.0$ was discovered. Until then, it had not been clear whether objects with metallicities lower than that of CD-38° 245 existed. This object, HE 0107-5240, is a faint ($V = 15.2$) red giant with $[\text{Fe}/\text{H}] = -5.3$ (Christlieb et al. 2002). In 2004, the bright ($V = 13.5$) subgiant HE 1327-2326 was identified and shown to have $[\text{Fe}/\text{H}] = -5.4$ (Frebel et al. 2005), corresponding to $\sim 1/250000$ of the solar iron abundance. This small stellar Fe number density translates to an actual iron mass that is about 100 times less than that of the earth’s iron core! Both stars were found in the Hamburg/ESO survey. Since then, no further objects with such record-low Fe values have been discovered. As outlined in Section 7 new surveys will provide additional chances to uncover more of these rare stars.

The paucity of stars with $-5.3 \lesssim [\text{Fe}/\text{H}] \lesssim -4.3$ sparked considerable interest among theorists, with some suggesting that there may be a physical reason for this apparent gap in the metallicity distribution function (e.g., Shigezuma et al. 2003). The discovery, however, of the red giant HE 0557-4840 (Norris et al. 2007) and the dwarf star SDSS J102915+172927 (Caffau et al. 2011) both with $[\text{Fe}/\text{H}] \sim -4.7$ (adopting 1D Fe abundances) confirmed that extremely limited discovery statistics below $[\text{Fe}/\text{H}] \sim -4.3$, driven by only four stars, are most likely the cause of the apparent gap.

In summary, as of mid-2010, numerous stars with $[\text{Fe}/\text{H}] < -3.0$ have been discovered and many (~ 130) have been analyzed with high-resolution spectroscopy. Stars with $[\text{Fe}/\text{H}] < -3.5$ are much rarer, but most likely all known examples (~ 25) of them have high-resolution spectroscopic analyses. Only four stars with $[\text{Fe}/\text{H}] < -4.3$ are known, of which two have $[\text{Fe}/\text{H}] < -5.0$.

2.5. The Lowest Observable Metallicity

What is the lowest abundance one might be able to observe in the Galactic halo? From a practical point of view, a useful limit is set by the abundance corresponding to a measured Ca II K line strength of $20 \text{ m}\text{\AA}$ (roughly 2–4 times the strength on the weakest lines measurable in high-resolution, high S/N , spectra such as those shown in Figure 2) in a cool red giant with $T_{\text{eff}} = 4500 \text{ K}$ and $\log g = 1.5$. (Ca II K is the strongest atomic feature in metal-poor stars, and its strength is greater in red giants than near-main-sequence dwarfs (due to the lower effective temperatures of the former). Also, the abundances of red giants are much less modified by accretion from the Galactic Interstellar Medium (ISM) than those of main-sequence stars, because of the deep outer convective regions in giants.)

Adopting a 1D LTE model atmosphere (see Section 3.1.1) with these parameters and $[\text{Fe}/\text{H}] = -4.0$ (the lowest available abundance in many grids, and which should be adequate for the task), a line strength of $20 \text{ m}\text{\AA}$ corresponds to $[\text{Ca}/\text{H}]_{\text{min}} = -9.4$. (For Fe I 3859.9 \AA , the intrinsically strongest Fe I line in the optical spectrum, a

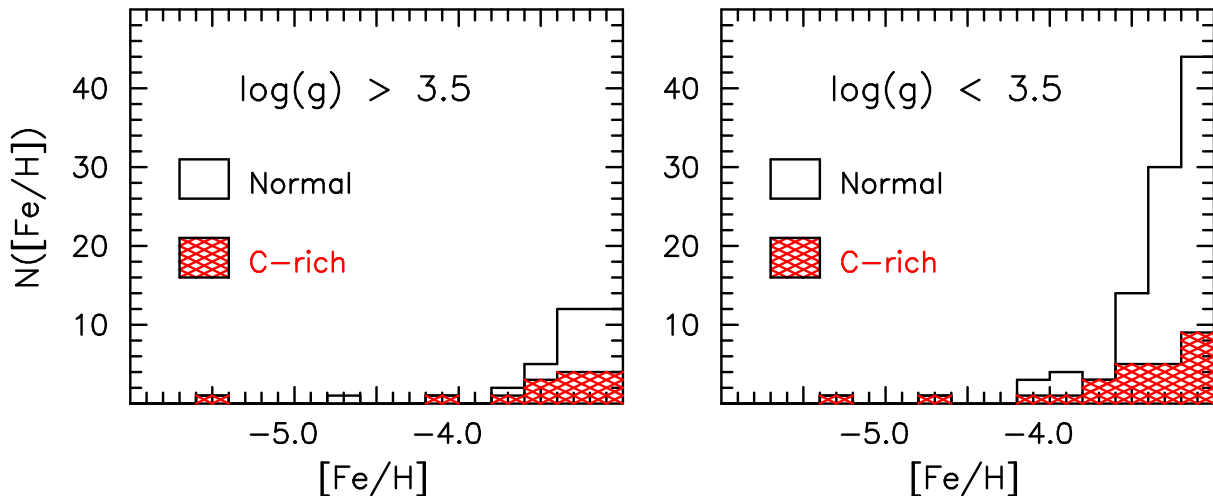


FIG. 4.— $[\text{Fe}/\text{H}]$ histogram for stars having high-resolution, high S/N , abundance analyses and $[\text{Fe}/\text{H}] < -3.0$, from the compilation of Frebel (2010). On the left are results for main-sequence and subgiant stars, while the right presents data for red giants. The shaded regions refer to C-rich stars. Note the rapid decline in the number of stars as $[\text{Fe}/\text{H}]$ decreases, accompanied by an increase in the proportion of carbon-rich objects.

line strength of $20 \text{ m}\text{\AA}$ results in a less stringent limiting abundance of $[\text{Fe}/\text{H}] = -7.2$.) If one were to assume that this hypothetical star had $[\text{Ca}/\text{Fe}] = 0.4$, similar to that found in the most metal-poor stars, its iron abundance would be $[\text{Fe}/\text{H}]_{\text{min}} = -9.8$. This can be taken as a rough estimate of the lowest metallicity practicably detectable.

Even, however, if such a star existed, one should not automatically interpret the above minimum abundance as the value with which it formed, given the possibility of accretion of material from the interstellar medium (ISM) during its ~ 13 Gyr lifetime. Using calculations described by Frebel et al. (2009), who compute the amount of material likely to have been accreted onto each of some 470 observed halo main-sequence stars, it was found that during its time on the RGB the average amount of material accreted onto a star would have increased an initial zero heavy element abundance to an observed atmospheric value of $[\text{Fe}/\text{H}] = -8.6$, with a dispersion of 0.8 dex (Here the large dispersion is driven by an extremely strong dependence of the accretion process on the relative velocity of the star with respect to the ISM.) From this information, it follows that a star that formed with $[\text{Fe}/\text{H}]_{\text{min}} = -9.8$, and experienced average ISM accretion would be observed during its RGB evolutionary phase as an object with $[\text{Fe}/\text{H}] \sim -8.6$. Alternatively, given the dispersion in possible accretion histories, one might also say that the probability of finding a star that initially had zero heavy-element abundance (i.e., Population III) and observed today during its RGB phase would have an “accreted” abundance of $[\text{Fe}/\text{H}] = -9.8$ or smaller, is ~ 0.07 .

Having assessed the technical feasibility of finding near-zero-metallicity, low-mass ($M < 1 M_{\odot}$) stars, one needs also to consider potential physical processes that may have played a role in the formation of the most metal-poor stars, and which lead to abundances between the current lowest observed level of $[\text{Fe}/\text{H}] \sim -5.5$ and the potentially detectable $[\text{Fe}/\text{H}] = -9.8$. As will be discussed in Section 6.1 the critical factor is the cooling mechanisms that determine the contraction and fragmentation of existing gas clouds. Two potentially important

cooling mechanisms are noted here, as well as the abundance limits they impose, following Frebel et al. (2009). The first is C II and O II fine-structure line cooling which leads to $[\text{Fe}/\text{H}]_{\text{min}} = -7.3$. The second is the major cooling due to dust grains, for which the limit might be 1 – 2 orders of magnitude lower, e.g., $[\text{Fe}/\text{H}]_{\text{min}} = -8.0$ to -9.0 . While more detailed knowledge on cooling mechanisms may well change these values, the above discussion shows that one should not be surprised to find stars with metallicities much lower than those of the most-metal-poor stars currently known.

3. DERIVED CHEMICAL ABUNDANCES

3.1. Abundance Determination

3.1.1. One-Dimensional Model Atmosphere Analyses

Most chemical abundance determinations are based on one-dimensional (1D) model stellar atmosphere analyses that assume hydrostatic equilibrium, flux constancy, Local Thermodynamic Equilibrium (LTE), and treat convection in terms of a rudimentary mixing length theory. (In most cases the configurations are plane parallel, but when necessary spherical symmetry is adopted for giants.) To first order, the basic atmospheric parameters that define the model are effective temperature (T_{eff}), surface gravity ($\log g$), and chemical composition. Given these, one may construct a model atmosphere and compute the emergent flux for comparison with observations. Then, on the assumption that the model well-represents the observed star, when one obtains a good fit between the model emergent flux (in particular the strengths of the atomic and molecular features) and the observed flux, one assumes the chemical abundances of the model correspond to those of the observed star. The student should consult Gray (2005) and Gustafsson et al. (2008) for the concepts associated with the process.

For completeness, it should be briefly noted that T_{eff} and $\log g$ are sometimes derived from atomic and molecular transitions (excitation temperature and ionization equilibrium, respectively) and sometimes from measurements of continuum colors, and the strengths of hydrogen

Balmer lines and the Balmer Jump. Surface gravity is also often derived from the star’s luminosity, T_{eff} , and mass. A basic shortcoming of 1D modeling is that an artificial, second-order, extra line-broadening called “microturbulence”, over and above the thermal broadening of the models, is always introduced into the formalism to satisfy the requirement that atomic lines of different strength yield the same abundance. This will not be discussed here further, except to say that the need for this “fudge factor” has proved to be unnecessary in the more physically realistic 3D modeling. Finally, best analysis involves an iterative process that demands the adopted T_{eff} , $\log g$, abundances, and microturbulence are consistent with both the adopted model atmosphere and all of the details in the star’s spectrum that are sensitive to these parameters.

As discussed in Section 1.2.2, the analysis produces stellar atmospheric abundances $\epsilon(X)$ for species X relative to hydrogen, expressed as $\log_{10}\epsilon(X) = \log_{10}(N_X/N_H) + 12$; in most cases values are published using the bracket notation $[X/H] = \log_{10}(N_X/N_H)_* - \log_{10}(N_X/N_H)_\odot$, which expresses the results relative to solar values. For completeness it should be noted that the *elemental* abundances derived in this way represent the contribution of all isotopes; additional isotope ratios can only be determined in a few cases (e.g., C). This contrasts nucleosynthesis models, which yield abundances of each individual calculated isotope abundance. (Publicly available model atmospheres and associated atomic and molecular data may be found, for example, at <http://kurucz.harvard.edu>, <http://vald.astro.univie.ac.at>, and <http://www.physics.nist.gov/PhysRefData/ASD/lines.form.html>, while codes for the computation of emergent fluxes and determination of chemical abundances may be found, for example, at <http://www.as.utexas.edu/~chris/moog.html>.) Given the power of modern computers, this is now a mature and straight-forward process, and 1D/LTE abundances, $[Fe/H]$ and $[X/Fe]$, based on high resolution, high S/N, data are currently available for a large number of metal-poor stars – for example, for resolving power $> 20,000$ and $[Fe/H] < -2.0$, data exist for some 600 objects. Two comprehensive compilations of published material are those of Suda et al. (2008) and Frebel (2010), the latter of which will be used in what follows. The precisions of these results are high, typically of order 0.10 dex (26%), and in some cases ~ 0.03 dex (7%).

3.1.2. Three-Dimensional Model Atmospheres

The question that remains to be answered is: how accurate are these 1D abundances? The issues have been addressed by Asplund (2005), to whom the reader is referred. Three-dimensional (3D) hydrodynamical models reveal temperature inhomogeneities, which lead to different temperature structures between 3D and 1D models. As metallicity decreases, the inhomogeneities become larger, resulting in significant negative abundance corrections. Figures 1 and 2 of Asplund illustrate the effect: at $T_{\text{eff}} = 5800$ K, $\log g = 4.4$, one finds that while at $[Fe/H] = 0.0$ the *average* temperature of the 3D model agrees reasonably well with that of its 1D counterpart, the situation is very different at $[Fe/H] = -3.0$, where the 3D model has temperatures lower by several hun-

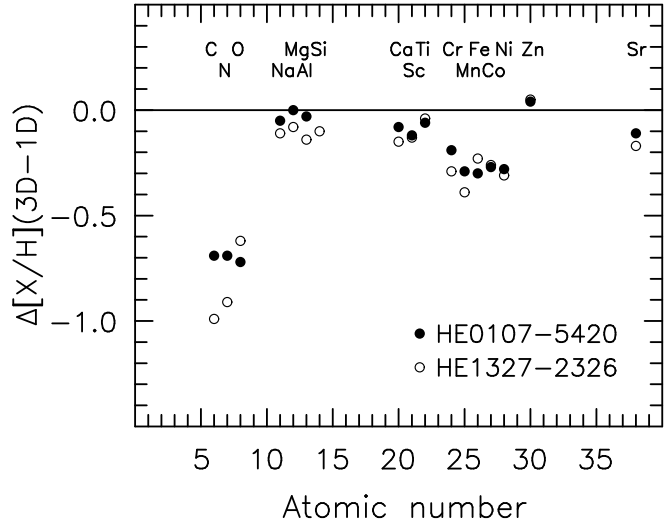


FIG. 5.— The difference in abundance, $[X/Fe]_{3D} - [X/Fe]_{1D}$, vs. atomic number, deduced from analyses based on three-dimensional and one-dimensional model atmospheres, for the two most metal-poor stars – the subgiant HE 1327–2326 and the red-giant HE 0107–5240, both with $[Fe/H]_{1D} \sim -5.5$. These stars show the so-far most extreme abundance differences between 1D and 3D analyses. (Data from Collet et al. 2006 and Frebel et al. 2008).

dred degrees in its upper layers. These in turn lead to significant differences between 1D and 3D abundances as a function of the metallicity of the star and the excitation potential of the observed line transition. Figure 8 of Asplund shows that for resonance lines of typical elements 1D abundances are too high by 0.1 – 0.6 dex, with the difference being smaller for lines of higher excitation potential. The strength of molecular features is very sensitive to the temperatures in the outer layers, resulting in dramatically lower abundances compared with those obtained in 1D analyses.

Abundance analysis utilizing 3D models is a computationally intensive exercise, and results are currently available for only relatively few stars selected for their astrophysical significance. Examples of this are the two most metal-poor stars HE 0107–5240 and HE 1327–2326, for which Figure 5 presents abundance differences $[X/Fe](3D) - [X/Fe](1D)$ versus atomic number from the work of Collet et al. (2006) and Frebel et al. (2008). Note the extremely large differences for C, N, and O – for which the cited results are determined from analysis of CH, NH, and OH, respectively. One must bear this in mind when seeking to interpret 1D chemical abundances.

3.1.3. Departures from Thermodynamic Equilibrium (Non-LTE)

In order to determine chemical abundances one needs to derive the populations of atomic and molecular energy levels, which depend on details of the radiative and collisional effects in the regions of line formation in the stellar atmosphere. The reader is once again referred to Asplund (2005) for a thorough discussion of this matter. The proper solution to the problem is sufficiently computationally intensive that most investigations to date have made the assumption of LTE. This approach assumes that collisional effects dominate over radiative ones, from

which it follows that the required populations can be determined by the Maxwell, Saha, and Boltzmann distributions, which involve only the local physical parameters temperature and electron pressure. To quote Asplund: “In LTE the strength of a line can be straightforwardly predicted from a few properties of the line and the species once the model atmosphere and continuous opacity are known. In non-LTE, in principle everything depends on everything else, everywhere else.” (For completeness, it should also be noted that a remaining uncertainty in current non-LTE analyses is the treatment of inelastic collisions with hydrogen atoms; see Asplund 2005, his Section 2.1.)

Given the time-consuming nature of non-LTE computations, the large majority of abundances analyses to date assume LTE. The advice of Asplund should, however, be recalled. “It is always appropriate to provide the LTE results for comparison purposes, but it is unwise to ignore the available non-LTE calculations when providing the final abundance values.” The present work follows this advice where possible, and considers (non-LTE – LTE) differences further in Section 3.2.2.

3.1.4. *Caveat Emptor*

Two caveats are offered in conclusion. The first is that essentially all of the abundances presented here have been determined using 1D/LTE model atmosphere analyses. In some cases, when 3D and/or non-LTE data are available, comments are included on the resulting differences between the two formalisms. The second point is that for a comprehensive improvement over 1D/LTE results, one needs to use both 3D and non-LTE and not just one of them: in the case of lithium, for example, and as will be discussed in Section 4.1, the 3D and non-LTE corrections are both large, but of opposite sign, and fortuitously largely cancel to give the 1D/LTE result.

3.1.5. *Post-Astration Abundance Modification*

The final question one must address is whether the abundances obtained from these exhaustive model atmosphere analyses are indeed the values in the protocloud from which the star formed. Here, very briefly, with source material pertinent to metal-poor stars, are important examples of processes that can modify the original abundance patterns in the observed surface layers.

- Accretion from the interstellar medium over the lifetime of a star (e.g., Frebel et al. 2009)
- Radiative and gravitational diffusion in the stellar surface layers (e.g., Behr et al. 1999)
- Macroscopic mixing of nucleosynthesis products from stellar interiors into their surface layers (e.g., Gratton et al. 2000)
- Post-asymptotic-giant-branch evolution, during which the sequence of element fractionation onto circumstellar grains, radiation-pressure-driven grain/gas separation, and the formation of a stellar atmosphere containing the remaining gas produce an Fe-poor, modified abundance pattern determined by the physics of gas/grain condensation (e.g., Giridhar et al. 2005)

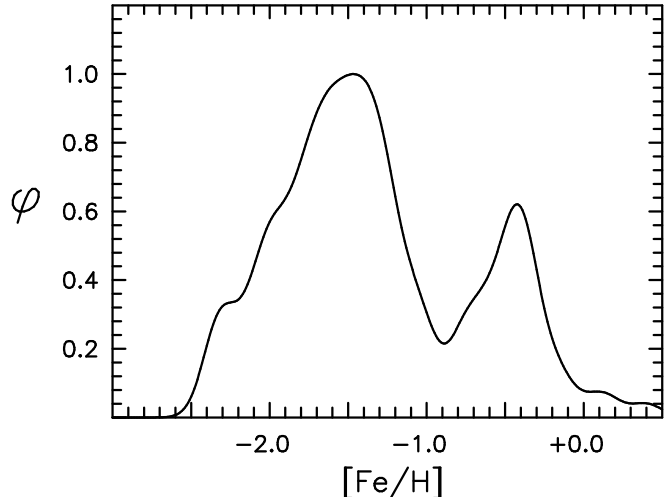


FIG. 6.— MDF of the Galactic globular clusters (data of Carretta et al. 2009). Note the clearly bimodal distribution, with peaks at $[\text{Fe}/\text{H}] = -1.5$ and -0.4 , corresponding predominantly to halo and disk/bulge material, respectively. (The histogram was generated with a gaussian kernel having $\sigma = 0.10$ dex.)

- Transfer of material across a multiple stellar system during post-main-sequence evolution (e.g., Beers & Christlieb 2005)

3.2. *Abundance Patterns*

3.2.1. *Metallicity Distribution Functions (MDF)*

The Galactic Globular Cluster System

With very few exceptions (which will be considered in Section 4.3.1) the Milky Way’s globular clusters are individually chemically homogeneous with respect to iron. The collective MDF of the cluster system is bimodal, as first definitively shown by Zinn (1985) and presented here in Figure 6 (based on the more recent abundance compilation of Carretta et al. 2009). The two components, initially designated “halo” and “disk” have mean metallicities $[\text{Fe}/\text{H}] \sim -1.5$ and -0.4 . This terminology, however, appears to be an oversimplification: some clusters with abundances as low as $[\text{Fe}/\text{H}] \sim -1.5$ have disk-like kinematics; some of the inner “disk” sub-population have been suggested to be members of the Galactic bulge; and consideration of the horizontal branch morphologies of globular clusters first led to the suggestion of old and young subgroups in the halo sub-population (Zinn 1993). Clearly, the situation is a very complicated one.

Field Stars

MDFs are also available for local metal-poor samples of both kinematically selected main-sequence dwarfs (Ryan & Norris 1991b) and (Carney et al. 1996), and spectroscopically selected giants (Schörck et al. 2009) and dwarfs (Li et al. 2010).

The field star distributions differ from that of the globular clusters in one important aspect: all halo field star samples contain objects having abundances considerably lower ($[\text{Fe}/\text{H}] = -4.0$ to -3.0) than that of the most metal-poor globular cluster ($[\text{Fe}/\text{H}] \sim -2.5$). According to Carney et al. (1996) the difference between halo

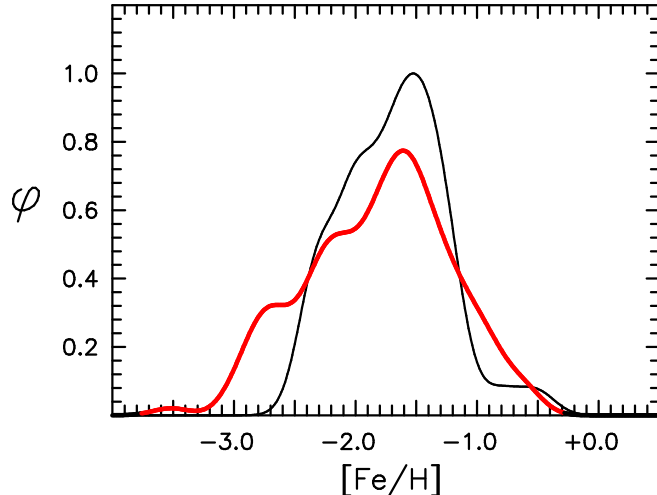


FIG. 7.— Comparison of the MDFs of the halo globular clusters (thin line) and kinematically chosen halo field main-sequence dwarfs (thick line). The selection of the halo samples follows Section 3.5 of Carney et al. (1996): for the clusters only objects more than 8 kpc from the Galactic center are included (with abundances from Carretta et al. 2009), while for the dwarfs the data are from Carney et al. (1996). (The histograms were generated with a gaussian kernel having $\sigma = 0.15$ dex.)

clusters and kinematically selected dwarfs is highly significant (at the 93 – 99.9% level); this effect is shown here in Figure 7, based on more recent data. For spectroscopically selected samples, on the other hand (which by definition have a strong abundance selection bias towards more metal-poor stars, not present in kinematically selected samples), the significance is less clear. According to Schörck et al. (2009): “A comparison of the MDF of Galactic globular clusters ... shows qualitative agreement with the halo [field star] MDF, derived from the HES, once the selection function of the latter is included. However, statistical tests show that the differences between these are still highly significant.” The problem with the spectroscopically chosen HK and HES samples is that the corrections that must be applied to compensate for the selection function are very large, as clearly shown in Figure 8 below (see also Schörck et al. 2009, their Figure 17).

The fundamental importance of metallicity distribution functions is that they provide essential constraints on galactic chemical enrichment (GCE) models. The starting point adopted for the present discussion is the simple model of halo chemical enrichment of Hartwick (1976), who assumed that initially the halo contained zero heavy elements, and was chemically enriched by the ejecta of massive stars on timescales short compared with those of the halo’s dynamical evolution (instantaneous recycling). He also assumed that the initial mass function was constant with time, and in order to reproduce the MDF of the halo globular clusters, postulated that gas was removed from the system at a rate proportional to that of star formation. The left panel of Figure 8 shows a comparison of this simple model (dotted line) with the observations of halo field dwarfs by Ryan & Norris (1991b). The solid line in the figure, which somewhat better fits the data, represents a model

of Tsujimoto et al. (1999) which involves star formation on shells swept up by the ejecta of the supernova explosions of massive stars.

A point worth reiterating from Section 2.2 is that the simple Hartwick model predicts the number of metal-poor stars should decrease by a factor of ten for each factor of ten decrease in abundance: Norris (1999) and Schörck et al. (2009) report that this appears to be the case down to $[\text{Fe}/\text{H}] = -4.0$ and -3.6 , respectively, below which there is a large dearth of stars. Recall also from Section 2.4 that only four stars with $[\text{Fe}/\text{H}] \lesssim -4.3$ are currently known.

Several other GCE models have been proposed which modify the basic assumptions of the Hartwick model. As an example, the right panel of Figure 8 shows the comparison between the spectroscopically selected halo giant sample of Schörck et al. (2009) and the model of Prantzos (2003) (which investigates improvement of the instantaneous recycling approximation and possible gaseous infall). The reader is referred to Schörck et al. (2009) and Li et al. (2010) for comparison of the observations with other GCE models from T. Karlsson (delayed chemical enrichment at the earliest times), S. Salvadori and co-workers (Λ CDM framework with a critical metallicity for low-mass star formation), and N. Prantzos (semi-analytical model within the hierarchical merging paradigm).

This section is concluded with a caveat concerning the above comparison of MDFs. There has been growing evidence over some two decades, beginning with the seminal works of Hartwick (1987) and Zinn (1993) that the Galactic halo comprises more than one component, with different properties as a function of Galactocentric distance; see Carollo et al. (2010) and Morrison et al. (2009), and references therein for details. The multiplicity of the Galactic halo will be discussed in Section 6.2. Suffice it here to say it makes little sense to compare the MDFs of samples (observational and/or theoretical) that have different properties (except to test the null hypothesis). It is essential to match the underlying characteristics of the theoretical models and observed samples that are being compared.

Dwarf Spheroidal Galaxies (dSph)

In stark contradistinction to the Milky Way’s globular clusters, its dwarf spheroidal galaxy satellites all show large internal spreads in the abundance of iron. The MDFs for five of the ~ 25 currently known systems are shown in Figure 9. (Also shown in the figure, for comparison purposes, is the MDF of ω Cen, the most massive Milky Way globular cluster, and one of only ~ 5 halo clusters known to exhibit a dispersion in iron greater than $\sigma[\text{Fe}/\text{H}] \sim 0.03$ dex.) In each panel the abundance dispersion $\sigma[\text{Fe}/\text{H}]$ and integrated absolute visual magnitude, $M_{V,\text{total}}$, are also shown.

It has been known for some time that the metallicities of elliptical galaxies and the more luminous dSphs collectively decrease as luminosity decreases (Mateo 1998). As reported by Kirby et al. (2008), the mean $[\text{Fe}/\text{H}]$ of dSphs continues to decrease with decreasing luminosity over the range of the ultra-faint systems as well. As shown here in Figure 10 the relationship holds over the range $3.5 \lesssim \log(L_{\text{tot}}/L_{\odot}) \lesssim 7.5$. This is a clear signal that the dwarf galaxies have undergone internal chemi-

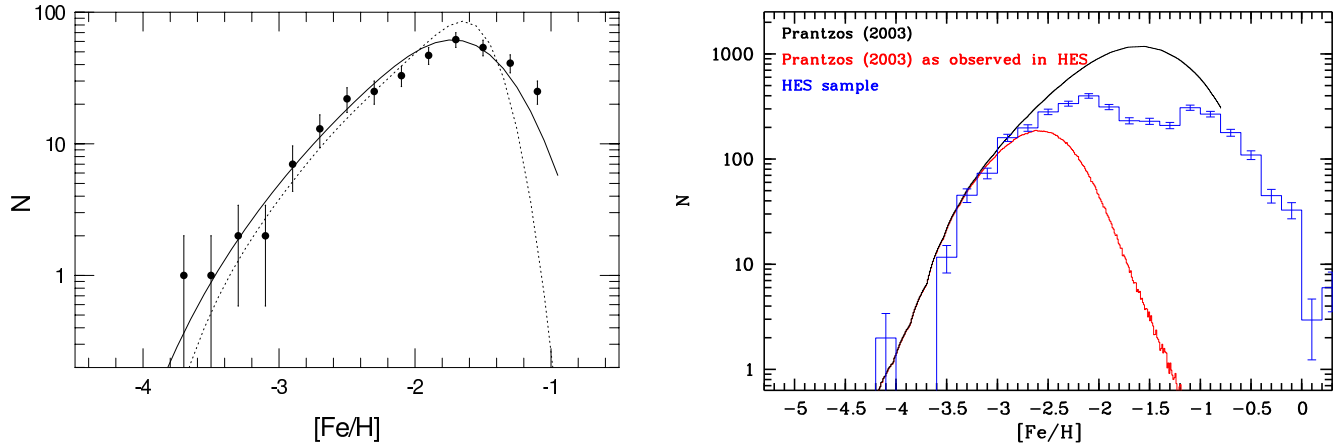


FIG. 8.— Left: comparison of the MDF of the kinematically selected halo main-sequence dwarf sample of Ryan & Norris (1991b) with the simple model (dotted line) of Hartwick (1976) and the more realistic supernova-induced star-formation model (solid line) of Tsujimoto et al. (1999). (The figure comes from Tsujimoto et al. 1999.) Right: MDF of the spectroscopically chosen halo giant sample of Schörck et al. (2009) in comparison with the GCE model of Prantzos (2003). Note the large correction necessary to modify the model (the upper continuous line) for the abundance incompleteness caused by the spectroscopic selection function (the lower continuous line) (from Schörck et al. 2009).

cal evolution. Examination of Figure 9 also shows that in the faintest of the dwarf systems ($M_{V, \text{total}} \lesssim -7$) there is a large fraction of stars with $[\text{Fe}/\text{H}] < -3.0$, suggesting a relationship between ultra-faint dwarf galaxies and the most metal-poor stars in the Milky Way halo. This topic will be further addressed in Section 4.3.2, but it is worth noting here that an essential difference between the Milky Way’s globular clusters and dSph systems is that (for objects with integrated magnitudes $M_{V, \text{total}} \gtrsim -10$) the dSphs are embedded in dark matter halos (with $M/L_V \sim 10 - 10^4$ in solar units), while almost all clusters contain relatively little or no dark matter ($M/L_V \lesssim 5$). This is almost certainly the essential difference behind the large $[\text{Fe}/\text{H}]$ dispersions observed in the dSph systems, but absent from the globular clusters.

3.2.2. Relative Abundances

Just as $[\text{Fe}/\text{H}]$ is adopted as proxy for a star’s overall metallicity, the abundances of the other elements are most often expressed relative to Fe, i.e., as $[X/\text{Fe}]$ for element X. (This is a somewhat arbitrary definition, driven by the practicality of the richness of the FeI spectrum, and from time-to-time the implications of adopting an alternative element as reference is investigated. For an example of this see Cayrel et al. (2004).) Element abundances are thus directly related to the element that represents the end stage of stellar evolution and provides a good indicator of core-collapse SN nucleosynthesis. Note that all such (relative) abundances are relative not only to Fe, but also to the abundances measured for the Sun (the bracket notation). This should be kept in mind when “reading” the chemical relative abundance trends in metal-poor stars in terms of Galactic chemical evolution.

To give the reader a feeling for the scope of the observed trends, Figure 11 shows the 1D/LTE relative abundances for metal-poor Galactic halo red giants from the work of Cayrel et al. (2004), Spite et al. (2005), and François et al. (2007), which covers the range $-4.5 < [\text{Fe}/\text{H}] < -2.0$, and is regarded by many as the “gold stan-

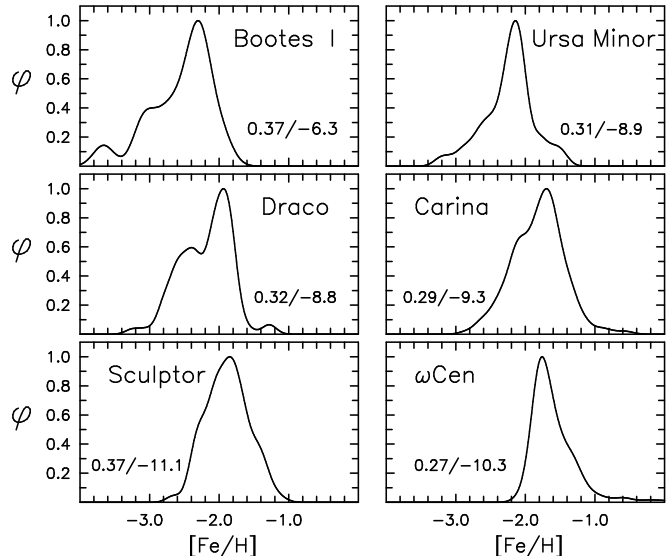


FIG. 9.— The Metallicity Distribution Functions for five Milky Way dwarf galaxies and the globular cluster ω Centauri. Also shown in each panel are $\sigma[\text{Fe}/\text{H}]/M_{V, \text{total}}$ (the dispersion in $[\text{Fe}/\text{H}]$ and the integrated absolute visual magnitude of the system). See Norris et al. (2010b) for source material. (The histograms were generated with gaussian kernels having $\sigma = 0.10 - 0.15$ dex.)

ard” of the state-of-the-art for this type of work. The reader should note that the scale in 16 of the 18 panels of Figure 11 is the same, with a range in $[X/\text{Fe}]$ of 2 dex. For the remaining two cases ($[\text{Sr}/\text{Fe}]$ and $[\text{Ba}/\text{Fe}]$) this is insufficient to cover the range in the early Universe, and for these the relevant panel range is 5 dex! The dotted lines in the figure correspond to the solar value. The solid lines in the panels of sodium through zinc represent the regression lines of Cayrel et al. (2004); for these elements these authors report errors of measurement $\sigma \sim 0.05 - 0.10$ dex, and dispersions about the regressions of $1 - 2\sigma$. Also shown, at the bottom right of each panel, are indica-

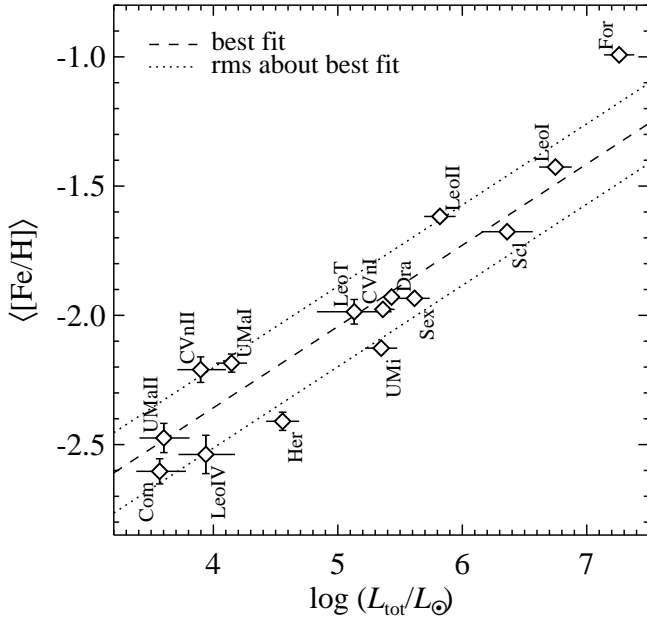


FIG. 10.— Mean $[Fe/H]$ vs. luminosity for the Milky Way’s dwarf spheroidal galaxies. Systems with $L_V \leq 10^5 L_{\odot}$ are designated “ultra-faint” dwarf galaxies, since they are fainter than the long-known “classical” dwarf galaxies. It is very likely, however, that there exists a continuous transition between the physical properties of the two groups. (Prepared by E. N. Kirby using data from Kirby et al. 2008, and references therein.)

tive 3D/non-LTE corrections for stars with $[Fe/H] \sim -3.0$ that have been gleaned from Asplund (2005) and other sources in the literature (such as the works of S. M. Andrievsky, D. Baumüller, M. Bergemann, D. V. Ivanova, L. Mashonkina, and co-workers).

By way of introduction to what follows, several aspects of the figure are highlighted.

- The large spreads in C, N, Sr, and Ba are real and tell us much about internal mixing during red giant evolution (C and N: Section 4.2.1), and the processes that produce the heavy neutron-capture elements (Sr and Ba: Section 4.2.2).
- Systematic enhancements of the α -elements Mg, Si, Ca, and (partially) Ti, lead to an explanation involving SNe of Type Ia and II, operating at different times (Sections 4.2.1 and 4.3.2).
- Tight solar-like correlations, such of those of the iron-peak elements Sc and Ni, suggest a close relationship between the production mechanisms of some of the iron-peak elements, indicative of processes similar to those responsible for the enrichment of the Sun.
- In contrast to the previous point, the trends shown by iron-peak elements such as Cr, Mn, and Co cast doubt on the previous suggestion. This “contradiction” is indicative perhaps of differences related to the location of the mass-cut radius within the progenitor of the SN explosion (above which all material is expelled) or to non-LTE effects (Section 4.2.1).

- Large corrections to some of the 1D/LTE abundances are clearly necessary to take into account 3D effects and a more realistic treatment of non-LTE before they may be closely and reliably compared with the prediction of stellar evolution and GCE computations.

4. THE CHEMICAL EVOLUTION OF THE UNIVERSE

4.1. Relics of the Big Bang

According to Standard Big Bang Nucleosynthesis (SBBN), some minutes after the singularity at the era of decoupling of radiation and matter, the only chemical elements in the Universe were hydrogen, helium and lithium. With the additional constraint of the results of the Wilkinson Microwave Anisotropy Probe (WMAP), the predicted relative mass densities of these elements are 0.75, 0.25, 2.3×10^{-9} , respectively (Spergel et al. 2007). All other elements have been produced subsequently.

4.1.1. Helium

No reliable spectroscopic determinations exist of the abundance of helium in the atmospheres of stars having $[Fe/H] < -1.0$. Most are too cool ($T_{\text{eff}} < 7000$ K) for lines of neutral helium to be currently useful for abundance analysis (see e.g., Dupree et al. 2011); and in metal-poor stars hot enough for the test to be made (the so-called blue-horizontal-branch stars), strong diffusive processes are clearly at work in their outer layers and preclude determination of the chemical abundances in the material from which they formed (Behr et al. 1999). The best estimates of primordial helium abundance based on spectral features of helium come from the analysis of helium lines in gaseous nebulae, for which Spergel et al. (2007) report a primordial helium abundance $Y_p = 0.232 - 0.258$.

4.1.2. Lithium

Spite & Spite (1982) first demonstrated that the Li abundance of metal-poor, near main-sequence-turnoff stars appears constant in the temperature range $T_{\text{eff}} = 5500 - 6250$ K, and concluded: “the abundance of lithium at the beginning of the Galaxy was: $N_{\text{Li}} = 11.2 (\pm 3.8) 10^{-11} N_{\text{H}}$ ”, i.e., $A(\text{Li}) = 2.05 \pm 0.16$. Astronomers today discuss this fundamental discovery not so much in respect of the Galaxy, to which it is certainly pertinent, but rather in terms of the Li abundance that emerged from the Big Bang.

The effect is shown in Figure 12, based on more recent observational data, where 1D/LTE values of $A(\text{Li})$ are presented as a function of T_{eff} and $[Fe/H]$. (It is noted here for completeness that the accepted temperature scale for metal-poor main-sequence stars has become some 300 K hotter since the work of Spite & Spite (1982).) One sees that the so-called Spite Plateau remains clearly defined, and as appreciated by Spite & Spite (1982), for $T_{\text{eff}} < 5900$ K on the new scale, lithium is destroyed by strong convective circulation that brings it into deeper and hotter regions. During extensive expansions on the original sample, some stars were found in which Li could not be detected. It has been suggested that these stars, which comprise only a small fraction of their parent population, have ultra-low lithium abundances as the result of phenomena related to binarity and blue stragglers, during which Li is converted into other

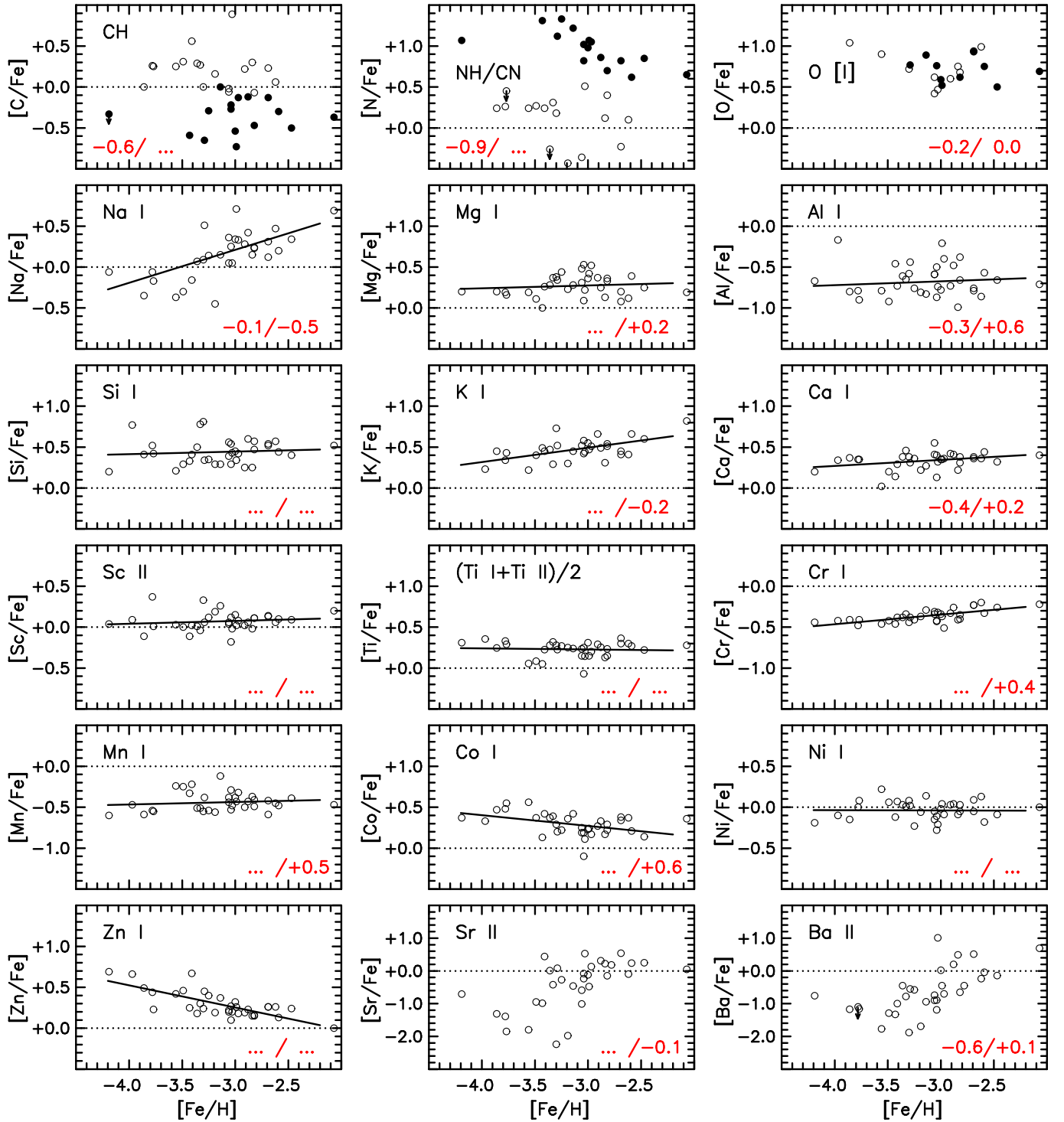


FIG. 11.— 1D/LTE relative abundances ($[X/Fe]$) vs. $[Fe/H]$ for metal-poor halo red giants from the work of Cayrel et al. (2004), Spite et al. (2005), and François et al. (2007). In the top row, filled and open circles refer to “mixed” and “unmixed” stars, respectively, as defined by Spite et al. (see Section 4.2.1). Also shown at the bottom of each panel are indicative $(3D - 1D)/(non-LTE - LTE)$, abundance differences as discussed in Section 3.1.2 (“...” indicates a potential incompleteness in our literature search or the absence of relevant information).

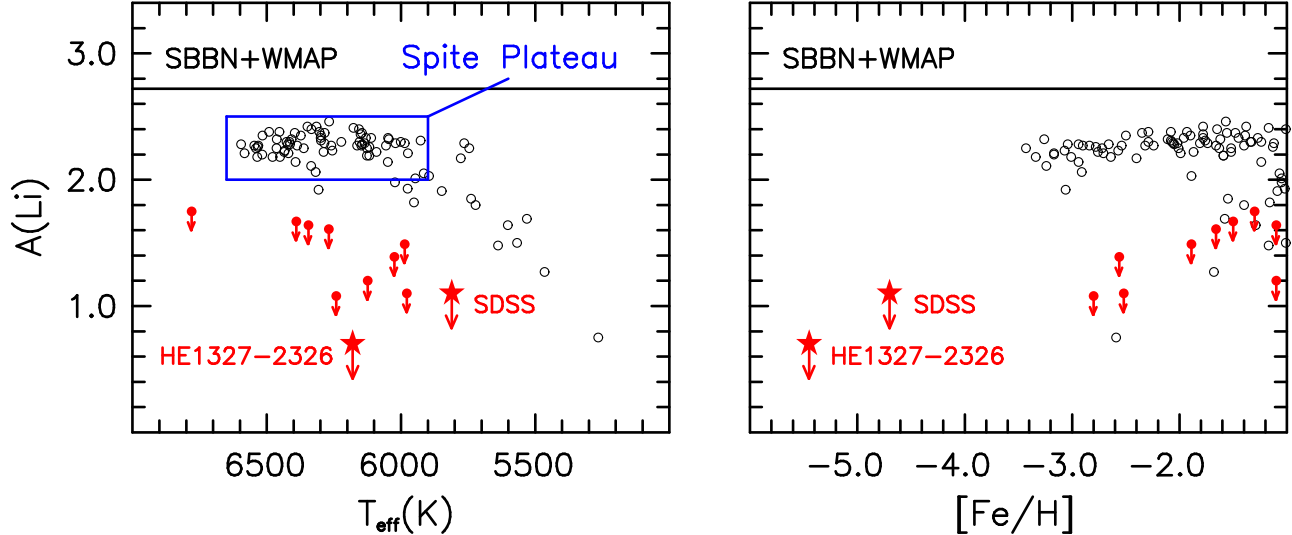


FIG. 12.— 1D/LTE lithium abundance, $A(\text{Li})$, as a function of T_{eff} (left) and $[\text{Fe}/\text{H}]$ (right), from the work of Frebel et al. (2008, HE 1327–2326) and Caffau et al. (2011, SDSS J102915+172927) (large filled stars), Meléndez et al. (2010, open circles), and Ryan et al. (2001, filled circles). The horizontal line in each panel is the value predicted from the observations by WMAP interpreted in terms of SBBN (Cyburt et al. 2008).

elements at the high temperatures experienced during convective mixing in their outer layers (see Ryan et al. 2001).

There are, however, two extremely important further points to be taken from Figure 12. The first is that, ignoring the obvious outliers, the mean abundance of the Plateau, $A(\text{Li}) = 2.28 \pm 0.01$, lies some 0.4 – 0.5 dex below the value that has been predicted from the results of WMAP, interpreted in terms of the predictions of SBBN of $A(\text{Li}) = 2.72^{+0.05}_{-0.06}$ (Cyburt et al. 2008). (Here the error in the mean abundance of the Plateau admits no slope or step as a function of T_{eff} , both of which have been claimed in the literature.)

The second point is that for the most metal-poor near-main-sequence-turnoff stars, HE 1327–2326 and SDSS J102915+172927 with $[\text{Fe}/\text{H}]_{\text{1D,LTE}} = -5.4$ and -4.7 , lithium is not detected, leading to the extremely puzzling limits of $A(\text{Li}) < 0.7$ and < 1.1 , respectively. Given that these objects have $T_{\text{eff}} = 6180\text{K}$ and 5810K , one would have expected them to lie on the Spite Plateau. (Note also that there is no evidence yet for binarity, or any other (non-abundance) peculiarity, for these stars.) This question will be addressed further in Section 6.1, where they are discussed in more detail.

Before proceeding, it should be noted that available 3D/non-LTE computations appear to be in agreement with those based on the 1D/LTE assumptions. The reader is referred to Asplund et al. (2003), who report that for two stars (with $T_{\text{eff}}/\log g/[\text{Fe}/\text{H}] = 5690/1.67/-2.50$ and $6330/2.04/-2.25$) the 3D and non-LTE corrections are both large, with absolute values of ~ 0.3 dex, but of opposite sign, which essentially cancel to yield a total correction of only ~ 0.05 dex. That is to say, 1D/LTE Li abundances are fortuitously valid.

Given the accuracy of the WMAP/SBBN prediction of the primordial Li abundance, the most widely held view seems to be that the abundance obtained from the analysis of observed Li line strengths in near-main-sequence-turnoff metal-poor stars is not the primordial

value, and that an explanation of the difference will lead to a deeper understanding of the astrophysics of stars and galaxies. The reader should consult Korn et al. (2007), Lind et al. (2009), and Meléndez et al. (2010) for recent examples of this approach, based on lithium abundances of field (Meléndez et al.) and globular cluster (Korn et al. and Lind et al.) near-main-sequence-turnoff stars. Meléndez et al. (2010) report “Models including atomic diffusion and turbulent mixing seem to reproduce the observed Li depletion ... which agrees well with current predictions from ... standard Big Bang nucleosynthesis”, while Lind et al. (2009) state “We confirm previous findings that some turbulence, with strict limits to its efficiency, is necessary for explaining the observations”. Both, on the other hand, issue a *caaveat emptor*: “We caution however that although encouraging, our results should not be viewed as proof of the ... models until the free parameters required for the stellar modeling are better understood from physical principles.” (Meléndez et al. 2010); and “However, these models fail to reproduce the behavior of Li abundances along the plateau, suggesting that a detailed understanding of the physics responsible for depletion is still lacking” (Lind et al. 2009).

4.2. The Milky Way Halo

The evolution of the chemical elements began shortly after the Big Bang, and is an ongoing process. It can be traced in detail in the Milky Way with stars of different metallicities, ranging from the most metal-deficient to the most metal-rich. Iron abundance serves as proxy not only for the overall metallicity of a star, but also for the evolutionary timescales it took to enrich the gas from which stars formed. It is not possible in most cases, however, to determine the ages of individual field stars, and what is known of Milky Way halo ages is derived from the fitting of globular cluster and field star near-main-sequence-turnoff color-magnitude diagrams to stellar evolution modeling, and nucleo-chronometry of

metal-poor field stars. (This topic is further addressed in Section 5.) As noted in Section 1.3 the present discussion is restricted principally to stars of the Galactic halo having $[\text{Fe}/\text{H}] < -1.0$. The Galactic age-metallicity relationship suggests that it took of order ~ 4 Gyr to reach this abundance (see e.g., Freeman & Bland-Hawthorn 2002). For comparison, the (one zone) galactic chemical enrichment model of Kobayashi et al. (2006) also takes ~ 4 Gyr to reach $[\text{Fe}/\text{H}] = -1.0$. The abundance trends discussed in the following thus describe the first ~ 5 Gyr of the evolution of the Milky Way – which, for the present discussion, is taken as a first approximation to the timescale for a similar enrichment of the Universe.

To understand the production of the elements and the observed trends found for metal-poor stars as a function of overall metallicity, most subsections below begin with a description of the relevant nucleosynthesis processes. Arnett (1996) and Wallerstein et al. (1997) provide general introductions to this topic. Woosley & Weaver (1995), among others, have carried out extensive core-collapse SN yield calculations to investigate the synthesis of the different isotopes during stellar evolution and subsequent supernova explosion. Progenitor masses of $11 - 40 M_{\odot}$ and different metallicities were considered. Since the details of the explosion mechanism of SNe remain largely unknown, a piston approximation (for the sudden injection of energy – the “explosion”) is employed so that the post-SN nucleosynthesis can be calculated. Fortunately, relatively few isotopes appear to be significantly affected by this uncertainty. The overall explosion energy and the “mass cut” (a specific radius above which material is ejected, rather than falling back onto the nascent black hole or neutron star) thus have significant impact on the final abundance distribution.

Mainly intermediate mass elements, with $Z \leq 30$, are produced and ejected by core-collapse supernovae. Traces of the so-called “neutron-capture” elements ($Z \gtrsim 30$) are believed to be produced by SNe and also during the asymptotic giant branch (AGB) phase of evolution of low and intermediate mass ($\sim 1 - 8 M_{\odot}$) stars. These heavier elements are about one million times less abundant than the lighter ones. Irrespective of their quantities, however, all elements play an important role in our understanding of galactic chemical evolution since each reflects the interplay of all the astrophysical processes and sites that produced the elements as they are known today.

In what follows, an unfortunately somewhat incomplete discussion is presented of many of the elements that are observed in metal-poor stars. Reasons for the incompleteness range from simple space limitations of this chapter to the fact that not all chemical elements can be observed in the relatively cool main-sequence and giant stars reviewed here.

4.2.1. The Evolution of Carbon through Zinc

Carbon, Nitrogen, Oxygen

C, N, and O are synthesized during quiescent stellar evolution, and in Type II (core-collapse) SN explosions. Carbon is produced in the triple- α process during advanced evolutionary stages such as the AGB phase. It is released into the interstellar medium during supernova explosions if the star is massive enough, or through stellar winds, if significant. Whenever the triple- α process is

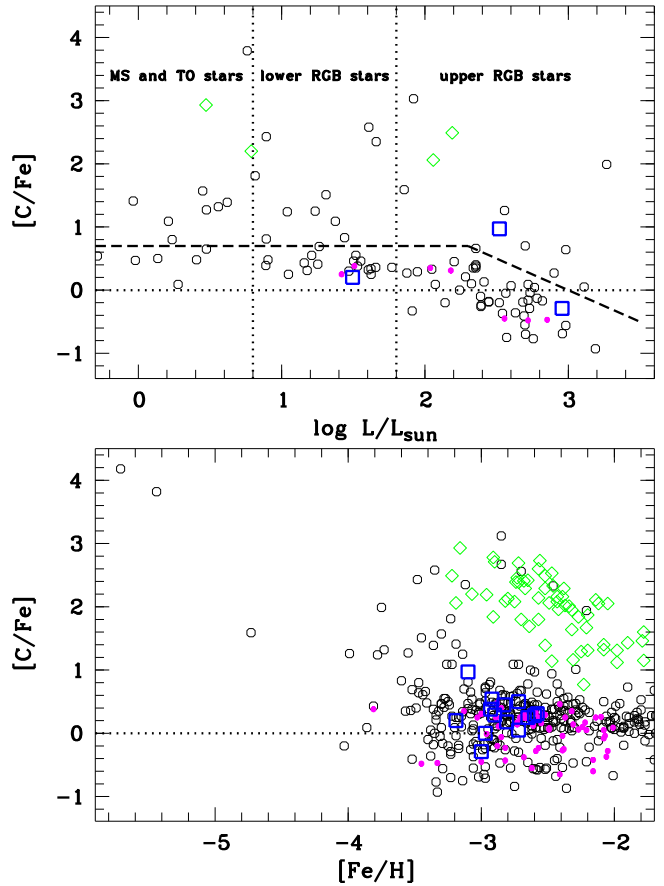


FIG. 13.— 1D/LTE $[\text{C}/\text{Fe}]$ abundances as a function of $[\text{Fe}/\text{H}]$ and luminosity (data from the Frebel 2010 compilation). In the top panel only stars with $[\text{Fe}/\text{H}] < -3.0$ are included. The definition for C-rich objects of $[\text{C}/\text{Fe}] > 0.7$ but with a luminosity dependent decline reflecting internal mixing processes is shown as a dashed line (see also Table 1). Open diamonds are used for s- and r+s-process-rich metal-poor stars, open squares refers to r-II and small filled circles to r-I r-process-rich objects, which are further discussed in Section 4.2.2.

at work, some oxygen is created as a by-product in the α -process. Hence, O can be regarded as an “ α -element” (see below), and abundance studies have shown that O does indeed exhibit this behavior in metal-poor stars (see Figure 11, top right, and the discussion below). Nitrogen is produced during H-burning in the CNO-cycle, during which C, N, and O act as catalysts. In this process, C and O abundances decrease while N increases, as the CNO-cycle approaches equilibrium. At the same time the $^{12}\text{C}/^{13}\text{C}$ ratio is driven to small values (~ 4). The production of nitrogen can be increased by stellar rotation: fast rotating, massive Population III stars (Meynet et al. 2006) may, for example, have been significant producers of the first enrichments in CNO elements.

In metal-poor stars, the abundances of each of C, N, and O can be determined from observations of their hydrides – the G-band of CH at $\sim 4300 \text{ \AA}$, the near-UV NH feature at 3360 \AA , and the UV features of OH at 3100 \AA . CN and/or C_2 bands can also provide constraints at optical wavelengths. The point that must be repeated here is that (as noted in Section 3.2.2) 1D/LTE abun-

dances determined from CH and NH may overestimate C and N abundances by up to ~ 0.7 dex. Atomic features of CI at $\sim 9070 \text{ \AA}$, together with the forbidden OI line at 6300 \AA and the OI triplet at $\sim 7770 \text{ \AA}$, provide other important constraints on the abundances of these elements. The three diagnostics involving oxygen yield different 1D/LTE abundances, driven by 3D and non-LTE effects. Again, the reader should consult Asplund (2005) for a thorough discussion of the problem: suffice it here to say that only for the forbidden OI line are the 1D/LTE abundances relatively unaffected. Recent results, taking into account various abundance corrections (e.g., Fabbian et al. 2009), indicate relatively small variation of $[\text{O}/\text{Fe}]$ as a function of $[\text{Fe}/\text{H}]$ in metal-poor stars.

Evolutionary mixing effects also modify initial surface abundances. Dredge-up events and mixing bring nuclei from interior layers to the surface, including CNO-processed material. The surface abundances of heavier elements are not affected by these mixing processes and their relative fractions remain unchanged. The effect is shown in Figure 11 where one sees a clear anticorrelation between C and N in “mixed” stars (filled circles; $[\text{C}/\text{Fe}] < 0.0$ and $[\text{N}/\text{Fe}] > +0.5$) and “unmixed” stars (open circles; $[\text{C}/\text{Fe}] \geq 0.0$ and $[\text{N}/\text{Fe}] < +0.5$), as defined by Spite et al. (2005). These mixing effects are observed in metal-poor stars with increasing luminosity on the upper RGB, as illustrated in the upper panel of Figure 13, where only stars with $[\text{Fe}/\text{H}] < -3.0$ are shown. A downturn of the $[\text{C}/\text{Fe}]$ ratio can be clearly seen at luminosity $\log L/L_{\odot} > 2$. When studying the CNO group, stellar evolutionary status must therefore be taken into account.

Many metal-poor stars show C abundances well in excess of the general carbon trend set by most Population II stars (and unrelated to abundance changes due to mixing) at all metallicities. Such “extra” C must have come either from additional sources that enriched the material from which the star formed or from enriched material that was added to the star at a later time. Carbon measurements in metal-poor stars thus provide important information on the various previous enrichment events and the nature of the first stars. The lower panel of Figure 13 shows $[\text{C}/\text{Fe}]$ as a function of $[\text{Fe}/\text{H}]$ for a large sample of metal-poor stars. The separation of stars with large carbon overabundances from those with more “normal” values is clearly seen. These **C**ar**bon E**nriched **M**etal **P**oor stars are referred to as CEMP stars, a significant fraction of which have $[\text{Fe}/\text{H}] > -3.0$ and inherited their carbon from a binary companion star through a mass transfer event. This type of enrichment is further discussed in Section 4.2.2. The origin of the carbon richness for the majority of stars with $[\text{Fe}/\text{H}] < -3.0$ remains the topic of intense interest, which is also described in Section 6.1.

α -Elements

The α -elements (Mg, Ca, Si, Ti) are built from multiples of He nuclei via α -capture during various stages of stellar evolution (carbon burning, neon burning, complete and incomplete Si burning). Although Ti ($Z = 22$) is not a true α -element, in metal-poor stars the dominant isotope is ^{48}Ti , which behaves like one. Produced in massive stars, these α -element nuclei are then dispersed during subsequent SN explosions. Abundance studies have shown that the majority of metal-poor stars

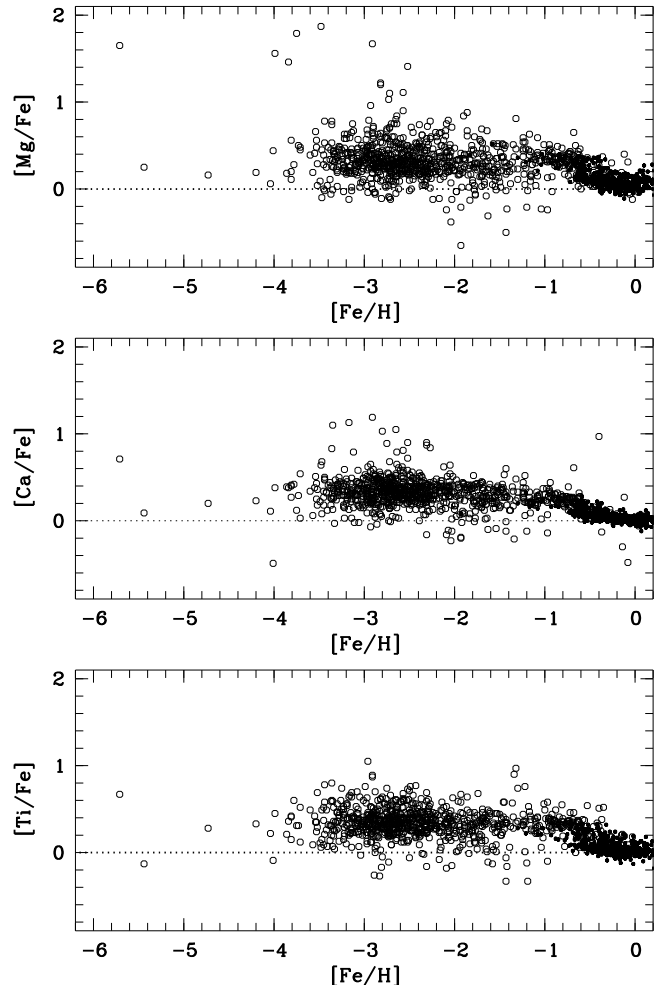


FIG. 14.— 1D/LTE α -element ratios $[\text{Mg}/\text{Fe}]$, $[\text{Ca}/\text{Fe}]$, and $[\text{Ti}/\text{Fe}]$ as a function of $[\text{Fe}/\text{H}]$. Open circles denote halo stars from the compilation of Frebel (2010). Small dots are more metal-rich thin and thick disk stars from the Venn et al. (2004) compilation. At $[\text{Fe}/\text{H}] > -1.0$, all three element ratios decrease with respect to the average halo value of $[\alpha/\text{Fe}] \sim 0.4$. This is due to the onset of SNe Ia, which contribute relatively high Fe to the chemical enrichment of the Galaxy. By $[\text{Fe}/\text{H}] \sim 0.0$, the solar ratio of $[\alpha/\text{Fe}]$ is reached.

with $[\text{Fe}/\text{H}] < -1.0$ show an enhanced $[\alpha/\text{Fe}]$ ratio compared with the solar value. Figure 14 illustrates that below this value $[\alpha/\text{Fe}]$ plateaus at ~ 0.4 due to the correlated production and release of α -elements and Fe. This characteristic overabundance in halo stars reflects an enrichment by core-collapse SNe in the early Universe. At later times (roughly 1 Gyr after the Big Bang), once the first lower-mass stars reached the end of their lifetimes, SNIa explosions began to dominate the production of Fe. The main yield of SNIa is C, O, and Fe-peak elements. This change in Fe producers can be seen in the abundance trends of metal-poor stars. Above metallicities of $[\text{Fe}/\text{H}] \sim -1.0$, the onset of SNIa and their Fe contribution to the chemical evolution of the Milky Way manifests itself in a pronounced decrease of the stellar $[\alpha/\text{Fe}]$ values (e.g., Ryan et al. 1996) until $[\alpha/\text{Fe}] = 0.0$ is reached at $[\text{Fe}/\text{H}] = 0.0$.

There are important exceptions to this generalization.

Some metal-poor stars show large Mg and Si abundances possibly due to unusual supernova explosions and associated nucleosynthesis processes (Aoki et al. 2002; Frebel et al. 2005). Others, as will be discussed in Sections 4.3.2 and 6.2, exhibit lower values, driven by the different star formation rates and different relative α /Fe contributions from Type II and Type Ia supernovae.

The α -elements also serve to highlight a further potentially important role of relative abundances as a function of $[\text{Fe}/\text{H}]$. Because the abundance of a given element contains the history of all the SNe that have contributed to the cloud from which a star forms, the dispersion of observed relative abundances contains potentially strong constraints on the relative yields of SNe, the stellar mass function, and the efficiency with which the ejecta of SNe have been mixed with the existing ISM. Several authors have emphasized the small values of the dispersion in $[\text{Mg}/\text{Fe}]$ ($\sim 0.06 - 0.10$ dex) in homogeneously selected and analyzed halo samples, which lead to interesting restrictions on the above possibilities.

Iron-peak Elements

In the early Universe, the iron-peak elements (V to Zn ; $23 \leq Z \leq 30$) were synthesized during the final evolution of massive stars, in a host of different nucleosynthetic processes before and during core-collapse SN explosions. These include direct synthesis in explosive burning stages (explosive oxygen and neon burning, and complete and incomplete explosive Si burning), radioactive decay of heavier nuclei or neutron-capture onto lower-mass Fe-peak elements during helium and later burning stages, and α -rich freeze-out processes.

In Figure 15, 1D/LTE relative abundances, $[\text{Sc}/\text{Fe}]$, $[\text{Cr}/\text{Fe}]$, and $[\text{Co}/\text{Fe}]$ are presented as a function of $[\text{Fe}/\text{H}]$, which demonstrate quite different behavior as $[\text{Fe}/\text{H}]$ increases. Figure 11 also presents data for other Fe-peak elements (Mn, Ni, and Zn) on the range $-4.0 \lesssim [\text{Fe}/\text{H}] \lesssim -2.5$. The abundance trends of Cr and Mn have a pronounced positive slope: their abundances at the lowest metallicities are subsolar ($[\text{Cr}, \text{Mn}/\text{Fe}] \sim -0.5$ at $[\text{Fe}/\text{H}] \sim -3.5$), becoming solar-like at $[\text{Fe}/\text{H}] \sim -1.0$. In contradistinction, the Co and Zn abundance trends are in the opposite sense. Their abundances decrease from $[\text{Co}, \text{Zn}/\text{Fe}] \sim +0.5$ at $[\text{Fe}/\text{H}] \sim -3.5$, to roughly solar values at higher metallicities ($[\text{Fe}/\text{H}] \sim -1.0$). Finally, Sc and Ni remain relatively unchanged with respect to $[\text{Fe}/\text{H}]$.

Investigations of these very different behaviors have involved two essentially different approaches. The first was to consider whether they could be explained in terms of the explosion energy and position of the mass-cut of core-collapse SN models (see Umeda & Nomoto 2005 and references therein), which has been only partially successful, and to which the reader is referred. Second, in the context of non-LTE effects, Bergemann and co-workers (e.g., Bergemann et al. 2010) have reported that for each of Cr I, Mn I, and Co I, abundance differences (in the sense $\Delta[\text{X}/\text{Fe}](\text{non-LTE} - \text{LTE})$), are small at high abundance and increase to $\sim +0.4$ to $+0.6$ at $[\text{Fe}/\text{H}] \sim -3.0$. Consideration of Figures 11 and 15 shows that while this acts to remove the downward trends for $[\text{Cr I}/\text{Fe}]$ and $[\text{Mn}/\text{Fe}]$ (and consistency then with $[\text{Cr II}/\text{Fe}]$ results), it exacerbates the upward behavior observed for $[\text{Co}/\text{Fe}]$, leading to an excess of 1 dex above the solar value at $[\text{Fe}/\text{H}] =$

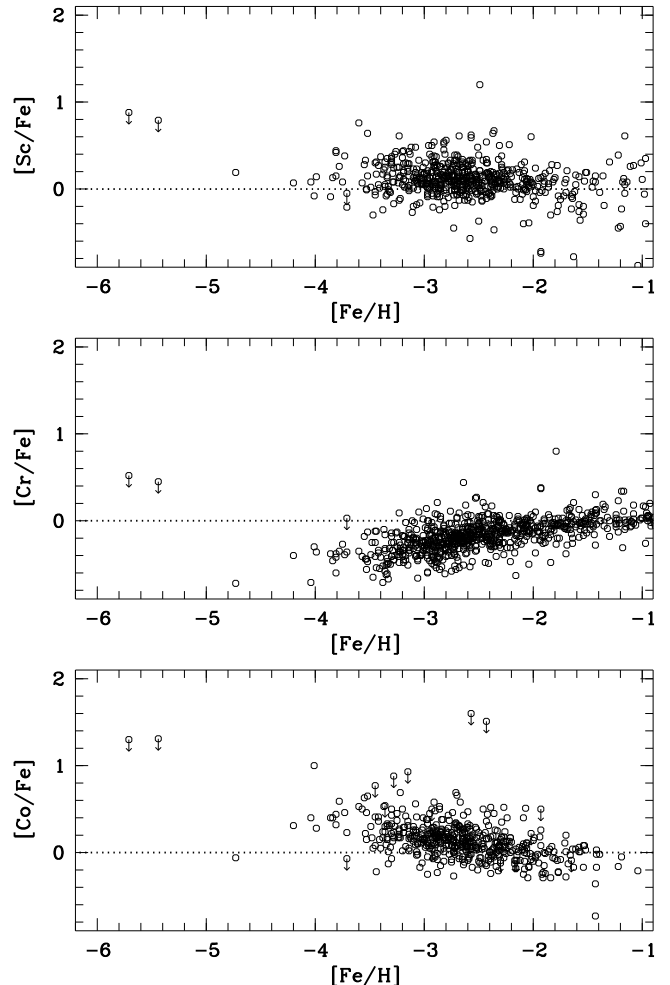


FIG. 15.— 1D/LTE Fe-peak relative abundances $[\text{Sc}/\text{Fe}]$, $[\text{Cr}/\text{Fe}]$, and $[\text{Co}/\text{Fe}]$ vs. $[\text{Fe}/\text{H}]$ (data from the compilation of Frebel 2010). See text for discussion.

-3.5 – providing an even larger challenge for an understanding of this abundance ratio.

4.2.2. The Evolution of Neutron-Capture Elements

Only elements up to zinc can be synthesized via nuclear fusion. Most heavier elements are built up by the slow neutron capture process, the s -process, and the rapid neutron capture process, the r -process (e.g., Meyer 1994 and references therein). The s -process operates under conditions of relatively low neutron densities ($n_n \sim 10^7$ neutrons cm^{-3}). In this regime the timescale for neutron capture is slower, in general, than the β -decay rate of unstable isotopes. In contradistinction, when an extremely strong neutron flux is present, the r -process occurs on timescales of only a few seconds so that neutron-capture takes place within the β -decay rates of the newly created unstable isotopes. The majority of elements with $Z > 30$ can be produced by either the s - or r -process and it is not trivial to disentangle the different production mechanisms. Metal-poor stars offer an opportunity to obtain “clean” nucleosynthetic signatures of each process, as will be described in this section. This opportunity provides unparalleled insight into the details of nucleosynthesis in

the early Universe and the onset of chemical evolution of the heaviest elements.

s-process

s-process nuclei are produced in the interiors of low and intermediate-mass AGB stars and in the He- and C-burning phases of massive stars. On timescales longer than that of a β -decay, neutrons are added to a seed nucleus (i.e., Fe) to build up heavier, stable nuclei. When neutron-capture creates a radioactive isotope, it will in general decay to its stable daughter isotope before capturing another neutron. In this way, nuclei along the “valley of β -stability” are created. The overall extent to which heavier and heavier isotopes are made is determined by the strength of the neutron flux and the timescale over which it operates. This is known as the time-integrated neutron-flux or neutron-exposure. As a consequence, the *s*-process is more efficient in low metallicity AGB stars due to a relatively larger ratio of neutrons to Fe seeds owing to the primary nature of the neutron source. In massive stars, however, the efficiency of the *s*-process strongly depends on whether the neutron source is of primary or secondary nature, and may depend on stellar rotation.

About half of the isotopes of the elements heavier than iron can be created through the *s*-process. Nuclei with atomic numbers that are equivalent to the magic numbers of neutrons, $A = 90$ ($N = 50$), $A = 140$ ($N = 82$), $A = 208$ ($N = 126$), are produced in larger quantities owing to their small neutron-capture cross-sections. (Here and in what follows, A refers to the mass number, Z to the atomic number, and N to the neutron number of a nucleus.) This results in three so-called “*s*-process peaks” that make up a distinct neutron-capture abundance signature. The first peak is located at Sr, Y, and Zr, the second at Ba, La, and Ce, and the third occurs at the end point of the *s*-process, Pb and Bi. For the Sun, the *s*-process component can be calculated, and subtracted from the total neutron-capture pattern to obtain the *r*-process contribution. Figure 16 shows the neutron-capture abundance distributions of both the *s*- and *r*-process. The *s*-process peaks are clearly seen, as well as the relative contributions of each process to a given element.

Overall, the *s*-process is rather well understood theoretically, even though there remain uncertainties with regard to the modeling of the amount of ^{13}C that acts as a major neutron source and other reaction rates associated with it (e.g., Arlandini et al. 1999; Sneden et al. 2008). The “main” component of the *s*-process occurs in the helium shells of thermally pulsing lower mass AGB stars and is believed to account for elements with $Z \geq 40$. Examples of *s*-process yields obtained from models of AGB stars with masses of 1 to $6 M_{\odot}$ and different metallicities can be found in Karakas & Lattanzio (2007).

The main neutron sources are α -captures on ^{13}C and ^{22}Ne nuclei. The former creates a low neutron density of $n_n \sim 10^7$ neutrons cm^{-3} , whereas the latter can provide a burst of neutrons with fluxes up to $n_n \sim 10^{13}$ neutrons cm^{-3} during convective thermal pulses. The concentration of ^{13}C and the low reaction rate at the temperatures under which the $^{13}\text{C}(\alpha, n)^{16}\text{O}$ reaction occurs in the He-shell maintain the *s*-process for thousands of years. Moreover, the repeated exposure of the He-shell to

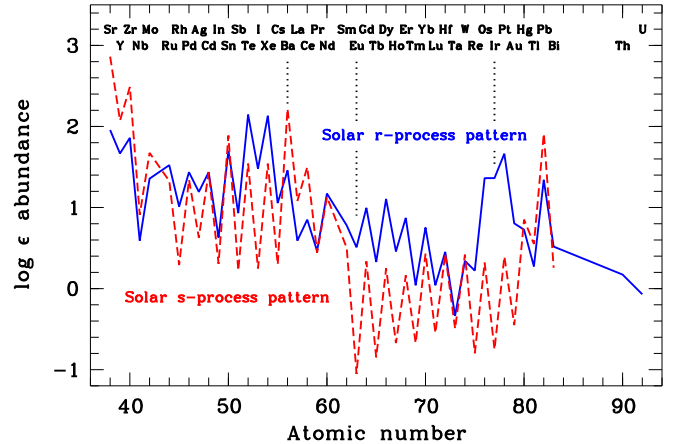


Fig. 16.— Solar *s*- and *r*-process patterns (dashed and full lines, respectively) (data from Burris et al. 2000). After billions of years of chemical evolution, the different contributions of the *s*- and *r*-processes are clearly seen. Sr and Ba are predominantly produced in the *s*-process, whereas Eu, Os, Ir and Pt originate mainly in the *r*-process. (The vertical dotted lines have been added to facilitate identification of Ba, Eu, and Ir.).

neutron fluxes is important for forming the heaviest elements in AGB stars. On the contrary, the $^{22}\text{Ne}(\alpha, n)^{25}\text{Mg}$ source has a timescale of only ~ 10 years. During the final stages of AGB evolution, *s*-process material is dispersed by stellar winds.

The so-called “weak” component of the *s*-process occurs in the He- and C-burning cores of more massive stars of roughly solar metallicity, and preferentially produces elements around $Z \sim 40$. These stars are just massive enough (perhaps around $8 M_{\odot}$) to eventually explode as core-collapse SNe during which the *s*-process material is ejected into the ISM. Regardless of the mass range, the AGB phase includes a series of dredge-up episodes that transport the newly created material to the surface. Through stellar winds, the ISM is immediately enriched with *s*-process elements, making AGB stars significant contributors to Galactic chemical evolution.

Given that many stars occur in binary systems, a common scenario is mass transfer during which *s*-process elements are transferred to a lower mass companion. This fortuitously provides an indirect method of studying a clean AGB nucleosynthesis signature. The process occurs not only in the early Universe, but also among higher metallicity stars. The so-called “Ba-stars” are the “receiver” stars within Population I binaries and the “CH stars” those within mild Population II systems. The characteristic *s*-process signature seen above in Figure 16 has been observed in many metal-poor stars as the result of a more massive companion going through the AGB phase and transferring some material onto its companion (e.g., Aoki et al. 2001). In Figure 17, abundances for several *s*-process-enhanced stars are shown in comparison with the scaled solar *s*-process pattern. (One should recall here that an abundance definition that classifies stars as *s*-process-rich is given in Table 1.) As may be seen in the figure, there is good agreement between the scaled solar pattern and the stellar abundances. (It should be remarked in passing that the relatively poor agreement

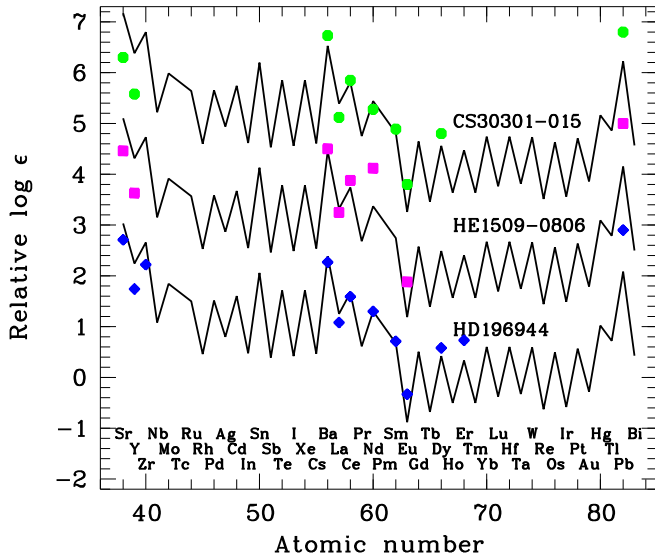


FIG. 17.— 1D/LTE abundances of s-process-enhanced metal-poor stars compared with the scaled solar s-process pattern. See text for discussion.

for Pb results from a significant underproduction of Pb in earlier s-process solar models, such as the one presented in Figure 17 (R. Gallino, private communication). Correspondingly, the scaled-solar r-process Pb predictions are too high. There remain disagreements, however, between the observed Pb abundances and the model predictions, suggesting that either our understanding of these processes is still rather limited or that there are systematic uncertainties in the abundance determinations, or both.)

This agreement is remarkable given the fact that the solar neutron-capture material is a product of ~ 8 Gyr of integrated chemical evolution, whereas the halo stars received these elements directly from one of the AGB stars that made s-process elements early in the Universe. Overall, the abundance match indicates a solid theoretical understanding of the s-process. This is also demonstrated by a small number of s-process stars that show extremely large enhancements of Pb, as predicted for third peak-elements (see Sneden et al. 2008). Additionally, since carbon is also produced during the AGB phase, the mass transfer usually includes large amounts of carbon. (s-process-enhanced stars are marked as such in Figure 13, with diamond symbols, to illustrate this point.) Most importantly, it should be kept in mind that the carbon excess in these stars is dominated by an extrinsic source and not representative of the intrinsic carbon abundance of the stars’ birth cloud. Finally, note that despite the mass transfer, the s-process-enhanced metal-poor stars exhibit lighter element ($Z < 30$) abundance patterns that are the same as those of other normal metal-poor halo stars. One exception is fluorine which, if significantly enhanced, is a signature of low-mass AGB pollution together with usual s-process-element and carbon-enhancement.

The evolution of representative neutron-capture elements as a function of $[\text{Fe}/\text{H}]$ is shown in Figure 18. Sr and Ba are predominantly produced in the s-process (89% and 85% in the Sun, respectively); see Burris et al. (2000) for details. Since the first lower mass stars in the

Universe reached their AGB phase ~ 1 Gyr after the Big Bang, s-process enrichment occurs with some delay with respect to core-collapse SN enrichment. This is indeed as observed: at a metallicity of $[\text{Fe}/\text{H}] \sim -2.6$, the s-process is in full operation, including significant neutron-capture element “pollution” of the Galaxy by AGB stars (Simmerer et al. 2004), as can be seen in the top panels of Figure 18. Metal-poor stars with an obvious s-process signature from a mass transfer event are also carbon-rich. At these and higher metallicities, all stars thus formed from gas that was intrinsically enriched in s-process elements, irrespective of whether or not they received extra s-process material from a companion. As can be seen in the bottom panels of the figure, there is a main branch in the $[\text{Ba}/\text{Fe}]$ vs. $[\text{Fe}/\text{H}]$ plane. Above $[\text{Fe}/\text{H}] \sim -2.6$, it is dominated by stars formed from AGB enriched gas.

There are some exceptions with respect to clean s-process signatures in metal-poor stars. A handful of objects display a mixed abundance signature originating from both the s- and the r-process (see e.g., Jonsell et al. 2006 for an extensive discussion on the origin of s-/r-mixtures observed in metal-poor stars). This includes some stars with $[\text{Fe}/\text{H}] < -2.6$, and their unusual chemical patterns are perhaps due to earlier more massive stars expelling some s-process elements when they exploded as core-collapse SNe. Several different scenarios have been invoked to explain the combination of the two neutron-capture processes originating at two very different astrophysical sites. No completely satisfactory explanation, however, has yet been found.

r-process

Heavy elements are also produced in the rapid (r-) process, which takes place over just a few seconds. Seed nuclei (e.g., C or Fe) are bombarded with neutrons ($\sim 10^{22}$ neutrons $\text{cm}^{-2} \text{sec}^{-1}$) to quickly form large radioactive nuclei far from stability. After the strong neutron flux ceases, the nuclei decay to form stable, neutron-rich isotopes. The r-process does not, however, produce infinitely large nuclei because of a significant decrease in the cross sections of neutron-capture nuclei with closed neutron shells. Other unfavorable reaction rates and problems with nuclear stability in the heavy-isotope region also play a role. These factors eventually terminate the r-process at nuclei around $A = 270$, far in the trans-uranium regime. Those nuclei all decay to eventually become Pb. Approximately half of the neutron-capture isotopes heavier than iron are produced in this way, including the heaviest, long-lived radioactive elements thorium and uranium.

The r-process also manifests itself in a characteristic abundance pattern, showing three large peaks at elements with $A \sim 80$ ($Z \sim 33$; Se-Br-Kr), $A \sim 130$ ($Z \sim 52$; Te-I-Xe) and $A \sim 195$ ($Z \sim 77$; Os-Ir-Pt), similar to the s-process peaks. The latter two of these may be seen in Figure 16. The peaks form because nuclei with closed neutron shells only reluctantly capture any neutrons (i.e., they have extremely small cross-sections). With their long β -decay lifetimes, they act as bottlenecks to additional neutron-captures creating even heavier nuclei. Hence, nuclei with atomic masses at or just below the closed-shell nuclei pile up during the process.

Unlike the situation for the s-process, the astrophysical site(s) that provide the extreme neutron fluxes required

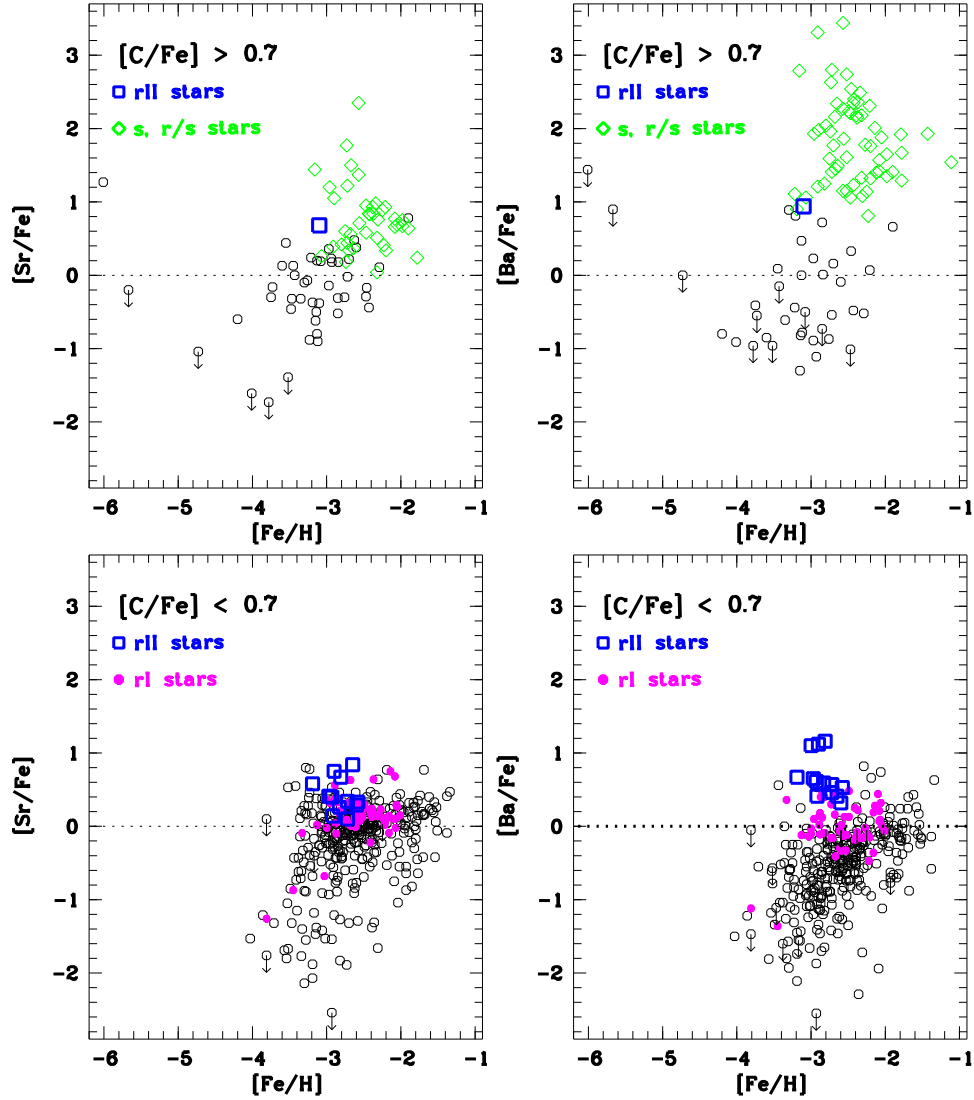


FIG. 18.— 1D/LTE neutron-capture element abundances ratios $[\text{Sr}/\text{Fe}]$ and $[\text{Ba}/\text{Fe}]$ as a function of $[\text{Fe}/\text{H}]$ for carbon-enhanced objects ($[\text{C}/\text{Fe}] \geq 0.7$; top panels) and other halo stars (bottom panels). The range in $[\text{Sr}/\text{Ba}]$ and $[\text{Ba}/\text{Fe}]$ is much larger than uncertainties or systemic differences between individual studies, indicating a cosmic origin. Below $[\text{Fe}/\text{H}] \sim -3.0$, the evolution is dominated by r-process enrichment. For $[\text{Fe}/\text{H}] \gtrsim -2.6$, the s-process significantly contributes neutron-capture material (see Simmerer et al. 2004). Arrows indicate upper limits, while the solar ratio is indicated by dotted lines.

for the r-process have not yet been identified. Neutron-star mergers have been considered, but their long evolutionary timescale prior to merging argues against them being the primary r-process site in the early Galaxy. Neutrino-driven winds emerging from the formation of a neutron-star during a core-collapse SN explosion are more promising locations (Qian & Wasserburg 2003). Since massive SNe dominate chemical enrichment in the early Universe (e.g., as documented through the α -element enhancement found in halo stars), the neutrino-driven wind model agrees naturally with such an early SN enrichment mode.

In order to learn about the details of the r-process and its site, it is of great importance to obtain actual data of a “clean” r-process signature. The best candidates for this are the r-II stars (see Table 1 for definitions), the most strongly r-process-enhanced objects,

which comprise about 5% of stars with $[\text{Fe}/\text{H}] \lesssim -2.5$ (see Barklem et al. 2005). All but one of the r-II stars have metallicities close to $[\text{Fe}/\text{H}] = -3.0$, with the outlier having an even lower $[\text{Fe}/\text{H}]$. The metallicities are thus distinctly lower than the value of $[\text{Fe}/\text{H}] = -2.6$ discussed above as corresponding to the onset for AGB s-process enrichment. (It should be recalled that mildly enriched r-I stars are found up to metallicities of $[\text{Fe}/\text{H}] \sim -2.0$; while at higher values, the signature becomes less clean since the more metal-rich star would have formed from material already significantly enriched in r-process elements.) This suggests that the r-process enhancement comes from stars slightly more massive than those that experience the s-process during AGB evolution.

The “main” r-process operates in the full range of neutron-capture elements, up to $Z = 92$. Model calculations have shown that it probably only occurs in

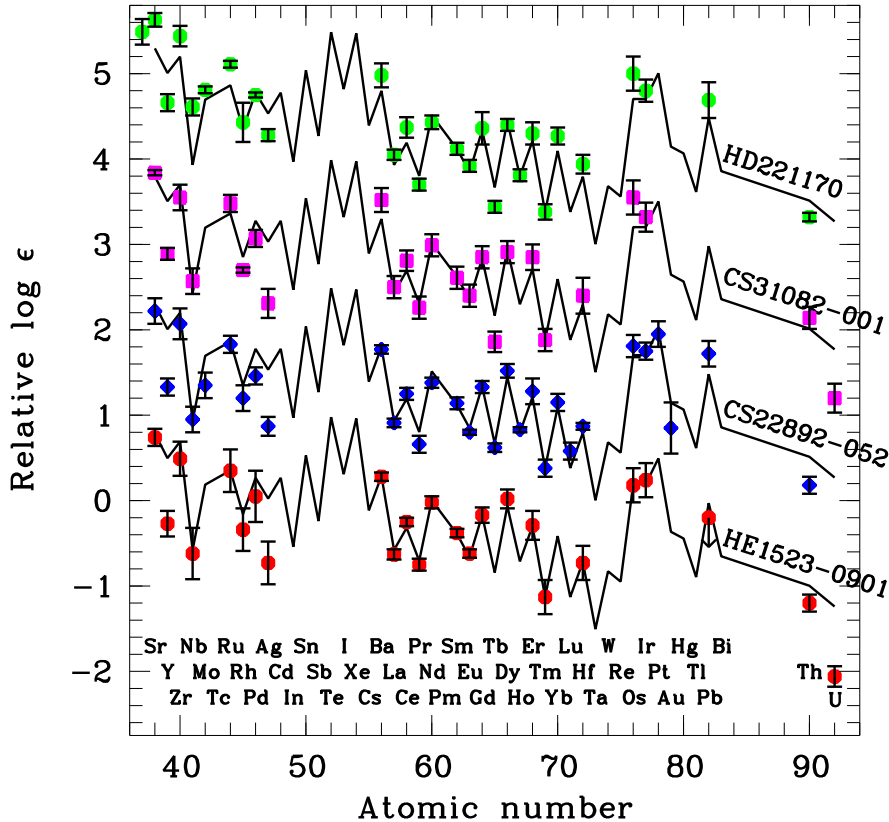


FIG. 19.— 1D/LTE abundances in r-process-enhanced metal-poor stars compared with the scaled solar r-process pattern. Note the remarkable agreement for elements heavier than Ba ($Z \geq 56$).

a specific, yet unidentified type of core-collapse SN, or perhaps only in a particular mass range ($\sim 8 - 10 M_{\odot}$; Qian & Wasserburg 2003). Examination of the ratios of the heavy ($Z > 56$) neutron-capture abundances in r-process enhanced stars (e.g., Sneden et al. 1996; Hill et al. 2002; Barklem et al. 2005; Frebel et al. 2007a) shows that the abundance distribution of each closely matches that of the scaled solar r-process pattern (e.g., Burris et al. 2000). Figure 19 shows data for four well-studied r-II stars. Given that the Sun was born ~ 8 Gyr later than these otherwise ordinary metal-poor stars, this is a remarkable finding. Assuming that the r-process takes place only in core-collapse SNe, the match of the stellar and solar patterns suggests that the r-process is universal: that is, no matter when and where it happens, it always produces its elements with the same proportions. Otherwise, the integrated pattern observed in the Sun would not resemble the individual pattern found in a ~ 13 Gyr old star.

While there is excellent agreement with the scaled solar r-process pattern for elements heavier than Ba, deviations have been found among the lighter neutron-capture species. This indicates that the origin of the lighter elements is more complex, with perhaps both the “main” and “weak” r-processes contributing in different mass ranges (see, e.g., Travaglio et al. 2004). The “weak” r-process is thought to produce mainly the lighter neutron-capture elements ($Z < 56$) and little or no heavier material, such as Ba. Possibly, this occurs mainly in massive ($\gtrsim 20 M_{\odot}$) core-collapse SNe (see e.g.,

Wanajo & Ishimaru 2006). A candidate for an observed “weak” r-process signature is provided by the r-process-poor, metal-poor star HD 122563 (Honda et al. 2006), which displays a depleted, exclusively light neutron-capture-element pattern. The $[\text{Sr}/\text{Ba}]$ ratio in this and other stars can be employed to learn about the relative contributions of the two r-processes, and potentially the origin of the overall abundance pattern. In this scenario, the “main” r-process would produce lower $[\text{Sr}/\text{Ba}]$ ratios than the “weak” one.

Overall, neutron-capture elements are produced in limited amounts. Their abundances in solar system material is about 6 orders of magnitude less than those of the Fe-peak elements. Nevertheless, they provide invaluable insight into various early nucleosynthesis processes. The enormous scatter of neutron-capture abundances (e.g., $[\text{Ba}/\text{Fe}]$), as a function of $[\text{Fe}/\text{H}]$, suggests that the production of neutron-capture elements is completely decoupled from that of Fe and other elements. As described earlier, and displayed in Figures 14 and 15, the α - and Fe-peak element abundances show very little scatter, probably because the ISM was already relatively well-mixed by $[\text{Fe}/\text{H}] \sim -4.0$. As can be seen in Figure 18, especially at $[\text{Fe}/\text{H}] \sim -3.0$, there is a range of ~ 6 dex in neutron-capture abundances. This must reflect strongly varying degrees of neutron-capture yields at the earliest times, and probably also different processes contributing different groups of these elements in various amounts (for example more Sr than Ba at the very lowest metallicities). Only at somewhat higher metallicities, when the

s-process begins to dominate the neutron-capture inventory, does the bulk of the stellar abundance ratios become more solar-like.

4.3. The Milky Way Globular Clusters and Dwarf Galaxies

4.3.1. Globular Clusters

The internal relative abundance patterns of the Galactic globular clusters are distinctly different in many respects from those of the Galactic halo, and require an explanation involving poorly understood intracluster self-enrichment processes. While this is a very important field of endeavor, insofar as it lies beyond the scope of the present chapter, a comprehensive description of this topic can not be provided here. Instead, some of the main differences between the globular cluster and halo field stars are briefly highlighted.

- Most clusters are chemically homogeneous with respect to iron, at the ~ 0.03 dex level. The clear exceptions among the halo clusters are ω Centauri, M22, and M54, where ranges of $\Delta[\text{Fe}/\text{H}] \sim 0.3$ to 1.5 dex have been observed. In Figure 9 the reader can see the MDF of ω Cen, the cluster with the largest spread; a large number (~ 5) of sub-populations, with distinctly different mean $[\text{Fe}/\text{H}]$ have been identified in this system.
- All globular clusters so far studied have been found to be chemically inhomogeneous in a number of light elements that are produced or modified in nucleosynthetic (p, γ) reactions. Beginning in ~ 1970 , observations and analyses of cluster members have over time added the following elements to the list – C, N, O, Mg, Na, and Al. Strong correlations and anti-correlations exist among the abundances of these elements; and within a given cluster, sub-populations have been identified based on abundance patterns involving them. Lithium and heavy-neutron-capture element variations have also been reported that correlate with those of the above elements in some clusters. Intermediate mass AGB stars are most commonly identified as the nucleosynthesis sites responsible for these variations, together in some cases with internal mixing high on the present-day RGB.
- Finally, some (but not all) of the most massive clusters (ω Cen, NGC 2808) show multiple main sequences in the color-magnitude diagram, for which the only empirically consistent explanation yet proposed is that there are sub-populations within these systems that have distinct helium abundances in the astoundingly large range $Y \sim 0.23 - 0.35$ (Y is the helium fraction by mass). No completely satisfactory explanation has yet been given, although several authors identify massive AGB stars in an early generation of cluster stars as the prime candidate.

Various models have been proposed that are unique to the globular cluster environment and which involve a number of stellar generations that chemically enrich the material from which subsequent generations form. An

example of such a model, which also provides references to the observational material described above is provided by Conroy & Spergel (2011).

4.3.2. Dwarf Galaxies

One of the important unsolved problems in cosmology is understanding the formation of galaxies. Studying the compositions of stars in dwarf galaxies provides information on the chemical evolution of these systems. The Milky Way’s dwarf galaxy satellites, with a large range in masses and luminosities very different from those of the Milky Way itself, permit a comparison of their chemical evolution histories, which in turn provides clues to the origin and overall evolution of different types of galaxies. Specifically, the connection between the surviving dwarf systems and those believed to have been captured and dissolved to form the Milky Way halo is best addressed by examining in detail the stellar chemical abundances of present-day dwarf galaxies (see also Section 6.2 on this topic). The most metal-poor (and hence oldest) stars in a given system permit unique insight into the earliest phases of star formation. Stars born at later times (and thus with higher metallicities) contain the integrated effects of internal chemical evolution in their atmospheric compositions. (See Kirby et al. 2011 for an overview of the history and current state of simple chemical evolution models.)

Dwarf spheroidal galaxies are relatively simple systems that allow us to study, both observationally and theoretically, the basic processes that led to their origin and evolution. They are generally old, metal-poor, have no gas, and thus no longer support star formation. On the other hand, a large fraction of their mass comprises dark matter, with the least luminous of them having mass-to-light ratios of order 10^3 (in solar units). Some 25 such systems are currently known orbiting the Galaxy today (see Tolstoy et al. 2009 for a review). The ~ 10 recently discovered “ultra-faint” dwarf galaxies ($L_V \leq 10^5 L_\odot$; Martin et al. 2008) are some orders of magnitude fainter than the more luminous, “classical”, Milky Way dwarf spheroidal galaxies. As has been outlined in Section 3.2.1, all of these dwarf systems follow a (metallicity, luminosity)–relationship, with the classical dwarfs being on average more metal-rich and containing more stars than their less luminous ultra-faint siblings.

With $[\text{Fe}/\text{H}] \gtrsim -2.0$, stars in the classical dwarf galaxies were found to have abundance ratios different from halo stars at the same metallicity (e.g., Shetrone et al. 2003; Geisler et al. 2005). Most strikingly, the α -element abundances are not enhanced to the SN II enrichment level of $[\alpha/\text{Fe}] \sim 0.4$. This indicates different enrichment mechanisms and longer timescales in the dwarf galaxies; due to a slower evolution, the Fe contribution from SN Ia occurred “earlier”, at a time when the entire system had not yet reached a metallicity of $[\text{Fe}/\text{H}] \sim -1.0$, the turn-down point of $[\alpha/\text{Fe}]$ vs. $[\text{Fe}/\text{H}]$ in the Milky Way (see Figure 14).

Only very recently, a handful of stars with metallicities of $[\text{Fe}/\text{H}] < -3.0$ was discovered in the classical dwarf galaxies, with some of them having $[\text{Fe}/\text{H}] \sim -4.0$ (Frebel et al. 2010a). While these dwarfs have been studied for many decades, problems with earlier search techniques had prevented the discovery of extremely metal-poor stars (Starkenburg et al. 2010). The existence of

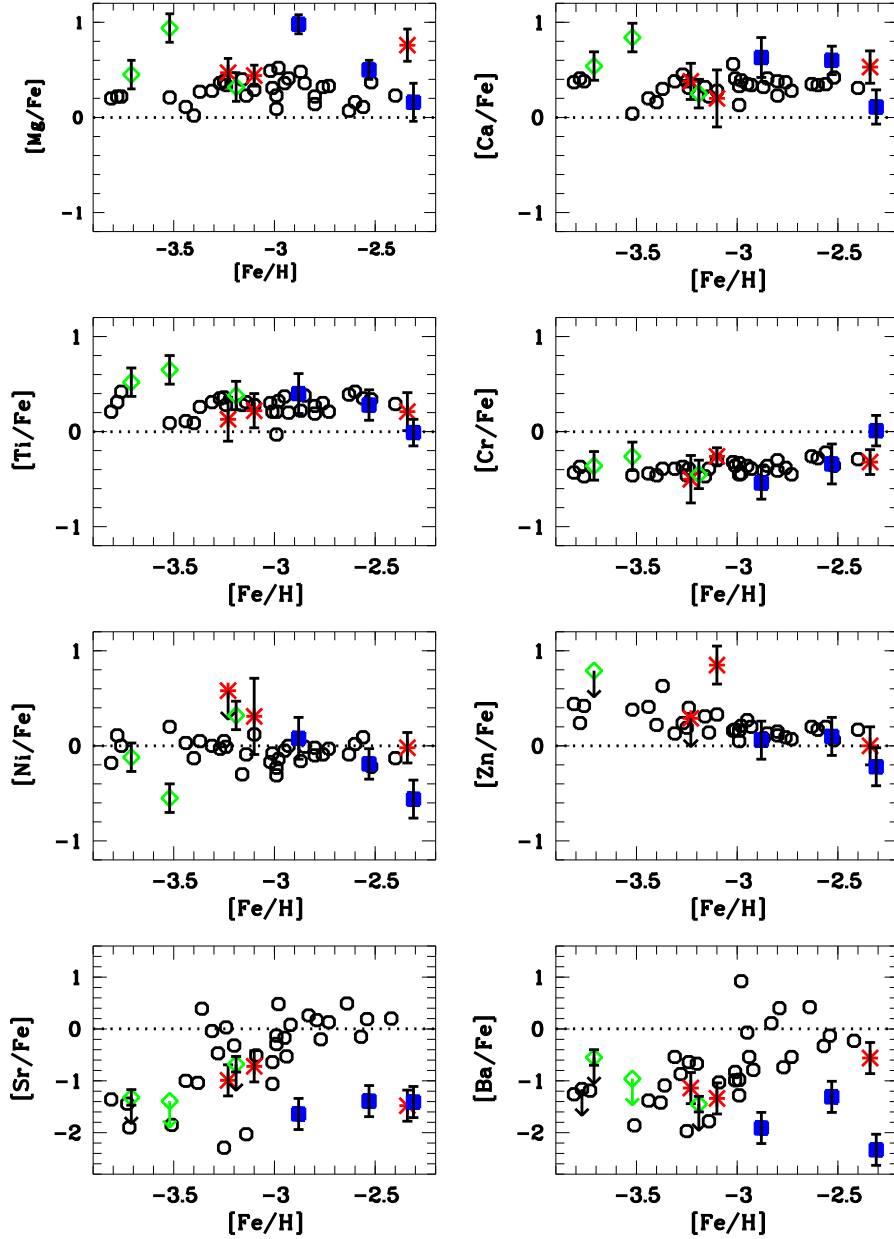


FIG. 20.— Comparison of stars in the Galactic halo (circles: Cayrel et al. 2004; François et al. 2007) and dwarf galaxies (asterisks: Ursa Major II, filled squares: Coma Berenices, diamonds: Segue 1, Bootes I and Leo IV) in the 1D/LTE relative abundances ($[X/Fe]$) vs $[Fe/H]$ diagram. While the light element abundances agree very well, dwarf galaxy stars have relatively low neutron-capture abundances, albeit still within the range of the halo stars.

such objects shows that a metallicity range of ~ 3 dex is present, at least in the Sculptor and Fornax dSphs. At $[Fe/H] < -3.0$, the chemical abundances, obtained from high-resolution spectra, are remarkably similar to those of Galactic halo stars at similar metallicities. This is in contrast to the deviations at higher $[Fe/H]$, and provides evidence for a change in the dominant enrichment mechanisms. For these types of dwarf galaxies, the transition from halo-typical abundance ratios (as a result of SN II enrichment) to more solar-like values (SN I-dominated Fe production) appears to take place around $[Fe/H] = -3.0$ (Cohen & Huang 2009; Aoki et al. 2009). As a consequence, chemical evolution may be a universal

process, at least at the earliest times, the very regime that is probed by the most metal-poor stars.

The first extremely metal-poor stars not belonging to the Galactic halo field population were found in some of the ultra-faint dwarf galaxies, even before such stars were discovered in the classical dwarfs (Kirby et al. 2008). Due to their distance and low stellar density these systems contain few stars brighter than $V = 19$, making the collection of spectroscopic data a challenge. Nevertheless, high-resolution spectra of a handful of individual metal-poor stars in Ursa Major II, Coma Berenices, Bootes I, Segue 1, and Leo IV (Frebel et al. 2010b; Norris et al. 2010c,a; Simon et al. 2010) have

been obtained. A large fraction of them are extremely metal-poor (i.e., $[\text{Fe}/\text{H}] < -3.0$). With one exception, all of their light element ($Z < 30$) abundances show the halo-typical core-collapse SNe signature, resembling those of similarly metal-poor Galactic halo stars. This may be clearly seen in the upper six panels of Figure 20, where the relative abundances of the metal-poor halo red giant sample of Cayrel et al. (2004) and François et al. (2007) (presented above in Section 3.2.2) are compared with those available for red giants in the ultra-faint dwarf galaxy stars. The exception is the CEMP-no star (see Table 1) Segue 1–7, a radial-velocity member of Segue 1, which has $[\text{Fe}/\text{H}] = -3.52$, $[\text{C}/\text{Fe}] = +2.3$, and $[\text{Ba}/\text{Fe}] < -1.0$ (Norris et al. 2010a). The 200-fold overabundance of carbon relative to iron in this extremely metal-poor star is quite remarkable. This shows that the CEMP-no phenomenon is not restricted to the Milky Way halo and may provide important clues to the origin of these stars.

Some abundances, however, indicate that the chemical evolution in these small systems may have been moderately inhomogeneous (see Section 3.2.1, Figure 9), with some stars perhaps reflecting enrichment by massive Population III stars. The chemical similarity to halo stars is also found at higher metallicity, up to $[\text{Fe}/\text{H}] \sim -2.0$, in contrast to what has been found for the classical dwarfs. This remarkable similarity between the abundance profiles of the halo and the dwarf galaxies supports the view that chemical evolution is independent of galaxy host mass in this metallicity regime. Moreover, this (together with the existence noted above of a CEMP-no star in the ultra-faint Segue 1) renews support for a scenario in which the metal-poor end of the Milky Way halo population was built up from destroyed dwarf galaxies (see Section 6.2).

Finally, neutron-capture abundances should be mentioned. These are extremely low in the ultra-faint systems, and as may be seen in the two bottom panels of Figure 20 in the range $-3.0 < [\text{Fe}/\text{H}] < -2.0$, the observed Sr and Ba values lie well below those found in typical Milky Way halo stars. A more general statement is that the mean values of $[\text{Sr}/\text{Fe}]$ and $[\text{Ba}/\text{Fe}]$ are significantly smaller in the ultra-faint dwarfs than in the halo. Comparably low values for Sr and Ba are also found in the more luminous dwarfs Hercules (Koch et al. 2008) and Draco (Fulbright et al. 2004) despite their sometimes relatively high Fe values of $[\text{Fe}/\text{H}] \sim -2.0$.

5. COSMO-CHRONOMETRY

Because of their low metallicity, metal-poor stars are usually regarded as having been formed at the earliest times, when the first elements heavier than helium were being synthesized. The most metal-poor stars are thus regarded as being almost as old as the Universe. Age determinations for field stars are, however, difficult, since they do not belong to a distinct single-age population such as a globular cluster. Cluster ages are based on fitting isochrones to their color-magnitude diagrams. The age dating of globular clusters will not be discussed here, and the reader is referred to Vandenberg et al. (1996) for details, and to Marín-Franch et al. (2009) for more recent results which are addressed further in Section 6.2. Suffice it to say that although the clusters are not as metal-poor as the most metal-poor field stars, the ages of the older of them range from 10 to 14 Gyr, placing them among

the oldest objects in the Universe. The main point of focus in this chapter is dating techniques for individual r-process-enhanced Galactic halo field stars.

5.1. Nucleo-Chronometry of Metal-Poor Field Stars

A fundamental way to determine the age of a *single* star is through radioactive decay dating. Elements suitable for this procedure are not, however, present in sufficient quantities in ordinary stars. There is also the problem of finding stars that have experienced enrichment from a single source so that the decay tracks the time from just one production event until the time of measurement. Fortunately, in strongly r-process-enhanced metal-poor stars, radioactive age dating is possible through abundance measurements of Th (^{232}Th , half-life 14 Gyr) and/or U (^{238}U , half-life 4.5 Gyr). These half-lives are sufficiently long for measurements of cosmic timescales, and stellar ages can be determined based on radioactive decay laws that lead to simple equations for different chronometer ratios involving Th, U, and stable r-process elements. Observed abundances in r-processed-enhanced stars provide determinations of their remaining radioactive material, e.g., $\log \epsilon(\text{Th}/r)_{\text{now}}$, with r being a stable element such as Eu, Os, and Ir, for which the following relationships (derived from radioactive decay laws in combination with known nuclear physics) obtain.

1. $\Delta t = 46.78[\log (\text{Th}/r)_{\text{initial}} - \log \epsilon(\text{Th}/r)_{\text{now}}]$ Gyr
2. $\Delta t = 14.84[\log (\text{U}/r)_{\text{initial}} - \log \epsilon(\text{U}/r)_{\text{now}}]$ Gyr
3. $\Delta t = 21.76[\log (\text{U}/\text{Th})_{\text{initial}} - \log \epsilon(\text{U}/\text{Th})_{\text{now}}]$ Gyr

Only theoretical r-process calculations can provide the initial production ratios ($\log (\text{Th}/r)_{\text{initial}}$ and $\log (\text{U}/r)_{\text{initial}}$) that describe how much r-process material, including Th and U, was made in the production event, i.e., the SN explosion. This implies that, technically, the SN is dated rather than the star. The time span, however, of the formation of the star after the SN is regarded as negligibly short compared to the star's age. Currently, the astrophysical site of the r-process remains unclear, and the associated initial conditions are not known, making yield predictions difficult. Nevertheless, some calculations involving various approximations are available (e.g., Schatz et al. 2002). It should be kept in mind that the universality of the r-process, noted in Section 4.2.2, (at least for $Z \geq 56$) is a major ingredient in predicting the relative elemental ratios, such as Th/ r .

The first r-II star, CS 22892-052, was discovered more than a decade ago in the HK survey (McWilliam et al. 1995). Its Th/Eu ratio yielded an age of 14 Gyr (Snedden et al. 2003). A second object, CS 31082-001, in which both Th and U were measurable, was then also shown to be 14 Gyr old, based on its U/Th abundance ratio (Hill et al. 2002). A large campaign was then initiated to observe metal-poor candidate stars from the Hamburg/ESO survey to discover such objects. Identifying stars with a strong Eu II line at 4129 Å, the main r-process indicator in stellar spectra, led to the discovery of several strongly r-process-enhanced (r-II) stars (see Barklem et al. 2005, and references therein) and dozens of mildly enriched (r-I) objects. With the exception of CS 31082-001, many of these r-process-enhanced stars could be dated with only the Th/Eu chronometer.

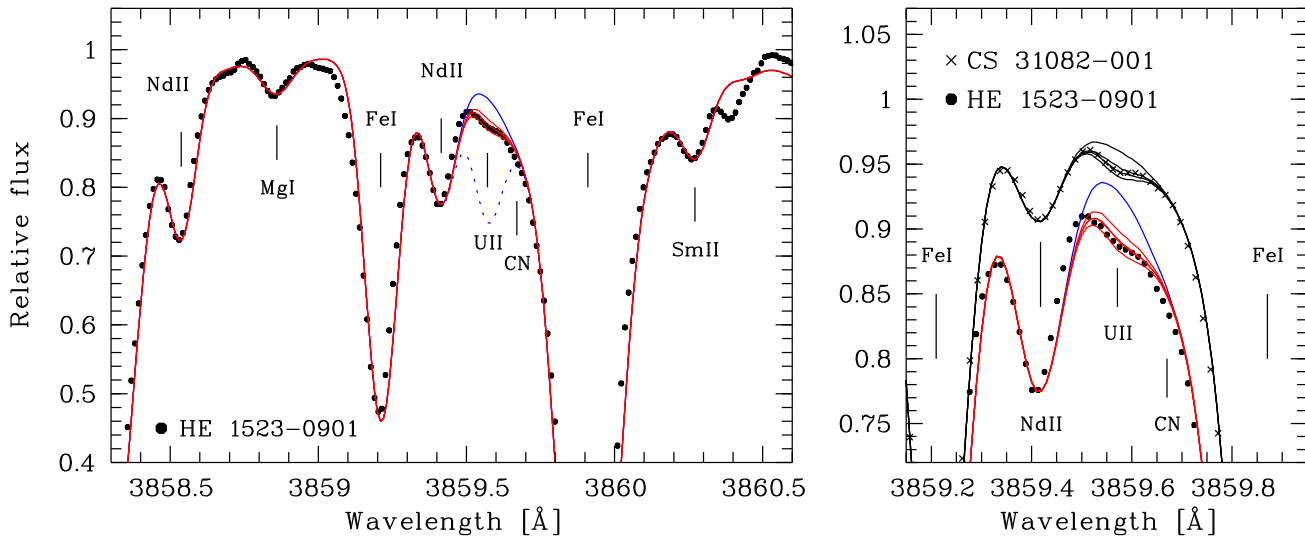


FIG. 21.— Spectrum synthesis of the U line region at 3860 Å in HE 1523–0901 (left panel, whole region; right panel, detailed view of just the line) and also CS 31082–001 (right panel only). Dots indicate the observed spectrum and continuous lines present synthetic spectra computed with a range of U abundances for comparison with the observed one. The latter are best illustrated in the right panel where the lowest three lines correspond to $\log \epsilon(\text{U}) = -1.96, -2.06,$ and $-2.16,$ and the uppermost line includes no U. The dotted line in the left panel represents a synthetic spectrum with an estimated U abundance if U was not radioactive and had not decayed over the past ~ 13 Gyr. From Frebel et al. (2007a).

In CS 31082–001, chronometer ratios involving any stable elements (e.g., Th/Eu) yielded *negative* ages. This is due to unusually high Th and U abundances compared with values expected for these elements from their overall r-process pattern (scaled to the Sun). Since only the elements heavier than the 3rd r-process peak are (equally) affected (Roederer et al. 2009), the U/Th ratio still gives a reasonable age for this star. The behavior was termed an “actinide-boost” (Schatz et al. 2002) and indicates an origin different from “normal” r-process-enhanced stars and/or multiple r-process sites (Hill et al. 2002). Since then, three more r-process-enhanced stars with such high Th/Eu ratios ($\sim 20\%$ of r-process stars) have been found (Honda et al. 2004; Lai et al. 2008). The underlying physical process(es) leading to the large fraction of the actinide-boost stars will need to be thoroughly investigated over the next few years. It is crucial to assess whether the apparent universality of the r-process of elements with $Z \geq 56$ seen in “regular” r-process-enhanced stars remains truly universal, or if it is simply an artefact of our limited understanding of the r-process and/or insufficient numbers of such stars.

For only one r-II star has it so far been possible to determine ages from more than just one chronometer ratio. The bright giant HE 1523–0901 ($V = 11.1$) has the strongest enhancement in r-process elements so far observed, $[\text{r}/\text{Fe}] = 1.8$ (Frebel et al. 2006, 2007a), and among the measured neutron-capture elements are Os, Ir, Th, and U. Its average stellar age of ~ 13 Gyr is based on seven chronometers Th/r, U/r and U/Th involving combinations of Eu, Os, Ir, Th and U. Only in cool r-II red giants can the many weak and often partially blended neutron-capture features be measured. The two most challenging examples are the extremely weak U II line at 3859 Å and the even weaker Pb I line at 4057 Å; these two lines are the strongest optical transitions of

the two elements. (It should be mentioned that both lines are blended with a strong CH feature. Hence, U and Pb can be detected best in stars with subsolar carbon abundances, which minimizes the blending effect. In CS 22892–052, a carbon-rich r-process-enhanced star, neither element will ever be measurable.)

Figure 21 shows the spectral region around the U line in HE 1523–0901. To be useful for age determination, r-II stars should be as bright as possible (preferably $V < 13$) so that very high-resolution spectra with very high S/N can be collected in reasonable observing times. A successful U measurement requires a high-resolution spectrum ($R > 60000$) with S/N of at least 350 per pixel at 3900 Å. A Pb measurement may be attempted in a spectrum with $S/N \sim 500$ at 4000 Å. Only *three* stars have had U measurements. They are HE 1523–0901, CS 31082–001, and a somewhat uncertain detection in BD +17° 3248, of which the age of HE 1523–0901 is currently the most reliable.

Compared with Th/Eu, the U/Th ratio is more robust against uncertainties in the theoretically derived production ratio because Th and U have similar atomic masses (for which uncertainties largely cancel out; e.g., Wanajo et al. 2002). Hence, stars displaying Th *and* U are the best for age determination. For the same reason, stable elements of the 3rd r-process peak ($76 \leq Z \leq 78$) are best used in combination with Th and U. Nevertheless, realistic age uncertainties range from ~ 2 to ~ 5 Gyr depending on the chronometer ratio (see Schatz et al. 2002, and Frebel et al. 2007a for discussions). In any case, age measurements of old stars naturally provide an important independent lower limit to the age of the Universe, currently inferred to be $13.73^{+0.16}_{-0.15}$ Gyr with WMAP (Spergel et al. 2007). In the absence of an age-metallicity relationship for field halo stars, the nucleochronometric ages thus demonstrate that these metal-

deficient stars, with $[\text{Fe}/\text{H}] \sim -3$, are indeed very ancient, leading to the corollary that stars of similar $[\text{Fe}/\text{H}]$, but with no overabundance in r-process elements, have a similar age.

The r-process-enhanced stars fortuitously bring together astrophysics and nuclear physics by acting as a “cosmic laboratory” for both fields of study. They provide crucial experimental data on heavy-element production that is not accessible to nuclear physics experiments. Since different r-process models often yield different final r-process abundance distributions, particularly in the heavy mass range, self-consistency constraints are very valuable. The stellar abundance triumvirate of Th, U, and Pb provides such constraints. These three elements are intimately coupled not only with each other but also to the conditions (and potentially also the environment) of the r-process. Pb is the β - plus α -decay end-product of all decay chains in the mass region between Pb and the onset of dominant spontaneous fission above Th and U. It is also built up from the decay of Th and U isotopes. All three measurements thus provide important constraints on the poorly understood decay channels. They offer an opportunity to improve r-process models which, in turn, facilitates the determination of improved initial production ratios necessary for the stellar age dating.

6. COSMOGONY

6.1. *The Early Universe*

Simulations of the hierarchical assembly of galaxies within the Cold Dark Matter (CDM) paradigm pioneered by White & Rees (1978) and today referred to as Λ CDM (e.g., Diemand et al. 2007; Springel et al. 2008) demonstrate that structure formation in the Universe proceeded hierarchically, with small dark matter halos merging to form larger ones which eventually led to the build-up of larger galaxies like the Milky Way. This is further described in Section 6.2. The very first stars (Population III) formed in small, so-called minihalos of $\sim 10^6 M_{\odot}$ that collapsed at $z \simeq 20 - 30$ (Tegmark et al. 1997) a few hundred million years after the Big Bang. Hydrodynamical cosmological simulations have shown that due to the lack of cooling agents in primordial gas, significant fragmentation was largely suppressed so that these first objects were very massive, of order $\sim 100 M_{\odot}$ (a “top-heavy” initial mass function; e.g, Bromm & Larson 2004 and references therein) and likely fast rotating. This is in contrast to low-mass stars ($< 1 M_{\odot}$) dominating today’s mass function (often referred to as the Salpeter mass function).

In this scenario, the massive first generation stars (designated Population III.1) soon exploded as core-collapse SNe leaving remnant black holes (for progenitor masses of $25 M_{\odot} < M < 140 M_{\odot}$ and $M > 260 M_{\odot}$), or even more energetic pair-instability SNe (PISNe; $140 M_{\odot} < M < 260 M_{\odot}$; Heger & Woosley 2002) with complete disruption. A specific, predicted “chemical fingerprint” of the putative PISN explosion has not (yet) been identified in any metal-poor star. (Given that luminous supernovae (having peak $M_V < -21$) in external galaxies have been associated with massive progenitor stars ($M > 100 M_{\odot}$) in low-metallicity regions (Neill et al. 2011) it can not be excluded, however, that such a signature will be found.) In their final stages, all these massive objects

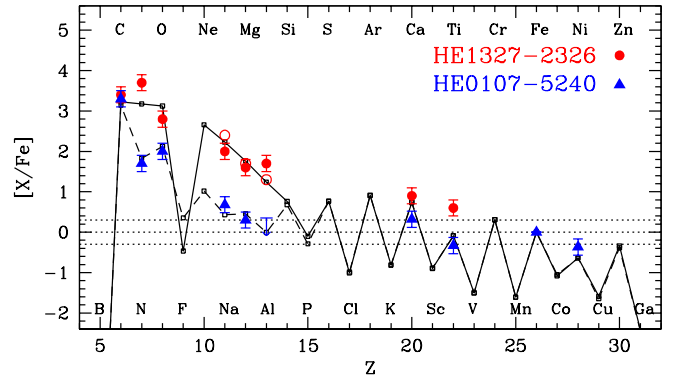


FIG. 22.— Abundance distribution vs. atomic number for the two most Fe-poor stars HE 0107–5240 and HE 1327–2326 (circle and triangles, respectively) compared with the best fit models of “mixing and fallback” core-collapse SNe from Nomoto et al. 2006). The middle dotted line shows the solar abundance ratio. See text for more details on the SNe models.

provided vast amounts of ionizing radiation (and some of the first metals) that changed the conditions of the surrounding material for subsequent star formation, even in neighboring minihalos. Partially ionized primordial gas supported the formation of first H_2 and then HD, which in turn facilitated more effective cooling than would be possible in neutral gas. Any metals or dust grains left behind from PISNe would have similar cooling effects. Hence, there likely was a second generation of metal-free stars (Population III.2) that, for the first time, included stars of somewhat smaller masses ($M \sim 10 M_{\odot}$.) This generation, however, was still top-heavy, in contrast to typical present-day stars ($M \sim 1 M_{\odot}$.) For a recent review of this topic, see Bromm et al. (2009). Soon thereafter, the first low-mass metal-poor stars were born. In their atmospheres they locked in the chemical fingerprint of the very first supernova explosions. Investigating the chemical abundances of the most metal-poor stars is thus the only way to gain detailed information of the nature and properties of the first stars without going to the very high redshift Universe. Even with the James Webb Space Telescope (see <http://www.jwst.nasa.gov>), the sensitivity will not be sufficient to directly observe the first stars. The first galaxies may, however, just be reachable.

As described in Section 2.4, four halo stars with the exceptionally low values of $[\text{Fe}/\text{H}] < -4.3$ are currently known. An immediate question arises: do their abundance patterns reflect the chemical yields of the first stars? Before attempting to answer this question, their detailed chemical abundances have to be considered. The most striking features in both stars with $[\text{Fe}/\text{H}] < -5.0$ are the extremely large overabundances of the CNO elements ($[\text{C,N,O}/\text{Fe}] \sim +2$ to $+4$). HE 0557–4840 (with $[\text{Fe}/\text{H}] = -4.8$) partially shares this signature by also having a fairly large value of $[\text{C}/\text{Fe}]$. SDSS J102915+172927, however, does not. This object has an abundance signature that resembles typical metal-poor halo stars, including its carbon signature, and no exceptional over- or underabundances. In contrast, other element ratios, $[\text{X}/\text{Fe}]$, are somewhat enhanced in HE 1327–2327 with respect to stars with $-4.0 < [\text{Fe}/\text{H}] < -2.5$, but less so for the giants HE 0107–5240 and HE 0557–4840. No

neutron-capture element was detected in HE 0107–5240, HE 0557–4840, or SDSS J102915+172927, whereas, unexpectedly, a large value of $[\text{Sr}/\text{Fe}] = 1.1$ was obtained for HE 1327–2326. Despite expectations, and as discussed in Section 4.1.2, lithium was not detected in either the relatively unevolved subgiant HE 1327–2326 or the dwarf SDSS J102915+172927. The lithium abundance upper limits are $\log \epsilon(\text{Li}) < 0.7$ (Frebel et al. 2008) and < 1.1 (Caffau et al. 2011), respectively. These results are extremely surprising. Given that HE 1327–2326 and SDSS J102915+172927 have $T_{\text{eff}} = 6180\text{K}$ and 5810K , respectively, one would expect them to lie on the Spite Plateau, with $\log \epsilon(\text{Li}) = 2.3$. Somewhat unsatisfactory conjectures that might explain the non-detection include: (1) Li at the epoch of lowest metallicity was below the abundance of the Spite Plateau due to its destruction early in the Universe (see e.g., Piau et al. 2006 for an interesting scenario), and (2) Li was destroyed by phenomena associated with (not yet detected) binarity. Progress will probably only be made when more near-main-sequence-turnoff stars with $[\text{Fe}/\text{H}] \lesssim -4.0$ are discovered which permit clarification of this issue.

Both HE 0107–5240 and HE 1327–2326 are benchmark objects with the potential to constrain various theoretical studies of the early Universe, such as the formation of the first stars, calculations of Population III SN yields, and the earliest chemical evolution. Several different scenarios have been offered that seek to explain the highly individual abundance patterns of both stars as early, extreme Population II, stars that display the “fingerprint” of just one Population III SN. These include: (1) “mixing and fallback” models (Umeda & Nomoto 2003; Iwamoto et al. 2005; Nomoto et al. 2006) of a faint (i.e., low energy) $25 M_{\odot}$ supernova in which a large amount of C, N, and O but little Fe is ejected, while a large fraction of Fe-rich ejecta is postulated to fall back onto the newly created black hole. (See Figure 22 for comparison of the observed and predicted abundances for HE 0107–5240 and HE 1327–2326); (2) the modeling of Heger & Woosley (2010) who fit the observed stellar abundances by searching for a match within a large grid of Population III SN yields. Their best fit involved typical halo stars with a power-law IMF in the range $M = 11 - 15 M_{\odot}$, low explosion energy, and little mixing; and (3) the investigation of Meynet et al. (2006) who explored the influence of stellar rotation on elemental yields of $60 M_{\odot}$ near-zero-metallicity SNe. Mass loss from rotating massive Population III stars qualitatively reproduces the CNO abundances observed in HE 1327–2326 and other carbon-rich metal-poor stars. In a somewhat different model, Suda et al. (2004) proposed a scenario in which the abundances of HE 0107–5240 originated in a Population III binary system that experienced mass transfer of CNO elements from the more massive companion during its AGB phase, together with subsequent accretion of heavy elements from the ISM onto the (less massive) component now being observed. Along the same lines, Campbell et al. (2010) suggested a binary model for HE 1327–2326 in terms of s-process nucleosynthesis and mass transfer via a stellar wind. Qualitatively, the high C,N,O and Sr stellar abundances could be explained this way if the star were in a wide binary. That said, neither HE 0107–5240 nor HE 1327–2326 shows radial velocity variations that would indicate close bina-

rity.

Stars with $[\text{Fe}/\text{H}] > -4.3$ and “classical” halo abundance signatures have also been reproduced with Population III SN yields. Average abundance patterns of four non-carbon-enriched stars with $-4.2 < [\text{Fe}/\text{H}] < -3.5$ were modeled with the yields of massive ($\sim 30 - 50 M_{\odot}$), high explosion energy ($\sim 20 - 40 \times 10^{51}$ ergs), Population III hypernovae (Tominaga et al. 2007) and also fit with integrated yields of a small number of Population III stars (Heger & Woosley 2010). Special types of SNe or unusual nucleosynthesis yields have been considered for stars with chemically peculiar abundances, e.g., high Mg. It is, however, often difficult to explain the entire abundance pattern in this way. Abundances of additional stars with $[\text{Fe}/\text{H}] < -4.0$, as well as a better understanding of the explosion mechanism and the effect of the initial conditions on SNe yields are required to arrive at a more comprehensive picture of the extent to which metal-poor stars reflect the ejecta of the original Population III objects or, alternatively, those of later generations of SNe.

Some metal-poor stars display abundance ratios of a few elements that differ by large amounts from the general halo trend (e.g., C, Mg). The level of chemical diversity also increases towards the lowest metallicities. For instance, as discussed in Section 4.2.1, a large fraction of the most metal-poor stars is very carbon-rich (i.e., $[\text{C}/\text{Fe}] > 0.7$). In the compilation of Frebel (2010) the C-rich fraction of stars with $[\text{Fe}/\text{H}] < -2.0$ is ~ 0.17 . Most significantly, the fraction increases with decreasing metallicity (see Figure 4); and indeed, three of the four stars with $[\text{Fe}/\text{H}] < -4.3$ are extremely carbon-rich. Reasons for this general behavior remain unclear. Could there be a cosmological origin for the large fraction of carbon-rich stars? Ideas for the required cooling processes necessary to induce sufficient fragmentation of the near-primordial gas to enable low-mass star formation include cooling based on enhanced molecule formation due to ionization of the gas, cooling through metal enrichment or dust, and complex effects such as turbulence and magnetic fields (Bromm et al. 2009). Fine-structure line cooling through CI and OII was suggested as a main cooling agent (Bromm & Loeb 2003). These elements were likely produced in vast quantities in Population III objects (see Section 4.2.1), and may have been responsible for the ISM reaching a critical metallicity, sufficient for low-mass star formation.

The existence and level of such a “critical metallicity” can be probed with large numbers of carbon and oxygen-*poor* metal-poor stars: if a threshold exists, all of these objects should have a combination of C and/or O abundances *above* the threshold for a critical metallicity. A transition discriminant was defined by Frebel et al. (2007b), which has since been slightly revised to $D_{\text{trans}} = \log(10^{[\text{C}/\text{H}]} + 0.9 \times 10^{[\text{O}/\text{H}]})$ (V. Bromm 2011, private communication). No low-mass metal-poor stars should exist below the critical value of $D_{\text{trans}} = -3.5$.

As can be seen in Figure 23, at metallicities of $[\text{Fe}/\text{H}] \gtrsim -3.5$, most stars have C and/or O abundances that place them well above the threshold. They simply follow the solar C and O abundances scaled down to their respective Fe values. Naturally, this metallicity range is not suitable for directly probing the very early time. Below $[\text{Fe}/\text{H}] \sim -3.5$, however, the observed C and/or O lev-

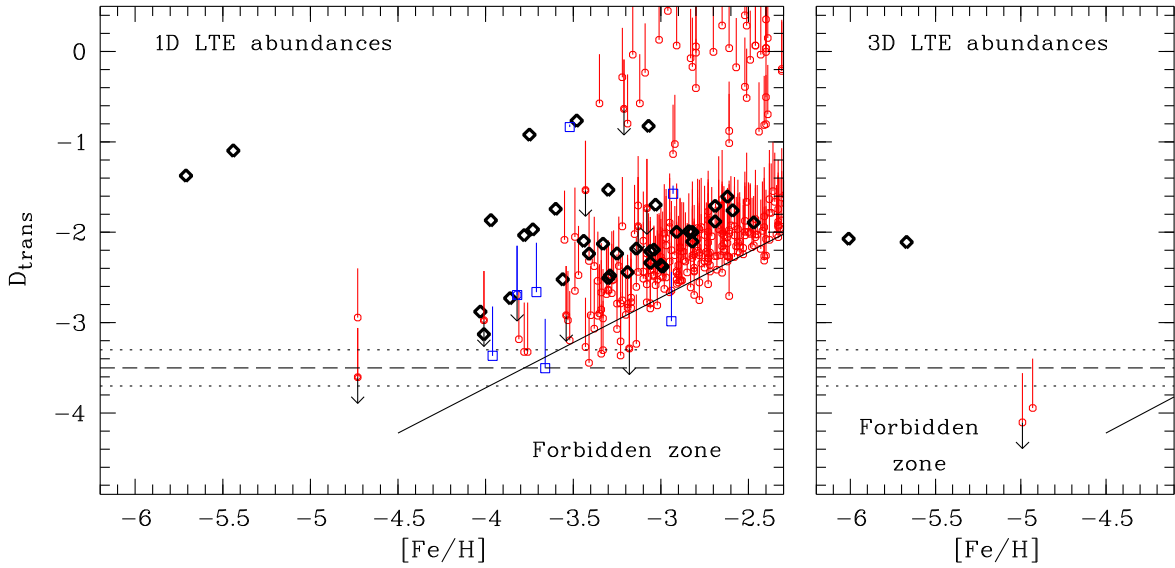


FIG. 23.— Left panel: Transition discriminant, D_{trans} , for Galactic halo (small red circles, thick black diamonds) and dwarf galaxy (blue squares) metal-poor stars as a function of $[\text{Fe}/\text{H}]$, based on 1D abundances. Black diamonds show stars with D_{trans} values calculated from their C and O abundances. Red circles and blue squares depict lower D_{trans} limits based on only a known C abundance. The corresponding vertical bars show the potential range of D_{trans} for a given star assuming O to be tied to C within the range $-0.7 < [\text{C}/\text{O}] < 0.2$. (If an upper limit on O is available and less than the maximal assumed O abundance, the bar is correspondingly shorter.) Circles or squares with bars plus additional arrows indicate interesting cases where only upper limits of C abundances are available and nothing is known about the O abundance. The solid line represents the solar C and O abundances scaled down with $[\text{Fe}/\text{H}]$, while dashed and dotted lines display the transition discriminant $D_{\text{trans}} = -3.5$ together with uncertainties. The “Forbidden zone” indicates the region with insufficient amounts of C and O for low-mass star formation. (Based on Figure 1 of Frebel et al. 2007b with recent additions from the literature such as Caffau et al. 2011). Right panel: Same as left panel, but for $[\text{Fe}/\text{H}] < -4.1$ and using 3D carbon and oxygen abundances, for the four most iron-poor stars.

els must be *higher* than the Fe-scaled solar abundances to be above the critical metallicity. Indeed, apart from one object, none of the known lowest-metallicity stars appear to have D_{trans} values or limits below the critical value, consistent with this cooling theory. The exception is SDSS J102915+172927, which has an upper limit for carbon of only $[\text{C}/\text{H}] < -3.8$ (1D) and < -4.3 (3D). Assuming the above $[\text{C}/\text{O}]$ range, this leads to $D_{\text{trans}} < (-3.6 \text{ to } -3.0)$ (1D) and $< (-4.1 \text{ to } -3.5)$ (3D). However, only with a known O abundance can this low D_{trans} value be conclusively determined. As can be seen in Figure 23, several other stars also have values that are close to $D_{\text{trans}} = -3.5$, based on their 1D abundances. Very high S/N spectra suitable for measurements of very weak CH and OH molecular features will be required to determine exactly how close the D_{trans} of these objects are to the critical value.

The likely exception of SDSS J102915+172927 and several interesting “border line” cases notwithstanding, this cooling theory suggests that at low metallicity, carbon excesses are a requirement for the formation of most low-mass metal-poor stars. This is qualitatively in line with the empirical finding of a large fraction of carbon-rich stars and may thus reflect a generic avenue for low-mass star formation. Individual objects, of course, could be the result of unusual circumstances or different mechanism. For example, SDSS J102915+172927 could have formed from a gas cloud that was primarily cooled by dust grains, rather than atoms, made by the first stars. If future data show that the *majority* of the most metal-poor stars have $D_{\text{trans}} < -3.5$, then dust cooling (induc-

ing a much lower critical metallicity) would be a dominant cooling mechanism in the early Universe.

6.2. The Milky Way

During the past half century, two basically different observationally driven paradigms were proposed for the formation of the Galactic halo. The first was the monolithic collapse model of Eggen et al. (1962) (hereafter ELS), and the second the accretion model of Searle & Zinn (1978) (hereafter SZ). At the same time, White & Rees (1978) proposed, in a more general context, their CDM hierarchical clustering paradigm in which “The entire luminosity content of galaxies ... results from the cooling and fragmentation of residual gas within the transient potential wells provided by the dark matter.” ELS predicted a very rapid collapse phase (of a few 10^8 yr), and a dependence of kinematics on abundance together with a radial abundance gradient for halo material. SZ, in contradistinction, predicted a longer formation period of a few 10^9 yr, no dependence of kinematics on abundance, and no radial abundance gradient. Not too surprisingly, perhaps, neither gives a complete explanation of the more complicated reality. On the one hand, early work revealed no dependence of kinematics on abundance for $[\text{Fe}/\text{H}] \lesssim -1.7$ (see Chiba & Beers 2000, and references therein), while on the other, globular cluster age measurements demonstrated that although some clusters were significantly younger than the majority, the age spread was small for the bulk of the system. Figure 24, from the recent work of Marín-Franch et al. (2009), presents the relative ages of 64 clusters as a func-

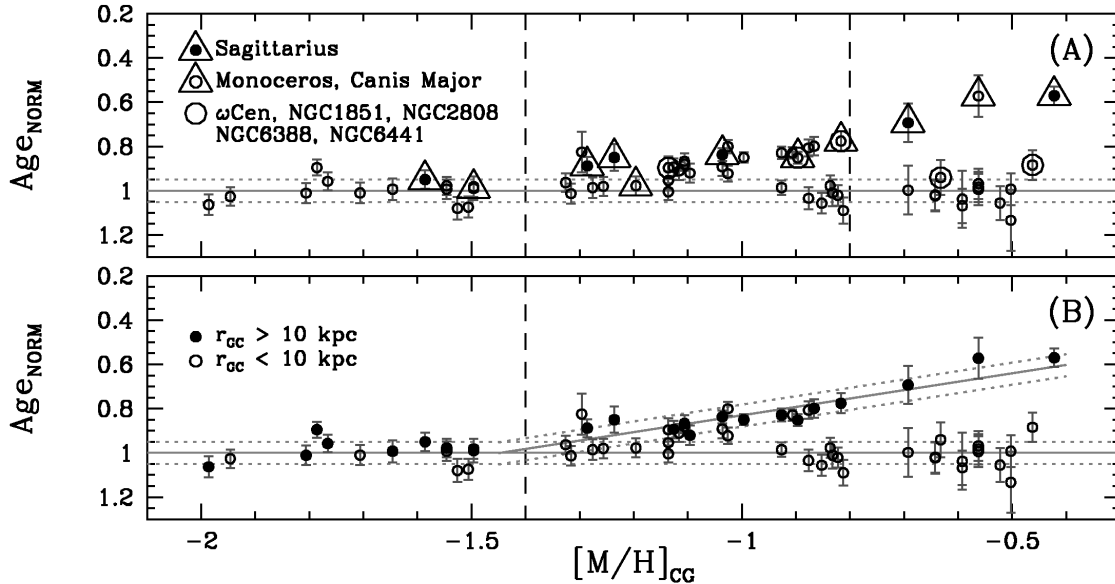


FIG. 24.— Relative ages, Age_{NORM} , for the Galactic globular clusters as a function of cluster metallicity, $[M/H]$ (where $[M/H] = [\text{Fe}/H] + \log(0.638f + 0.362)$, and $\log(f) = [\alpha/\text{Fe}]$), from the work of Marín-Franch et al. (2009, Figure 13). Approximate absolute ages may be obtained as $12.8 \times \text{Age}_{\text{NORM}}$.

tion of metallicity, $[M/H]$, which illustrates this point.

A turning point in the discussion came with the discovery by Ibata et al. (1995) of the Sagittarius dwarf galaxy, which has been captured by the Milky Way and is currently being torn apart in its gravitational field. Some six of the Galactic globular clusters are believed to have once been part of the Sgr system. Marín-Franch et al. (2009) comment on similar over-densities in Monoceros and Canis Major that may contain several other globular clusters and be associated with similar accretions. Against this background, it is then very instructive to consider the detail of Figure 24. Marín-Franch et al. (2009) identify two groups of globular clusters: “a population of old clusters with an age dispersion of $\sim 5\%$ (i.e., ~ 0.6 Gyr) and no age-metallicity relationship, and a group of younger clusters with an age-metallicity relationship similar to that of the globular clusters associated with the Sagittarius dwarf galaxy.” Two thirds of the sample belong to the old group, one third to the younger.

As noted above in Section 3.2.1, there has been growing evidence that the field halo stars of the Milky Way comprise more than one population. The reader should consult Carollo et al. (2010) for the development of the case that the Galaxy’s halo contains an inner and an outer component. They report the following essential differences between the two components, which are dominant interior and exterior to ~ 15 kpc: (1) the inner component is more flattened than the outer component, with axial ratio (c/a) values of ~ 0.6 and 1.0 , respectively; (2) the inner component has small prograde systemic rotation, $\langle V_\phi \rangle = +7 \pm 4 \text{ km s}^{-1}$ (i.e., rotating in the same sense as the Galactic disk), while the outer has retrograde rotation $\langle V_\phi \rangle = -80 \pm 13 \text{ km s}^{-1}$; and (3) the inner component is more metal-rich, with peak metallicity $[\text{Fe}/H] = -1.6$, while the outer one has peak metallicity $[\text{Fe}/H] = -2.2$.

Against this background, Morrison et al. (2009) have reported another, more highly flattened halo component, with $c/a \sim 0.2$, which has “a small prograde rotation ... supported by velocity anisotropy, and contains more intermediate-metallicity stars (with $-1.5 < [\text{Fe}/H] < -1.0$) that the rest of [the] sample”.

While the detailed nature and relationships of these components remain to be fully understood, it seems likely the answer will be found within the hierarchical Λ CDM paradigm reported above. The work of Zolotov et al. (2009), for example, while supporting the SZ paradigm of halo formation, also produces a dual halo configuration of “*in situ*” and “*accreted*” components, not unlike those envisaged in the ELS and SZ observational paradigms. Remarkably, these paradigms were first established on essentially observational grounds only. They are now being explained in terms of a theoretical framework based on tracing the dark matter evolution from initial density fluctuations early in the Universe.

Further support for a two component model comes from recent work of Nissen & Schuster (2010), who have investigated the abundances of α -elements in the abundance range $-1.6 < [\text{Fe}/H] < -0.4$, as a function of kinematics, with a view to comparing (in Zolotov et al. 2009 terminology) the “*in situ*” and “*accreted*” components. Their results are shown in Figure 25. In the right panel one sees a large spread in $[\alpha/\text{Fe}]$, at fixed $[\text{Fe}/H]$, that correlates strongly with position in the kinematic (so-called “Toomre”) diagram on the left. The simplest and also extremely significant interpretation of this figure is that stars with $[\alpha/\text{Fe}] \sim +0.3$ to $+0.4$, with prograde kinematics, are part of the “*in situ*” component, while those with $[\alpha/\text{Fe}] \lesssim +0.3$, on principally retrograde orbits, belong to the “*accreted*” component. The reader will recall from Section 4.3.2 that low $[\alpha/\text{Fe}]$ is a key signature of the Milky Way’s dwarf galaxies in the range $-1.5 < [\text{Fe}/H] < 0.0$ (see also Tolstoy et al. 2009, their Figure 11). Said

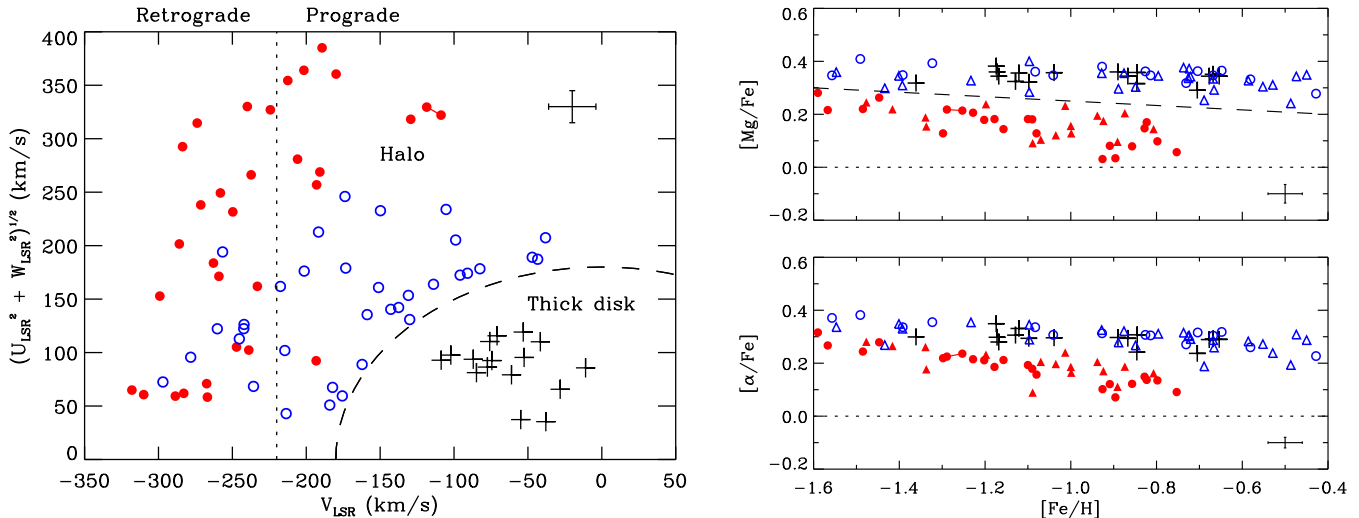


FIG. 25.— Left: kinematics (in which U , V , W are velocity components in the Galactic frame) and right: $[\alpha/\text{Fe}]$ vs. $[\text{Fe}/\text{H}]$ for metal-poor Milky Way stars, from the work of Nissen & Schuster (2010). Circles and triangles refer to halo (and crosses to thick disk) stars, respectively. Note the strongly correlated relative positions of the filled and open circles in the two panels. See text for discussion.

differently, Figure 25 is consistent with the view that dwarf galaxies have played an important role in the formation of the Milky Way halo.

A complementary way to study the origin of the Milky Way, its halo, and similar large galaxies more generally, is through large-scale Λ CDM simulation of the growth of structure formation. A prominent issue with Milky Way-size halos at redshift $z = 0$ is the predicted large number of CDM substructures that surround such a galaxy. The number of observed dwarf galaxies surrounding the Milky Way is, however, much lower and does not agree with such predictions. This mismatch has been termed the “missing-satellite” problem (e.g., Moore et al. 1999).

It is thus apparent that many more questions about galaxy assembly and evolution still need to be resolved. Crucially, it remains to be seen to what extent small dark halos contained baryonic matter, subsequently observed as gas and stars, and how they evolved with time. One way to learn about the luminous content of small sub-halos is to investigate in detail the surviving dwarf galaxies, in particular the ultra-faint systems, that orbit the Milky Way. Studying the onset of star formation and associated chemical evolution in these satellites will provide some of the currently missing information for our understanding of how the observed properties of small, faint systems relate to the dark matter substructures that built up larger galaxies.

7. CONCLUSIONS & FUTURE PROSPECTS

Old metal-poor stars can be employed as tools to learn about the conditions in the early Universe. The scientific topics that can be addressed in this way are numerous, and this chapter describes the most prominent questions to which metal-poor stars can provide unique insights. These include the origin and evolution of the chemical elements, the relevant nucleosynthesis processes and sites, and the overall chemical and dynamical history of the Galaxy. By extension, the abundance patterns in metal-poor stars provide constraints on the nature of the first stars and the initial mass function, and the chemical

yields of first/early SNe. Moreover, studying metal-poor stars in dwarf galaxies opens up ways to learn about early star and early galaxy formation processes, including the formation of the Galactic halo through hierarchical assembly.

Our review has highlighted the tension between the approximations inherent in 1D/LTE model atmosphere abundance analyses, on the one hand, and the more physically realistic 3D/non-LTE (and more computationally challenging) formalism, on the other. Given abundance differences $\sim 0.5 - 0.9$ dex between the two formalisms for many elements, there is an urgent need for comprehensive investment in self-consistent 3D/non-LTE modeling of the relevant regions of $T_{\text{eff}}/\log g/[\text{Fe}/\text{H}]$ space.

The most metal-deficient stars are extremely rare, but past surveys for metal-poor halo stars have shown that they can be systematically identified through several selection steps. Typically, the metal-poor halo stars found to date are located no further away than $\sim 10 - 15$ kpc, with $B \lesssim 16$. This brightness limit ensures that adequate S/N spectra can be obtained in reasonable observing times with existing telescope/instrument combinations. The outer halo beyond ~ 15 kpc, however, is largely unexplored territory, at least in terms of high-resolution spectroscopy. Recent work has shown that the ultra-faint dwarf galaxies orbiting the Galaxy contain larger fractions of extremely metal-poor stars (i.e., $[\text{Fe}/\text{H}] < -3.0$) than does the Galactic halo. That said, there is a high price to be paid in order to observe these objects because most of them are extremely faint. Those that are currently observable with 6 - 10 m telescopes are only the brightest in a given system, and these are usually located on the upper RGB. At the limit are objects at 19th magnitude that can just be observed at high spectral resolution, requiring exposure times up to ~ 10 h per star in order to reach the minimum useful S/N ratio in the final spectrum. This is feasible only for individual stars, not for large-scale investigations. Objects lower on the RGB or even the main sequence (> 21 mag) are out

of reach, even for medium-resolution studies.

Over the next few years all of these brightest dwarf galaxy stars will have been observed. What then? Either new larger telescopes, or additional dwarf galaxies that harbor more observable stars, are required. Addressing both options is currently underway. To chemically characterize the Galactic halo in detail (including its streams, substructures and satellites) wide-angle surveys with large volumes are needed. The Australian SkyMapper photometric survey (to begin in 2011) is optimized for stellar work. It will provide a wealth of metal-poor candidates in need of detailed high-resolution follow up to determine their abundances. The footprint of this project will be some three times larger than that of the HES. Newly discovered stars with $B \lesssim 16$ will enable an important advance in stellar archaeology by (hopefully) trebling the number of “bright” objects available for high-resolution abundance studies with existing facilities. A significant fraction of SkyMapper candidates will, however, be too faint for practical and efficient follow-up observations. In particular, the most metal-poor stars require high S/N to enable the detection of very weak absorption features. These will be the target of the high-resolution spectrographs on the new generation of 20 – 30 m telescopes. Among these new discoveries, it is expected that more of the most metal-poor stars (e.g., those with $[Fe/H] < -5.0$; Christlieb et al. 2002 and Frebel et al. 2005) will be found.

With SkyMapper, many more faint dwarf galaxies are expected to be found. Even though the brightest stars in them will still be at the observational limit for high-resolution spectroscopy, having more of these dwarf galaxy stars available for detailed studies will provide new insights into the nature and evolution of these small systems and their relationship to the building-up process(es) of the Milky Way. Other photometric surveys such as Pan-Starrs and LSST are also expected to yield new dwarf galaxies. These surveys, however, will be useful for the search for metal-poor stars in dwarf galaxies only if coupled with additional follow-up efforts, due to the lack of sufficiently metal-sensitive filters.

In addition to these photometric surveys, the Chinese LAMOST spectroscopic survey will provide numerous metal-poor candidates in the northern hemisphere, all based on medium-resolution spectra. GAIA is an astrometric space mission led by ESA, scheduled to begin observations in 2012. It will obtain high-precision phase-space information for one billion stars in the Galaxy, along with the physical parameters and the chemical composition of many of these stars. These new data will revolutionize our understanding of the origin, evolution, structure, and dynamics of the Milky Way as a whole and of its components. In particular, the kinematic information (e.g., proper motions) that will become available for many known metal-poor stars will enable detailed studies of how the abundances of different populations depend on kinematics. Furthermore, a precise selection of low-metallicity candidate stars based on, for example, extreme kinematic signatures, will become feasible. Since this is currently beyond reach for most metal-poor halo

giants, the GAIA astrometry should increase the yield of fainter metal-poor stars at larger distances.

By having the opportunity to access fainter stars in the outer Galactic halo and dwarf galaxies, the next major frontier in stellar archaeology and near-field cosmology can be tackled. High-resolution follow-up of faint stars may become a reality with the light-collecting power of the next generation of optical telescopes, the Giant Magellan Telescope, the Thirty Meter Telescope and the European Extremely Large Telescope. All three telescopes are currently in the planning and design phase with completions scheduled around 2020. When equipped with high-resolution spectrographs, such facilities would not only permit in-depth analysis of new metal-poor stars in the Galaxy’s outer halo and dwarf galaxies, but also make it feasible to obtain very high- S/N data of somewhat brighter stars, to permit investigation, for example, of isotopic ratios such as ${}^6\text{Li}/{}^7\text{Li}$ and r-process-enhanced stars, to provide crucial empirical constraints on the nature of the site and details of critical nucleosynthesis processes. This is currently possible only for the very brightest stars. At the faintest magnitudes, individual stars in the Magellanic Clouds and perhaps even the brightest objects in Andromeda could be observed with high-resolution spectroscopy. Studying massive dwarf galaxies and another spiral system that resembles the Milky Way would provide unprecedented new insight into the chemical evolution of large systems and their formation process(es).

All of these new observations will be accompanied by an increased theoretical understanding of the first stars and galaxies, SN nucleosynthesis, the mixing of metals into the existing gaseous medium, and feedback effects in the early Universe, as well as cosmic chemical evolution. New generations of hydrodynamical, high-resolution cosmological simulations will enable a direct investigation of chemical evolution by including more than one SN and corresponding feedback(s), for example, in first-galaxy simulations. These will be sufficient for tracing the corresponding metal production and spatial distributions and enable direct comparisons with abundance measurements in the stars of dwarf galaxies. This in turn will shed new light on the question of whether the least-luminous dwarf galaxies resemble the first galaxies, and if they are early analogs of the building blocks of the Galactic halo.

A. F. acknowledges support through a Clay Fellowship administered by the Smithsonian Astrophysical Observatory. J. E. N. acknowledges support from the Australian Research Council (grants DP03042613, DP0663562, and DP0984924) for studies of the Galaxy’s most metal-poor stars and ultra-faint satellite systems. It is a pleasure to thank M. Asplund, T. C. Beers, N. Christlieb, G. L. Harris, A. Karakas, and H. L. Morrison for their perceptive comments, which led to improvement to the manuscript. The authors also thank N. Christlieb and E. N. Kirby for supplying the high-resolution spectrum of HE 0107–5240 presented in Figure 2 and Figure 10, respectively.

REFERENCES

- Aoki, W., Arimoto, N., Sadakane, K., Tolstoy, E., Battaglia, G., Jablonka, P., Shetrone, M., Letarte, B., Irwin, M., Hill, V., Francois, P., Venn, K., Primas, F., Helmi, A., Kaufer, A., Tafelmeyer, M., Szeifert, T., & Babusiaux, C. 2009, *A&A*, 502, 569
- Aoki, W., Beers, T. C., Christlieb, N., Norris, J. E., Ryan, S. G., & Tsangarides, S. 2007, *ApJ*, 655, 492

- Aoki, W., Norris, J. E., Ryan, S. G., Beers, T. C., & Ando, H. 2002, *ApJ*, 576, L141
- Aoki, W., Ryan, S. G., Norris, J. E., Beers, T. C., Ando, H., Iwamoto, N., Kajino, T., Mathews, G. J., & Fujimoto, M. Y. 2001, *ApJ*, 561, 346
- Arlandini, C., Käppeler, F., Wisshak, K., Gallino, R., Lugaro, M., Busso, M., & Straniero, O. 1999, *ApJ*, 525, 886
- Arnett, D. 1996, *Supernovae and nucleosynthesis. An investigation of the history of matter, from the Big Bang to the present* (Princeton: Princeton University Press)
- Asplund, M. 2005, *ARA&A*, 43, 481
- Asplund, M., Carlsson, M., & Botnen, A. V. 2003, *A&A*, 399, L31
- Asplund, M., Grevesse, N., Sauval, A. J., & Scott, P. 2009, *ARA&A*, 47, 481
- Baade, W. 1944, *ApJ*, 100, 137
- Bahcall, J. N. & Soneira, R. M. 1980, *ApJS*, 44, 73
- Barklem, P. S., Christlieb, N., Beers, T. C., Hill, V., Bessell, M. S., Holmberg, J., Marsteller, B., Rossi, S., Zickgraf, F.-J., & Reimers, D. 2005, *A&A*, 439, 129
- Beers, T. C. & Christlieb, N. 2005, *ARA&A*, 43, 531
- Beers, T. C., Preston, G. W., & Shectman, S. A. 1992, *AJ*, 103, 1987
- Behr, B. B., Cohen, J. G., McCarthy, J. K., & Djorgovski, S. G. 1999, *ApJ*, 517, L135
- Bergemann, M., Pickering, J. C., & Gehren, T. 2010, *MNRAS*, 401, 1334
- Bessell, M. S. & Norris, J. 1984, *ApJ*, 285, 622
- Bromm, V. & Larson, R. B. 2004, *ARA&A*, 42, 79
- Bromm, V. & Loeb, A. 2003, *Nature*, 425, 812
- Bromm, V., Yoshida, N., Hernquist, L., & McKee, C. F. 2009, *Nature*, 459, 49
- Burbidge, E. M., Burbidge, G. R., Fowler, W. A., & Hoyle, F. 1957, *Reviews of Modern Physics*, 29, 547
- Burris, D. L., Pilachowski, C. A., Armandroff, T. E., Sneden, C., Cowan, J. J., & Roe, H. 2000, *ApJ*, 544, 302
- Caffau, E., Bonifacio, P., François, P., Sbordone, L., Monaco, L., Spite, M., Spite, F., Ludwig, H.-G., Cayrel, R., Zaggia, S., Hammer, F., Randich, S., Molaro, P., & Hill, V. 2011, *Nature*, 477, 67
- Campbell, S. W., Lugaro, M., & Karakas, A. I. 2010, *A&A*, 522, L6
- Carney, B. W., Laird, J. B., Latham, D. W., & Aguilar, L. A. 1996, *AJ*, 112, 668
- Carney, B. W. & Peterson, R. C. 1981, *ApJ*, 245, 238
- Carollo, D., Beers, T. C., Chiba, M., Norris, J. E., Freeman, K. C., Lee, Y. S., Ivezić, Ž., Rockosi, C. M., & Yanny, B. 2010, *ApJ*, 712, 692
- Carretta, E., Bragaglia, A., Gratton, R., D'Orazi, V., & Lucatello, S. 2009, *A&A*, 508, 695
- Cayrel, R., Depagne, E., Spite, M., Hill, V., Spite, F., François, P., Plez, B., Beers, T., Primas, F., Andersen, J., Barbuy, B., Bonifacio, P., Molaro, P., & Nordström, B. 2004, *A&A*, 416, 1117
- Chamberlain, J. W. & Aller, L. H. 1951, *ApJ*, 114, 52
- Chiba, M. & Beers, T. C. 2000, *AJ*, 119, 2843
- Christlieb, N., Bessell, M. S., Beers, T. C., Gustafsson, B., Korn, A., Barklem, P. S., Carlsson, T., Mizuno-Wiedner, M., & Rossi, S. 2002, *Nature*, 419, 904
- Christlieb, N., Schörck, T., Frebel, A., Beers, T. C., Wisotzki, L., & Reimers, D. 2008, *A&A*, 484, 721
- Cohen, J. G. & Huang, W. 2009, *ApJ*, 701, 1053
- Collet, R., Asplund, M., & Trampedach, R. 2006, *ApJ*, 644, L121
- Conroy, C. & Spergel, D. N. 2011, *ApJ*, 726, 36
- Cooke, R., Pettini, M., Steidel, C. C., Rudie, G. C., & Jorgenson, R. A. 2011, *MNRAS*, 412, 1047
- Cybart, R. H., Fields, B. D., & Olive, K. A. 2008, *JCAP*, 11, 12
- Diemand, J., Kuhlen, M., & Madau, P. 2007, *ApJ*, 667, 859
- Dupree, A. K., Strader, J., & Smith, G. H. 2011, *ApJ*, 728, 155
- Eggen, O. J., Lynden-Bell, D., & Sandage, A. R. 1962, *ApJ*, 136, 748
- Fabbian, D., Asplund, M., Barklem, P. S., Carlsson, M., & Kiselman, D. 2009, *A&A*, 500, 1221
- François, P., Depagne, E., Hill, V., Spite, M., Spite, F., Plez, B., Beers, T. C., Andersen, J., James, G., Barbuy, B., Cayrel, R., Bonifacio, P., Molaro, P., Nordström, B., & Primas, F. 2007, *A&A*, 476, 935
- Frebel, A. 2010, *Astronomische Nachrichten*, 331, 474
- Frebel, A., Aoki, W., Christlieb, N., Ando, H., Asplund, M., Barklem, P. S., Beers, T. C., Eriksson, K., Fechner, C., Fujimoto, M. Y., Honda, S., Kajino, T., Minezaki, T., Nomoto, K., Norris, J. E., Ryan, S. G., Takada-Hidai, M., Tsangarides, S., & Yoshii, Y. 2005, *Nature*, 434, 871
- Frebel, A., Christlieb, N., Norris, J. E., Beers, T. C., Bessell, M. S., Rhee, J., Fechner, C., Marsteller, B., Rossi, S., Thom, C., Wisotzki, L., & Reimers, D. 2006, *ApJ*, 652, 1585
- Frebel, A., Christlieb, N., Norris, J. E., Thom, C., Beers, T. C., & Rhee, J. 2007a, *ApJ*, 660, L117
- Frebel, A., Collet, R., Eriksson, K., Christlieb, N., & Aoki, W. 2008, *ApJ*, 684, 588
- Frebel, A., Johnson, J. L., & Bromm, V. 2007b, *MNRAS*, 380, L40
- , 2009, *MNRAS*, 392, L50
- Frebel, A., Kirby, E. N., & Simon, J. D. 2010a, *Nature*, 464, 72
- Frebel, A., Simon, J. D., Geha, M., & Willman, B. 2010b, *ApJ*, 708, 560
- Freeman, K. & Bland-Hawthorn, J. 2002, *ARA&A*, 40, 487
- Fulbright, J. P., Rich, R. M., & Castro, S. 2004, *ApJ*, 612, 447
- Geisler, D., Smith, V. V., Wallerstein, G., Gonzalez, G., & Charbonnel, C. 2005, *AJ*, 129, 1428
- Gilmore, G., Wyse, R. F. G., & Kuijken, K. 1989, *ARA&A*, 27, 555
- Giridhar, S., Lambert, D. L., Reddy, B. E., Gonzalez, G., & Yong, D. 2005, *ApJ*, 627, 432
- Gratton, R. G., Sneden, C., Carretta, E., & Bragaglia, A. 2000, *A&A*, 354, 169
- Gray, D. F. 2005, *The Observation and Analysis of Stellar Photospheres*, 3rd Edition (Cambridge: Cambridge University Press)
- Gustafsson, B., Edvardsson, B., Eriksson, K., Jørgensen, U. G., Nordlund, Å., & Plez, B. 2008, *A&A*, 486, 951
- Hartwick, F. D. A. 1976, *ApJ*, 209, 418
- Hartwick, F. D. A. 1987, in *NATO ASIC Proc. 207: The Galaxy*, ed. G. Gilmore & B. Carswell, 281
- Heger, A. & Woosley, S. E. 2002, *ApJ*, 567, 532
- , 2010, *ApJ*, 724, 341
- Hill, V., Plez, B., Cayrel, R., Nordström, T. B. B., Andersen, J., Spite, M., Spite, F., Barbuy, B., Bonifacio, P., Depagne, E., François, P., & Primas, F. 2002, *A&A*, 387, 560
- Honda, S., Aoki, W., Ishimaru, Y., Wanajo, S., & Ryan, S. G. 2006, *ApJ*, 643, 1180
- Honda, S., Aoki, W., Kajino, T., Ando, H., Beers, T. C., Izumiura, H., Sadakane, K., & Takada-Hidai, M. 2004, *ApJ*, 607, 474
- Ibata, R. A., Gilmore, G., & Irwin, M. J. 1995, *MNRAS*, 277, 781
- Iwamoto, N., Umeda, H., Tominaga, N., Nomoto, K., & Maeda, K. 2005, *Science*, 309, 451
- Jonsell, K., Barklem, P. S., Gustafsson, B., Christlieb, N., Hill, V., Beers, T. C., & Holmberg, J. 2006, *A&A*, 451, 651
- Karakas, A. & Lattanzio, J. C. 2007, *PASA*, 24, 103
- Kirby, E. N., Cohen, J. G., Smith, G. H., Majewski, S. R., Sohn, S. T., & Guhathakurta, P. 2011, *ApJ*, 727, 79
- Kirby, E. N., Simon, J. D., Geha, M., Guhathakurta, P., & Frebel, A. 2008, *ApJ*, 685, L43
- Kobayashi, C., Umeda, H., Nomoto, K., Tominaga, N., & Ohkubo, T. 2006, *ApJ*, 653, 1145
- Koch, A., McWilliam, A., Grebel, E. K., Zucker, D. B., & Belokurov, V. 2008, *ApJ*, 688, L13
- Korn, A. J., Grundahl, F., Richard, O., Mashonkina, L., Barklem, P. S., Collet, R., Gustafsson, B., & Piskunov, N. 2007, *ApJ*, 671, 402
- Lai, D. K., Bolte, M., Johnson, J. A., Lucatello, S., Heger, A., & Woosley, S. E. 2008, *ApJ*, 681, 1524
- Li, H. N., Christlieb, N., Schörck, T., Norris, J. E., Bessell, M. S., Yong, D., Beers, T. C., Lee, Y. S., Frebel, A., & Zhao, G. 2010, *A&A*, 521, A10
- Lind, K., Primas, F., Charbonnel, C., Grundahl, F., & Asplund, M. 2009, *A&A*, 503, 545
- Marín-Franch, A., Aparicio, A., Piotto, G., Rosenberg, A., Chaboyer, B., Sarajedini, A., Siegel, M., Anderson, J., Bedin, L. R., Dotter, A., Hempel, M., King, I., Majewski, S., Milone, A. P., Paust, N., & Reid, I. N. 2009, *ApJ*, 694, 1498
- Martin, N. F., de Jong, J. T. A., & Rix, H.-W. 2008, *ApJ*, 684, 1075
- Mateo, M. L. 1998, *ARA&A*, 36, 435

- McWilliam, A. 1997, *ARA&A*, 35, 503
- McWilliam, A., Preston, G. W., Sneden, C., & Searle, L. 1995, *AJ*, 109, 2757
- Meléndez, J., Casagrande, L., Ramírez, I., Asplund, M., & Schuster, W. J. 2010, *A&A*, 515, L3
- Meynet, G., Ekström, S., & Maeder, A. 2006, *A&A*, 447, 623
- Moore, B., Ghigna, S., Governato, F., Lake, G., Quinn, T., Stadel, J., & Tozzi, P. 1999, *ApJ*, 524, L19
- Morrison, H. L., Helmi, A., Sun, J., Liu, P., Gu, R., Norris, J. E., Harding, P., Kinman, T. D., Kepley, A. A., Freeman, K. C., Williams, M., & Van Duyne, J. 2009, *ApJ*, 694, 130
- Neill, J. D., Sullivan, M., Gal-Yam, A., Quimby, R., Ofek, E., Wyder, T. K., Howell, D. A., Nugent, P., Seibert, M., Martin, D. C., Overzier, R., Barlow, T. A., Foster, K., Friedman, P. G., Morrissey, P., Neff, S. G., Schiminovich, D., Bianchi, L., Donas, J., Heckman, T. M., Lee, Y., Madore, B. F., Milliard, B., Rich, R. M., & Szalay, A. S. 2011, *ApJ*, 727, 15
- Nissen, P. E. & Schuster, W. J. 2010, *A&A*, 511, L10
- Nomoto, K., Tominaga, N., Umeda, H., Kobayashi, C., & Maeda, K. 2006, *Nuclear Physics A*, 777, 424
- Norris, J. E. 1999, in *Astronomical Society of the Pacific Conference Series*, Vol. 165, *The Third Stromlo Symposium: The Galactic Halo*, ed. B. K. Gibson, R. S. Axelrod, & M. E. Putman, 213
- Norris, J. E., Christlieb, N., Korn, A. J., Eriksson, K., Bessell, M. S., Beers, T. C., Wisotzki, L., & Reimers, D. 2007, *ApJ*, 670, 774
- Norris, J. E., Gilmore, G., Wyse, R. F. G., Yong, D., & Frebel, A. 2010a, *ApJ*, 722, L104
- Norris, J. E., Ryan, S. G., & Beers, T. C. 2001, *ApJ*, 561, 1034
- Norris, J. E., Wyse, R. F. G., Gilmore, G., Yong, D., Frebel, A., Wilkinson, M. I., Belokurov, V., & Zucker, D. B. 2010b, *ApJ*, 723, 1632
- Norris, J. E., Yong, D., Gilmore, G., & Wyse, R. F. G. 2010c, *ApJ*, 711, 350
- Pagel, B. E. J. 1997, *Nucleosynthesis and Chemical Evolution of Galaxies* (Cambridge: Camb. University Press)
- Piau, L., Beers, T. C., Balsara, D. S., Sivarani, T., Truran, J. W., & Ferguson, J. W. 2006, *ApJ*, 653, 300
- Prantzos, N. 2003, *A&A*, 404, 211
- Qian, Y.-Z. & Wasserburg, G. J. 2003, *ApJ*, 588, 1099
- Roederer, I. U., Kratz, K., Frebel, A., Christlieb, N., Pfeiffer, B., Cowan, J. J., & Sneden, C. 2009, *ApJ*, 698, 1963
- Ryan, S. G., Beers, T. C., Kajino, T., & Rosolankova, K. 2001, *ApJ*, 547, 231
- Ryan, S. G. & Norris, J. E. 1991a, *AJ*, 101, 1835
- . 1991b, *AJ*, 101, 1865
- Ryan, S. G., Norris, J. E., & Beers, T. C. 1996, *ApJ*, 471, 254
- Ryan-Weber, E. V., Pettini, M., Madau, P., & Zych, B. J. 2009, *MNRAS*, 395, 1476
- Sandage, A. 1986, *ARA&A*, 24, 421
- Schatz, H., Toenjes, R., Pfeiffer, B., Beers, T. C., Cowan, J. J., Hill, V., & Kratz, K.-L. 2002, *ApJ*, 579, 626
- Schörck, T., Christlieb, N., Cohen, J. G., Beers, T. C., Shectman, S., Thompson, I., McWilliam, A., Bessell, M. S., Norris, J. E., Meléndez, J., Ramírez, S., Haynes, D., Cass, P., Hartley, M., Russell, K., Watson, F., Zickgraf, F., Behnke, B., Fechner, C., Fuhrmeister, B., Barklem, P. S., Edvardsson, B., Frebel, A., Wisotzki, L., & Reimers, D. 2009, *A&A*, 507, 817
- Searle, L. & Zinn, R. 1978, *ApJ*, 225, 357
- Shetrone, M., Venn, K. A., Tolstoy, E., Primas, F., Hill, V., & Kaufer, A. 2003, *AJ*, 125, 684
- Shigezumi, T., Tsujimoto, T., & Yoshii, Y. 2003, *ApJ*, 586, L57
- Simmerer, J., Sneden, C., Cowan, J. J., Collier, J., Woolf, V. M., & Lawler, J. E. 2004, *ApJ*, 617, 1091
- Simon, J. D., Frebel, A., McWilliam, A., Kirby, E. N., & Thompson, I. B. 2010, *ApJ*, 716, 446
- Sneden, C., Cowan, J. J., & Gallino, R. 2008, *ARA&A*, 46, 241
- Sneden, C., Cowan, J. J., Lawler, J. E., Ivans, I. I., Burles, S., Beers, T. C., Primas, F., Hill, V., Truran, J. W., Fuller, G. M., Pfeiffer, B., & Kratz, K.-L. 2003, *ApJ*, 591, 936
- Sneden, C., McWilliam, A., Preston, G. W., Cowan, J. J., Burris, D. L., & Amorsky, B. J. 1996, *ApJ*, 467, 819
- Songaila, A. 2001, *ApJ*, 561, L153
- Spergel, D. N., Bean, R., Doré, O., Nolta, M. R., Bennett, C. L., Dunkley, J., Hinshaw, G., Jarosik, N., Komatsu, E., Page, L., Peiris, H. V., Verde, L., Halpern, M., Hill, R. S., Kogut, A., Limon, M., Meyer, S. S., Odegard, N., Tucker, G. S., Weiland, J. L., Wollack, E., & Wright, E. L. 2007, *ApJS*, 170, 377
- Spite, F. & Spite, M. 1982, *A&A*, 115, 357
- Spite, M., Cayrel, R., Plez, B., Hill, V., Spite, F., Depagne, E., François, P., Bonifacio, P., Barbuy, B., Beers, T., Andersen, J., Molaro, P., Nordström, B., & Primas, F. 2005, *A&A*, 430, 655
- Springel, V., Wang, J., Vogelsberger, M., Ludlow, A., Jenkins, A., Helmi, A., Navarro, J. F., Frenk, C. S., & White, S. D. M. 2008, *MNRAS*, 391, 1685
- Starkenbug, E., Hill, V., Tolstoy, E., González Hernández, J. I., Irwin, M., Helmi, A., Battaglia, G., Jablonka, P., Tafelmeyer, M., Shetrone, M., Venn, K., & de Boer, T. 2010, *A&A*, 513, A34
- Suda, T., Aikawa, M., Machida, M. N., Fujimoto, M. Y., & Iben, I. J. 2004, *ApJ*, 611, 476
- Suda, T., Katsuta, Y., Yamada, S., Suwa, T., Ishizuka, C., Komiya, Y., Sorai, K., Aikawa, M., & Fujimoto, M. Y. 2008, *PASJ*, 60, 1159
- Tegmark, M., Silk, J., Rees, M. J., Blanchard, A., Abel, T., & Palla, F. 1997, *ApJ*, 474, 1
- Timmes, F. X., Woosley, S. E., & Weaver, T. A. 1995, *ApJS*, 98, 617
- Tolstoy, E., Hill, V., & Tosi, M. 2009, *ARA&A*, 47, 371
- Tominaga, N., Umeda, H., & Nomoto, K. 2007, *ApJ*, 660, 516
- Travaglio, C., Gallino, R., Arnone, E., Cowan, J., Jordan, F., & Sneden, C. 2004, *ApJ*, 601, 864
- Tsujimoto, T., Shigezumi, T., & Yoshii, Y. 1999, *ApJ*, 519, L63
- Umeda, H. & Nomoto, K. 2003, *Nature*, 422, 871
- Umeda, H. & Nomoto, K. 2005, *ApJ*, 619, 427
- Vandenbergh, D. A., Bolte, M., & Stetson, P. B. 1996, *ARA&A*, 34, 461
- Venn, K. A., Irwin, M., Shetrone, M. D., Tout, C. A., Hill, V., & Tolstoy, E. 2004, *AJ*, 128, 1177
- Wagoner, R. V., Fowler, W. A., & Hoyle, F. 1967, *ApJ*, 148, 3
- Wallerstein, G., Iben, Jr., I., Parker, P., Boesgaard, A. M., Hale, G. M., Champagne, A. E., Barnes, C. A., Käppeler, F., Smith, V. V., Hoffman, R. D., Timmes, F. X., Sneden, C., Boyd, R. N., Meyer, B. S., & Lambert, D. L. 1997, *Reviews of Modern Physics*, 69, 995
- Wanajo, S. & Ishimaru, Y. 2006, *Nuclear Physics A*, 777, 676
- Wanajo, S., Itoh, N., Ishimaru, Y., Nozawa, S., & Beers, T. C. 2002, *ApJ*, 577, 853
- Wheeler, J. C., Sneden, C., & Truran, Jr., J. W. 1989, *ARA&A*, 27, 279
- White, S. D. M. & Rees, M. J. 1978, *MNRAS*, 183, 341
- Woosley, S. E. & Weaver, T. A. 1995, *ApJS*, 101, 181
- Zinn, R. 1985, *ApJ*, 293, 424
- Zinn, R. 1993, in *Astronomical Society of the Pacific Conference Series*, Vol. 48, *The Globular Cluster-Galaxy Connection*, ed. G. H. Smith & J. P. Brodie, 38
- Zolotov, A., Willman, B., Brooks, A. M., Governato, F., Brook, C. B., Hogg, D. W., Quinn, T., & Stinson, G. 2009, *ApJ*, 702, 1058